TECHNISCHE UNIVERSITÄT WIEN
Vienna University of Technology

MEDIZINISCHE UNIVERSITÄT WIEN

Diploma Thesis

Instrumentation of an Industry Tricycle for Cycling with FES Activated Denervated Muscles

Scientific work to obtain the academic degree Dipl.-Ing.
Under supervision by

Univ.Prof. Dipl.Ing. Dr.techn. Winfried Mayr
E325
Institute of Mechanics and Mechatronics
and
340
Center for Medical Physics and Biomedical Engineering

Submitted at the Vienna University of Technical
Faculty of Mechanical and Industrial Engineering

by

Thomas Egger
e0525730
Thaliastraße 16/16, 1160-Vienna

Vienna, January 2015

Abstract/Zusammenfassung

In case of a spinal cord injury, leading to paraplegia, affected people do suffer severe limitations based on the loss of mobility. This loss leads necessarily to further severe secondary complications like cardio vascular disease, type II diabetes, massive muscle atrophy in lower limps and a loss of bone mineral density. Electrical stimulation (ES) is an uncomplicated to use possibility for minimizing these secondary complications. A further advantage of ES is that it is completely free of possible negative side-effects when applied properly. Therefore, functional electrical stimulation cycling (FESC) is a gladly used method in rehabilitation and the positive effects are documented in many studies. But the existence of a flaccid paralysis is an excluding criterion to take part in studies concerning FESC. In near past, studies, like project RISE, have shown that it is possible to train and to partly recover denervated muscles. Within the scope of project RISE parameters were defined which are necessary to allow functional electrical stimulation (FES) of denervated muscles.

It was the aim of this study to adapt a recumbent bicycle, to enable people suffering from flaccid paraplegia to perform FESC test trials. The used bicycle has two different driving possibilities. One possibility is to drive the bicycle by pedaling, called pedaling mode (p-mode), the other one is by a movement similar to rowing, called extension drive mode (ed-mode). For both driving possibilities mechanical and electro technical adaptations needed to be done. To stimulate the muscles a prototype of a stimulator for denervated muscles was used. To use the stimulator, in combination with the bicycle, it was necessary to design a controller and the suitable stimulation program. To assure the proper function of the bicycle and the designed mechanical and electrical components, function tests were performed.

With the ed-mode it was possible to perform extensive development tests. The tests lead to the assumption that the ed-mode would also be feasible for persons with denervated muscles because of its straightforward movement. It was not possible to achieve equally successful test demonstrations of the p-mode functionality due to difficulties to overcome a dead zone in the pedaling angle where no driving moment is produced. One reason was the limitations in available stimulation channels (2 per leg), but as the main problem the non-lockable freewheel construction of the commercial bicycle was identified. Even able-bodied subjects were not able to overcome the dead zone. After further instrumentation of the tricycle with an auxiliary electrical motor support also p-mode FESC should be possible for paraplegic with denervated muscles.

Im Fall einer Querschnittverletzung, mit resultierender Lähmung der unteren Extremitäten, erleiden die betroffenen Personen gravierende Einschränkungen ihrer Mobilität. Dieser Verlust führt zwangsläufig zu weiteren schweren Sekundärkomplikationen wie Herz-Kreislauf Beschwerden, Typ II Diabetes, massiver Muskel Atrophie in den unteren Gliedmaßen sowie einer Abnahme der Knochendichte. Elektrostimulation (ES) ist eine unkompliziert anzuwendende Möglichkeit um diese Sekundärkomplikationen zu minimieren. Ein weiterer Vorteil der Elektrostimulation liegt darin, vollkommen frei von etwaigen negativen Nebenwirkungen zu sein, vorausgesetzt die Anwendung wird ordnungsgemäß durchgeführt. Fahrradfahren mittel funktioneller Elektrostimulation (FESC) ist daher eine in der Rehabilitation gerne angewendete Methode und die positiven Auswirkungen sind in zahlreichen Studien dokumentiert. Das Vorhandensein einer schlaffen Lähmung gilt bis jetzt als Ausschlusskriterium, um an FES-Radfahrstudien teilzunehmen. Forschungsprojekte, wie das Projekt RISE, haben in naher Vergangenheit bewiesen, dass es möglich ist, denervierte Muskulatur zu trainieren und nach Degeneration teilweise wiederherzustellen. Zusätzlich wurden im Rahmen des Projektes geeignete elektrische Parameter für die funktionale Elektrostimulation denervierter Muskulatur definiert.

Es war Zweck dieser Arbeit ein Liegefahrrad zu adaptieren um Testfahrten mit Personen, die an denervierter Muskulatur leiden, durchführen zu können. Das verwendete Fahrrad besitzt über zwei verschiedene Antriebsmöglichkeiten. Einen Pedallierbetrieb, Pedallier-Modus (p-mode) genannt, und eine Antriebsmöglichkeit, die der Bewegung beim Rudern, Extensions-Modus (ed-mode) genannt, nachempfunden ist. Für beide Betriebsarten mussten sowohl mechanische als auch elektrotechnische Anpassungen am Fahrrad vorgenommen werden. Zur Stimulation der Muskulatur wurde ein Prototyp eines Stimulators für denervierte Muskulatur verwendet. Um das Fahrrad mit dem Stimulator betreiben zu können, war es nötig ein Steuergerät, inklusive der benötigten Programmierung, zu entwickeln. Um die Funktion des Fahrrades, sowie der konstruierten mechanischen und elektrischen Komponenten, zu gewährleisten, wurden entwicklungsbegleitende Funktionstests durchgeführt.

Mit dem ed-mode war es möglich ausführliche Entwicklungs Fahrtests durchzuführen. Dabei wurde dieser, vor allem aufgrund des einfach umzusetzenden Bewegungsablaufes, als auch bei denervierter Muskulatur durchführbar erachtet. Im p-modus war es nicht möglich erfolgreiche Testfahrten im Zuge der Entwicklungstests durchzuführen, da ein nichtüberwindbarer Totpunkt im Pedalkurbelwinkel auftrat, in dem kein Antriebsmoment produziert wurde. Einerseits konnte der zur Verfügung gestellte Stimulator (vier Stimulationskanäle) nur zwei Muskelgruppen pro Bein aktivieren andererseits war es auch ohne Lähmung für Probanden nicht möglich ein positives Antriebsmoment über den gesamten Tretkurbelwinkel aufrechtzuerhalten. Als Hauptproblem wurde ein nicht blockierbarer Freilauf des Fahrrades identifiziert. Als Lösung ist die Implementierung eines unterstützenden Elektromotors für die Überbrückung der Antriebslücke geplant. Mit dieser Maßnahme sollte auch das Radfahren für Paraplegiker mit denervierter Muskulatur mittels FES im p-Mode möglich sein.

Acknowledgement

First I want to thank Univ.Prof. Dipl.Ing. Dr.techn. Winfried Mayr, my supervisor from the Center for Medical Physics and Biomedical Engineering of the Medical University of Vienna and the Institute of Mechanics and Mechatronics of the Vienna University of Technology, for his extensive expertise and guidance. Without him this thesis would not have been possible.

Further thanks go to Ing. Ewald Unger, Research Assistant, MSc Mathias Krenn and MSc Michael Haller from the Center for Medical Physics and Biomedical Engineering of the Medical University of Vienna for their profound knowledge and support in the areas of electrical engineering and microcontrollers.

I want to thank Dr. Christian Hofer of the Research and Development Department of Otto Bock Healthcare Products GmbH for his time and support concerning the stimulator for denervated muscles. As well as Otto Bock Healthcare Products GmbH for providing the recumbent bicycle for this thesis.

I give special thanks to my mother, my godmother Gerti and my uncle and aunt, Josef and Katja, for their financial and moral support over the duration of my study. With their help it was possible to reach my goal.

I would particularly like to thank my girlfriend Verena for her understanding and consideration while the partial time-consuming study phases. Furthermore I want to thank her for proofreading my thesis.

For Verena and Marie

Table of Contents

Abstract/Zusammenfassung II

Acknowledgement IV

Table of Contents VI

Index of Abbreviations IX

List of Tables X

Table of Images XI

1 Objective of the Study 14

2 Introduction 14
- 2.1 Anatomical and Physiological Background 14
  - 2.1.1 The Human Muscle and its Anatomical Structure 14
  - 2.1.2 The Action Potential (AP) and the Excitation Propagation in Motor Neurons 16
  - 2.1.4 Anatomical and Histological Changes of Denervated Musculature 18
- 2.2 Functional Electrical Stimulation 19
  - 2.2.1 Functional Electrical Stimulation of Denervated Muscles 19
  - 2.2.2 Benefits of FES-Cycling for Persons with Paraplegia 20
  - 2.2.3 FES-Cycling Review 21
  - 2.2.4 Selected Applications of Functional Electrical Stimulation for Paraplegic Persons 24

3 Concept, Material and Methods 26
- 3.1 The Bicycle 26
- 3.2 System Concept 28
  - 3.2.1 Safety 28
  - 3.2.2 Requirements 32
  - 3.2.3 System Draft 32
  - 3.2.4 Resulting Concept 42
- 3.3 Equipment 42
  - 3.3.1 Stimulation Equipment 42
  - 3.3.2 Sensory and Measurement Equipment 45
- 3.4 Stimulation Concepts 48
  - 3.4.1 Extension Drive Mode 48
  - 3.4.2 Pedalling-Mode 50
- 3.5 Stimulation Program 52
- 3.6 Calculations 52
  - 3.6.1 Calculation of the Drag Force (FD) 54
  - 3.6.2 Calculation of the Translational Inertial Force (FIT) 55

3.6.3 Calculation of the Rotational Inertial Forces (FIR) 55
3.6.4 Calculation of the Bicycle Resistance Forces (FBR) 56
3.6.5 Power Calculation 58

4 Bicycle Modifications 59
4.1 Construction of the Control Panel Mounting (CPM) 60
4.2 Construction of the Crank Fixation 60
4.3 Construction of the Bottom Bracket Shaft (BBS) 61
4.4 Construction of the Limit Switch Mounting 62
4.4.1 Mechanical Design 62
4.4.2 Electrical Design 62
4.4.3 Electrical Functional Description 62
4.5 Limit Switch Fence 63
4.6 Construction of the Stimulation Button Casing (SBC) 63
4.6.1 Mechanical Design 63
4.6.2 Electrical Design 64
4.6.3 Electrical Functional Description 64
4.7 Construction of the Controller 65
4.7.1 Mechanical Design 65
4.7.2 Electrical Design 65
4.7.3 Electrical Functional Description 66
4.8 Construction of the Emergency Button Casing (EBC) 67
4.8.1 Mechanical Design 67
4.8.2 Electrical Design 68
4.8.3 Electrical Functional Description 68
4.9 Construction of the Pedal End Stop (PES) 69
4.10 Construction of the End Stop Clamp (ESC) 69
4.10.1 Mechanical Design 69
4.10.2 Finite Element Analysis (FEM) 70
4.10.2.1 FEM Analysis of the Horizontal Beam 70
4.10.2 FEM Analysis of the Clamping Jaws 72
4.11 Construction of the Battery Clamp (BC) 77
4.12 Construction of the Chain Tensioner Adapter (CTA) 77

5 Development Accompanying Function Tests 78
5.1 Investigation of the Bicycle Resistance Force (BRF) 78
5.1.1 Measurement of the BRF 78
5.1.2 Measurement of the BRF - Test Setup and Calculations 79
5.1.3 Calculation of the BRF 80
5.2 Extension Drive Mode-Function Test 80
5.2.1 Test Preparations 81
5.2.2 Documentation of the Test Setup: 84
5.2.3 Test Data 84
5.2.4 Test Results 91

5.2.5 Assessment of the Designed Bicycle Components 95
5.3 Pedalling Mode – Function Test 97
5.3.1 Test Preparations 97
5.3.2 Test device – Function Test 99
5.3.3 Test Track – Function Test 100
5.3.4 Assessment of the Designed Bicycle Components 101

6 Conclusion and Outlook 101

Bibliography 103

Appendix 107
A1 Technical Drawings 107
A2 Circuit Diagrams 135
A3 Calculation 140
A3.1 Function Test Calculation 140
A3.2 ESC Calculation 159
A4 Test Trial Checklist 163

Index of Abbreviations

ADP	Adenosine diphosphate
AP	Action potential
API	Application programming interface
AS	Analogue switch
ATP	Adenosine triphosphate
BBS	Bottom bracket shaft
BC	Battery clamp
BC	Bicycle computer
BRF	Bicycle resistance force
CNS	Central nervous system
CPM	Control panel mounting
CTA	Chain tensioner adapter
DP	Depolarisation
EBC	Emergency button casing
ed-mode	Extension drive mode
ES:	Electrical stimulation
ESC	End stop clamp
FB	Fubarino mini v15 board
FEM	Finite element method
FES	Functional electrical stimulation
FESC	Functional electrical stimulation cycling
FESR	Functional electrical stimulation rowing
ICSP	In circuit serial programming
LED	Light emitting electrodes
LCD	Liquid crystal display
MBF	Musculus biceps femoris
MEP	Motor end plate
MQF	Musculus quadriceps femoris
PES	Pedal end stop
p-mode	Pedalling mode
RP	Repolarisation
SBC	Stimulation button casing
SCI	Spinal cord injury
SPST-NO	Single pole, single throw-normally open
ST	Smith trigger
TFES	Transcutaneous functional electrical stimulation
VO2	Maximal oxygen uptake
WTB	Wire to board

List of Tables

Table 1 Comparison of stimulation parameters for TES of innervated and denervated muscles. Under assumption of a frequency range from 20-50Hz and a pulse width of 0,5ms per phase 20
Table 2 Technical data of the Reha-Funtrike 27
Table 3 Technical data of the used stimulator 43
Table 4 Technical data of the controller 44
Table 5 Technical data of the implemented limit switches 46
Table 6 Selected technical data of the BC 46
Table 7 Selected technical data of the shaft encoder 47
Table 8 Selected technical data of the LCD 48

Table of Images

Figure 1 Anatomical composition of a striated muscle 15
Figure 2 Anatomical composition of a sacromere 15
Figure 3 Membrane voltage (AP) of a nerve cell depicted over time 17
Figure 4 Description of the transition from an electrical AP to a chemical transmission at a synapse 17
Figure 5 Displays the mechanism which is responsible for the filament sliding 18
Figure 6 Muscle biopsy of denervated muscle tissue 18
Figure 7 Histological appearance of a healthy muscle vs. a denervated muscle. 19
Figure 8 FES-ergometer for leg cycling only 23
Figure 9 FES-trainer for leg and arm cycling 23
Figure 10 FES assisted recumbent bicycle for leg cycling 23
Figure 11 FES assisted wheelchair-bicycle combination for leg and arm cycling 23
Figure 12 Parastep walker including switches 26
Figure 13 Parastep stimulator 26
Figure 14 Picture of the bicycle in extension drive mode 27
Figure 15 Simplified Time-Current-Regions 29
Figure 16 Body impedance and resulting contact currents 30
Figure 17 Body resistance at dry contact conditions 31
Figure 18 System Draft of the bicycle 33
Figure 19 User controller interface 34
Figure 20 Stimulation lever force relationships 35
Figure 21 Position of the BC (A) and the battery (B) inside of the stimulator 37
Figure 22 Position of the Limit Switch Mounting including the Limit Switches 38
Figure 23 Placement of the Limit Switch Fence (A) 38
Figure 24 ESC (A), clamped onto the guide rails, in bottom position 39
Figure 25 Position of the PES on the left side, in driving direction, in end position. 39
Figure 26 Position of the Crank Fixation (A) 40
Figure 27 Position of the BBS (A), the installed gears (B) and the encoder (C) 41
Figure 28 Position of the CTA (A) with the chain tensioner (B) 41
Figure 29 Sketch of the resulting system concept 42
Figure 30 Image of the stimulator front panel with the connected controller 43
Figure 31 Picture of self adhesive electrodes for transcutaneous electric stimulation 45
Figure 32 Safety electrodes with conductive layer pointing upward 45
Figure 33 Circuit diagram of the SPST-NO switch 45
Figure 34 Possible evaluation methods of the angular encoder 47
Figure 35 Flowchart for the ed-mode. 49
Figure 36 Flowchart for the pedalling movement of one leg 51
Figure 37 Diagram of forces acting on a bicycle while driving 53

Figure 38 Symbolic depiction of the bicycle including driver, the occurring forces and their effective direction while driving 53
Figure 39 Cropped picture used to determine the wind contact surface 55
Figure 40 Draft of the occurring forces and their effective direction while the test trial 58
Figure 41 Exploded drawing of the CPM 60
Figure 42 Exploded drawing of the Crank Fixation 61
Figure 43 Exploded drawing of the BBS and the encoder gear 61
Figure 44 Exploded drawing of the Limit Switch Mounting 62
Figure 45 Exploded drawing of the Limit Switch Fence 63
Figure 46 Exploded drawing of the Stimulation Button Casing 64
Figure 47 Controller housing with the main body (1) and the lid (2) 66
Figure 48 View into the controllers inside 66
Figure 49 Exploded drawing of the EBC 68
Figure 50 Exploded drawing of the PES 69
Figure 51 Exploited drawing of the ESC 70
Figure 52 Picture of the applied mesh, position of the fixed surfaces and the applied loads 71
Figure 53 Analysis results of the horizontal beam, in vertical direction 72
Figure 54 Picture of the rectangular version of one clamping jaw 72
Figure 55 Picture of one clamping jaw version with 0.5° chamfer 72
Figure 56 Depiction of the mesh applied to the ESC model. 73
Figure 57 Depiction of the ESC surfaces and their applied contact conditions and constraints 74
Figure 58 ESC model with applied forces 74
Figure 59 Picture of a guide rail section with clamping jaw. 75
Figure 60 Guide rail section without clamping jaw 76
Figure 61 Guide rail section without clamping jaw 76
Figure 62 Exploded drawing of the BC 77
Figure 63 Exploded drawing of the CTA 78
Figure 64 Sketch of the forces acting on the bicycle if the potential force, the inertia force and the drag force are neglected 79
Figure 65 Adjusted knee angle in end position. 82
Figure 66 Position of the stimulation electrodes on the left femur 83
Figure 67 Velocity of the first test trial 85
Figure 68 Acceleration of the first test trial 85
Figure 69 Velocity of the second test trial 86
Figure 70 Acceleration of the second test trial 86
Figure 71 Velocity of the third test trial 87
Figure 72 Acceleration of the third test trial 87
Figure 73 Recorded velocity of the first test trial in dependence of the driven time. 88
Figure 74 Resulting acceleration of the first test trial in dependence of the driven time 88
Figure 75 Recorded velocity of the second test trial in dependence of the driven time. 89
Figure 76 Resulting acceleration of the second test trial 89

Figure 77 Recorded velocity of the third test trial in dependence of the driven time. ... 90
Figure 78 Resulting acceleration of the third test trial 90
Figure 79 Diagram of the BRF in dependence of the driving velocity 91
Figure 80 Diagram of the forces acting to the bicycle while accelerating 92
Figure 81 Diagram of the achieved power 92
Figure 82 Diagram of the forces acting to the bicycle while accelerating 93
Figure 83 Diagram of the achieved power for the second trial. 93
Figure 84 Diagram of the forces acting to the bicycle while accelerating for the third test trial. 94
Figure 85 Diagram of the achieved power for the third trial. 94
Figure 86 Adjusted seat position for the p-mode 98
Figure 87 Position of the dorsal femural surface electrodes 99
Figure 88 Angular stimulation regions with the best results to produce a pedal movement 100

1 Objective of the Study

Cycling, supported by Functional electrical stimulation (FES), is frequently used today as therapy for people with paraplegia. But up to now, it is an exclusion criterion for Functional electrical stimulation cycling (FESC), if paraplegia with denervated musculature exists.

Therefore study´s aims are:

1. Adapt an existing bicycle for the use as FES-Bicycle
2. Design and produce the necessary equipment
3. Investigate if FESC is possible with flaccid paralysis

The study was performed in cooperation with another student about to take his diploma [1]. The areas of responsibility were separated as following. The mechanical design was part of this work while the programming of the designed hardware was part of the other work. The electrical components were largely designed in cooperation.

2 Introduction

2.1 Anatomical and Physiological Background

2.1.1 The Human Muscle and its Anatomical Structure

The human muscle tissue is one of the soft tissues. As a unique property, muscle tissue is able to contract. This contraction leads to a shortening of the muscle and furthermore to movement of the locomotion system. The contraction of the muscle is based on electrical and chemical processes. The muscle of the human body can be grouped in two, structural different, types. The smooth muscle and the striated muscle whereby striated muscles can further be divided in two different groups, called skeletal muscle and cardiac muscle. Smooth muscles do exist mainly in the inner organs like the intestines and the vascular system. Cardiac muscles occur only at the heart. Both, the smooth and the cardiac muscle, cannot be contracted voluntary. The striated musculature appears mainly in the locomotion system and can be contracted voluntary. Since only striated muscles are needed for FESC, the further explanations refer only to striated musculature.

The anatomical structure from the macroscopic to the microscopic scale is given by following sequence. A muscle fascia is building the outer layer of the muscle, this fascia

has a fluently transition into a tendon which connects the muscle to the bone. Both, the fascia and the tendon consist of fibrous connective tissue. Inside the fascia, muscle fibres are grouped into so called muscle bunches. These bunches are capsulated by the perimysium, a loose connective tissue layer. The muscle fibres, inside of the bunches, are the muscle cells and can achieve a length up to 20 cm (Figure 1).

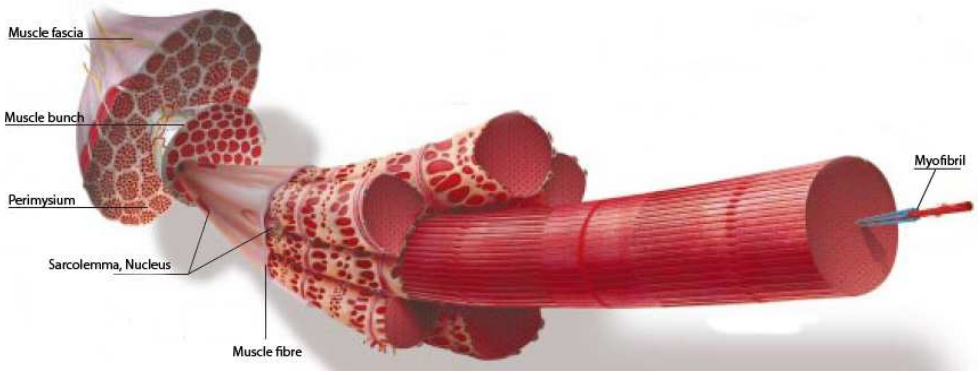

Figure 1 Anatomical composition of a striated muscle. (Figure adapted from [2])

A muscle cell itself consists of myofibrils which are orientated parallel to each other. A myofibril consists furthermore of huge number of sarcomeres which are placed longitudinal one to another. Longitudinal myofibriles are separated by partition walls, called Z-lines. One sarcomere is the smallest functional unit of a muscle. The structure of one sacromere is given by two Z-lines parallel to each other and with proteins as functional elements between them. The proteins are named actin, myosin and titin. The actine filaments are directly attached, in a circular way, on both Z-lines. Within the actine filaments, thin myosin filaments are orientated also in a circular way. The myosin filaments are also attached to the Z-lines by titin filaments on the outer side and directly to the so called M-line, placed in the middle of the sacromere. Because of this orientation and separation the muscle shows a striated appearance under the microscope (Figure 2) [3][4].

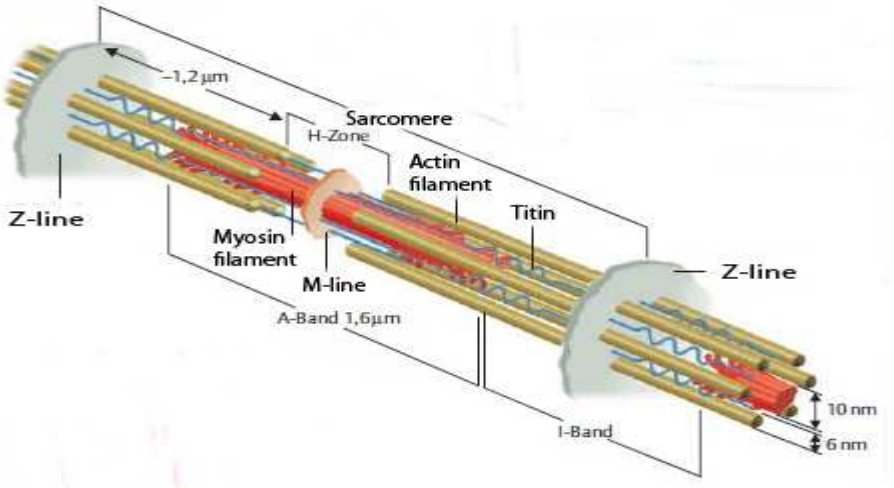

Figure 2 Anatomical composition of a sacromere. (Figure adapted from [4])

2.1.2 The Action Potential (AP) and the Excitation Propagation in Motor Neurons

To initiate a muscle contraction a chain reaction of electrical and chemical processes is necessary. At the beginning of this reaction a relative constant, negative voltage difference, named resting potential, is dominant between the outside and the inside of a motor neuron. This resting potential is achieved by a difference in the ion concentration between the intra cellular space and the extra cellular space of the nerve cell. The physiological reaction starts with the generation of an action potential at the axon hillock of the neuron. An action potential means a decrease of the voltage difference between outside and inside of the nerve cell until a positive value is achieved. This phase is called depolarisation (DP). The DP phase is followed by the repolarisation phase (RP), which reverses the ion concentration difference between intracellular and extracellular space. At the end of the RP phase the AP shows a short negative overshoot, called hyperpolarisation (HP) (Figure 3). To start the reaction, which leads to an action potential, it is necessary to reduce the potential difference to a certain threshold. Reaching this threshold, ion channels in the nerve cell membrane do open and an action potential is initiated. This AP is propagated, inside of the nerve cell, along the nerve axon to the synapses placed at the end of a nerve fibre. At the synapse the process is transformed from an electrical process to a chemical process. The arriving action potential leads to a depolarisation of the synapse cell membrane. This again leads to an opening of ion channels and diffusion of ions from the extra cellular space into the intra cellular space. This results in a formation of small vesicles, filled with neurotransmitter, in the intracellular space. In a next step, these vesicles merge with the presynaptic membrane of the synapse, and do release the neurotransmitter into the synaptic cleft. The neurotransmitter diffuses through the synaptic cleft and binds to a receptor on the postsynaptic side. The receptor again opens ion channels and leads to a depolarisation of the postsynaptic membrane (Figure 4). A postsynaptic membrane can either be another nerve cell or a muscle cell. In case of excitation propagation from a motor axon to a muscle fibre the postsynaptic side is called motor end plate. The motor end plate is the location where a muscle is innervated by its motor neurons [4].

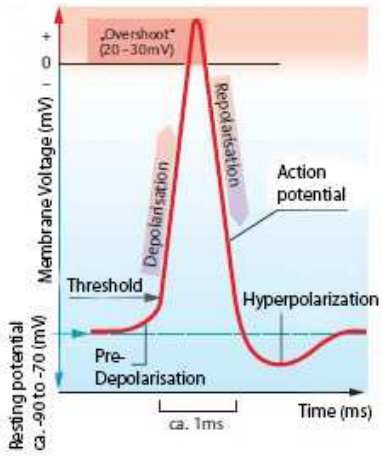

Figure 3 Membrane voltage (AP) of a nerve cell depicted over time (Figure adapted from [4])

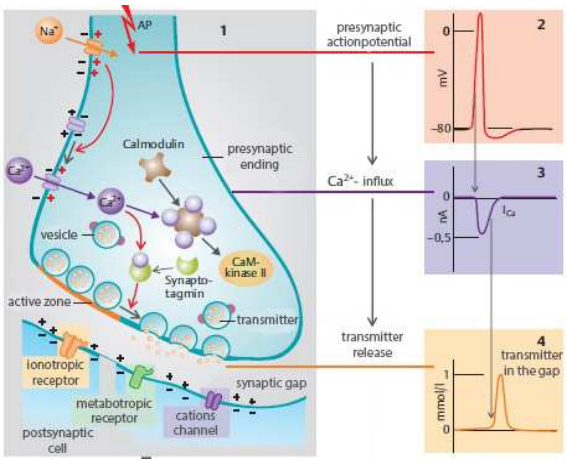

Figure 4 Description of the transition from an electrical AP to a chemical transmission at a synapse (Figure adapted from [4])

2.1.3 Excitation of Muscle Tissue and Muscle Contraction

The excitation and contraction of a muscle is a combination of electrical, chemical and mechanical mechanisms. The AP, which is produced at the motor end plate, is propagated along the Sarcolemma by the opening of ion channels. On this way the AP is distributed along the whole muscle surface. Along the T-system, consisting of transversal tubules, the AP is lead into the depth of the muscle. While travelling along the T-tubules, the AP is activating ion channel of the Sarcoplasmatic Reticulum. This leads to the release of calcium-ions into the Sacromere and starts the contraction mechanism. The calcium-ions bind to a molecule named tropomyosin which prevents the myosin filament from binding to the actin filament. By binding of the calcium-ion to the tropomyosin, the tropomyosin is moving and permits the myosin head to bind to the actin. For binding to the actin, the myosin itself needs to absorb adenosine triphosphate (ATP). As next step a single phosphate is released from the ATP molecule and forms adenosine diphosphate (ADP). As a result, the myosin head is twisted about 40°. Then the ADP is released which leads to a further twist of about 5°. By twisting its heads, the myosin is sliding the actin filament and as a result, the muscle contracts. To solve the binding between the actin and myosin filament, again ATP needs to bind to the myosin head. This leads also to the reset of the myosin heads angled orientation (Figure 5). Since the movement of one single myosin head leads to a distance of about 4-10 nm, high oscillation frequencies and the cooperation of a huge number of myosin heads is necessary to fulfil a muscle contraction [4].

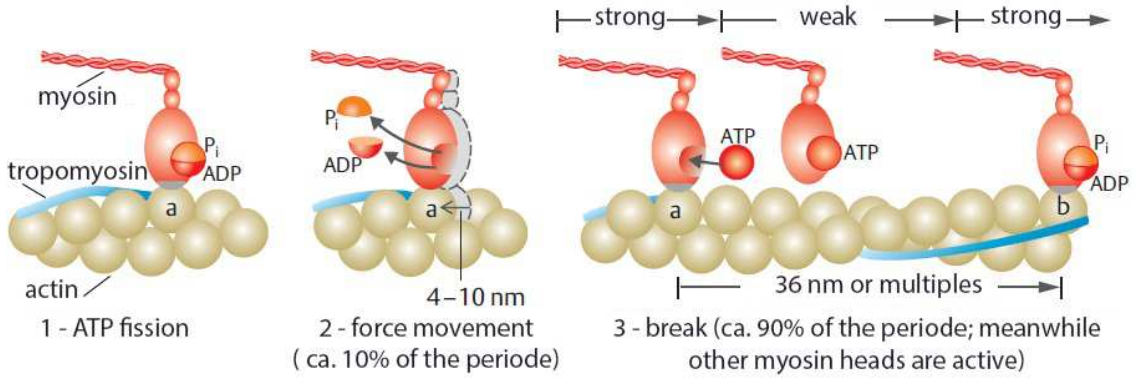

Figure 5 Displays the mechanism which is responsible for the filament sliding. Step one depicts the fission of phosphor (P) and ADP. As second step the release of a single phosphor and the remaining ADP as well as the bending of the myosin head is shown. This leads to step three, the adsorption of ATP and the resting phase of the myosin head. (Figure adapted from [4])

2.1.4 Anatomical and Histological Changes of Denervated Musculature

Denervated muscles lack completely of innervation by a motor neuron. This can happen because of neuropathological conditions or due to a traumatic event. This denervation leads to dramatic changes of the anatomical and histological structure of the muscle fibres as well as to severe atrophy. In the first year after the spinal cord injury (SCI) about 70% of a biopsy section consists of preserved atrophic myofibrils. Two years after the traumatic event, biopsies showed already a mean value of only 31.5% preserved atrophic myofibrils. The remaining 68.5% of the biopsy cross section consists of connective and adipose tissue (Figure 6). A permanent denervation of the muscle leads also to a complete disassembling of the microscopic myofibril structure. Sarcomeres show wavy or widened Z-lines and do often lack completely of M-lines. The intermyofibrilar space is widened and filled with clustered mitochondria. The sarcoplasmatic reticulum is incomplete and the transverse tubules are distorted (Figure 7) [5],[6].

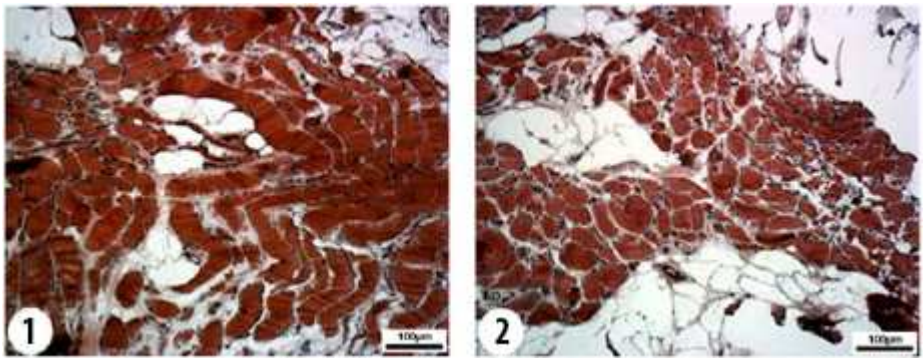

Figure 6 Muscle biopsy of denervated muscle tissue. Picture number 1 shows a muscle biopsy, taken from a patient, 1,3 years after the SCI. On the right side on picture number 2 a muscle biopsy of a patient, 3,3 years after the SCI, is displayed. The biopsy, taken 3,3 years after the SCI, shows clearly the increase of adipose and connective tissue gradually, compared with the biopsy taken 1,3 years after the SCI. (Figure adapted from [5])

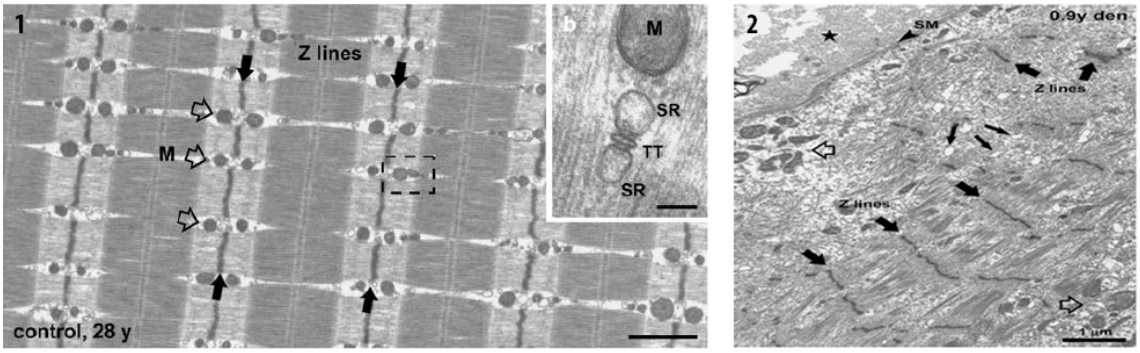

Figure 7 Histological appearance of a healthy muscle vs. a denervated muscle. On the left side, picture number 1 shows a muscle tissue biopsy of a healthy 28 year old person. The histological appearance shows well arranged sarcomeres, mitochondria (M), sarcoplasmatic reticula (SR) and transversal tubule (TT). Z lines are highlighted with fully black arrows. Picture number 2, on the right side, depicts a muscle biopsy of a patient 0,9 years after denervation. The sacromere structures are already dissolved. Z lines (full black arrows) are wavy in shape and dislocated. Mitrochondria are clustered (empty broad arrow) and the SR is located randomly far away from the z lines (small black arrows). (Figures adapted from [6], [7])

2.2 Functional Electrical Stimulation

2.2.1 Functional Electrical Stimulation of Denervated Muscles

In a physiological healthy person an action potential is triggered by the Central Nervous System (CNS). Further it is propagated by a motor neuron to the muscle which is innervated by this neuron and triggers a muscle contraction (see chapter 2.1.2, 2.1.3). When FES is necessary the motor neuron is damaged between the CNS and the muscle. This leads to an incomplete spinal cord injury. Therefore the motor neuron is not able to propagate the AP reliably. One possibility to use FES for incomplete SCI is transcutaneous-FES (TFES). When using TFES an electrode pair is placed on the skin surface, directly above the muscle which is to stimulate. The most effective position is to place one electrode direct above the motor end plate (MEP) which is the innervation location of the muscle. When a stimulation impulse is send from the stimulator the ion channels of the motor neuron are opened and on this way an AP is triggered artificially. The further propagation of the AP along the muscle happens the same way as it would in a physiological healthy person.

A complete SCI exists if the motor neuron is completely disrupted. Then the muscle is denervated and the associated motor neuron is inoperable. In this case it is not possible to stimulate the motor neuron or the MEP and trigger an AP artificial. Therefore the muscle fibers have to be depolarized directly. This can be achieved by using large electrodes which cover the majority of the muscle. Another reason to use large electrodes when stimulating denervated muscles is that the pulse rate has to be kept low. Dependent on the time past since the traumatic event, more or less long impulses are necessary.

To guarantee charge balance, in the tissue surrounding the electrodes, a biphasic impulse shape is required for stimulation of denervated muscles. The needed pulse width, for both phases, varies in a range from 36-150ms dependent on the physical condition of the muscle [8].

Comparison of Stimulation Parameters for Transcutaneous Electrical Stimulation (TES) of Innervated and Denervated Muscle with Biphasic Pulse Shape:

	Innervated Muscle	**Denervated Muscle**
Amplitude constant voltage	Up to ±100V	Up to ±100V
Amplitude constant current	Up to ±300mA	Up to ±300mA
Pulse width	Typically 0,5ms per phase	36-150ms for both phases
Impulse break	15-50ms*	10-400ms

Table 1 Comparison of stimulation parameters for TES of innervated and denervated muscles. Under assumption of a frequency range from 20-50Hz* and a pulse width of 0,5ms* per phase

2.2.2 Benefits of FES-Cycling for Persons with Paraplegia

A lot of negative secondary complications are caused by paraplegia mainly through massive decreased capability of voluntary movement. The most obvious complication affects the muscular system. Through the inability to activate the muscles voluntarily these muscles are affected by severe atrophy. This leads to a reduction of muscle mass and an increase of fat to muscle ratio. Furthermore the muscle strength is reduced as well as the fatigue resistance and the oxygen capacity of the muscle. With frequently FESC training it is possible to increase to muscle mass and muscle strength as well as to increase the muscle to adipose tissue ratio. This leads furthermore to increased maximal power output and endurance. Persons with a SCI usually suffer from spasticity. Spasticity is the involuntary convolution of affected muscles. These convolutions can be strong and lead to joint movements. Therefore spasticity can lead to discomfort, disruption of the activities of the daily life and functional disabilities. The results concerning the alterations of spasticity after FESC are controversial. Some results show a reduced spasticity while other results reveal that the frequency of the spasticity is reduced but the convolutions are growing in strength.

Another complication is osteoporosis for people with SCI, caused by loss of bone mineral density. The loss of mineral density is predominant in the paralyzed limps. During the first year after the SCI the bone mineral density is reduced by 20%. In comparison to able bodied persons, the risk of fractures is twice higher for people with SCI. Several studies found no increase in bone mineral density after FESC whereas others found a decreased rate of bone loss or even an increase of bone density after frequent FESC training. These differences statements seem to be the result of different training dura-

tions and intensities. Long time immobilization leads furthermore to degeneration of articular cartilage and to loss of bone mineral density in articular bones. One study indicates that FESC may contribute to reduce this problem.

Also the cardiovascular system is negatively influenced in persons with SCI. Caused by lack of exercise the cardiopulmonary system adapts by reducing the diameters of arteries and the decrease of capillarization. These adaptions lead to a decrease of baseline and peak blood flow in the lower limps. FESC is an effective and easy way to increase the arterial diameters, reinforce the capillary density and therefore increase the blood flow in the lower limps. Further studies showed that persons with SCI have a higher risk of developing cardiovascular diseases. This diseases result in decreased cardiopulmonary and metabolic activity. But also this risk can be reduced by FESC by increasing the left ventricular mass and the left ventricular end-diastolic volume.

A frequent problem in the SCI population is the occurrence of pressure sores which represent a great health risk. Pressure sores mainly occur at areas where only a thin tissue layer is between skin and bone and pressure is applied for extended time. This leads to a reduced blood flow and oxygen supply in this area which ultimately results in tissue necrosis[9]. A study by Petrofsky found out that the occurrence of pressure sores can be reduced by 90%. This reduction is achieved by muscle atrophy and therefore an increase of soft tissue and the enhanced blood flow and therefore oxygen supply.

Some studies pointed out that type 2 diabetes is more frequent in SCI Population than in able-bodied persons. This increase in type 2 diabetes is due to reduced glucose tolerance in the lower limps. With FESC it is also possible to increase the insulin uptake in the muscles of the lower limps.

An advantage which should not be neglected is the positive psychological effect. Patients who attempted at a study for patients perceptions concerning FESC reported of improved self image and appearance [10]. This has a positive influence on social abilities and can also be an important training motivation. Also the functional performance and the actions of daily life are improved after frequent FESC training [11].

2.2.3 FES-Cycling Review

At the beginning of the 1980s different research groups published their FESC attempts [12] [13],[14]. The motivation was to design a training device for SCI patients, to increase muscle strength, muscle size and cardiovascular fitness. In 1986 it was reported that the main reason for mortality in SCI population is due to cardiovascular diseases [15]. Based on this report it was searched for a possibility to reinforce the cardiovascular system of people with SCI. FESC was already known as feasible training method. A further reason to choose FESC instead of FES walking is that FESC is safer to perform than FES walking. FES walking has a much higher risk of falling than FESC with a tricycle. And only FESC can provide an independent mobility opportunity since a per-

son, riding an outdoor FES-bicycle, is not dependent on help of another person. Therefore more research groups started investigations concerning FESC. To access the cardiovascular benefit of a training method the maximal oxygen uptake (VO2) is used. The VO2 is proportional to the oxygen transport in the cardiovascular system and the oxygen utilization in the muscles of the locomotion system, the heart, smooth muscles, organs and nerve cells. Therefore it is logical that the VO2 can also be increased by including the voluntary controllable muscle when training persons with SCI. This attempt was used by several research groups in 1990 and 1992 [16],[17]. They started to combine voluntary arm movement with electrical stimulation of the legs and reported a VO2 increase by 54% compared to only leg or arm exercises.

Bicycle Designs

Several different designs were developed over the last thirty years. They can be distinguished basically between stationary and movable designs. Stationary designs can be further distinguished in ergometers and trainers. An ergometer (Figure 8) is an independent device which does not need further tools or additional devices for usage. A trainer (Figure 9) provides the mechanics necessary for the training but does not supply a seat. For sitting the user's personal wheel chair is required. Moveable designs can also be divided into two groups. The first group are recumbent bicycles (Figure 10). Like stationary ergometers they supply all necessary parts for driving. The second group is a combination of the user´s own wheel chair and an additional mechanical system which is fixed to it (Figure 11). Both, stationary and mobile designs are available in two different versions. With one version only the legs can be trained, the second version combines leg training with training of the arms.

Figure 8 FES-ergometer for leg cycling only. (Therapeutic Alliances [18])

Figure 9 FES-trainer for leg and arm cycling. (Restorative Therapies [19])

Figure 10 FES assisted recumbent bicycle for leg cycling. (Hasomed [20])

Figure 11 FES assisted wheelchair-bicycle combination for leg and arm cycling (Berkel Bike [21])

Manufacturers

Five manufacturers are producing FES-bicycles currently. The oldest one is Therapeutic Alliances (USA) [18]. Therapeutic Alliances produce their own FES-ergometer since 1984 which is currently available in its third version. RECK-Technik GmbH & Co. KG (Germany) producing their own stationary trainer for leg cycling only [22]. The company Berkel Bike (Netherlands) has the largest range of products [21]. They are specialized on recumbent bicycles with combined leg and arm drive and provide pure recumbent bicycles as well as a wheelchair-bicycle combination. They also offer a stationary trainer for leg and arm movement. Restorative Therapies (USA) uses motor assisted trainer, from the company Medica Medizintechnik (Germany), in combination with their own stimulation equipment [19],[23]. They offer stationary trainers with either leg movement only or leg and arm movement. The company Hasomed (Germany) provides a trainer for the legs only as well as a recumbent bicycle, also only for the legs [20]. The mechanical components of the trainer are produced by Reck and Hasomed applies their stimulation equipment. The recumbent bicycle is produced by the company Hase Bikes (Germany) [24]. The necessary adaptations are made by Hasomed and they use their stimulation equipment.

2.2.4 Selected Applications of Functional Electrical Stimulation for Paraplegic Persons

Already at the time of the Roman Empire naturally electrical sources were used to heal various pain conditions. Later at the end of the 18th and the beginning of the 19th century the invention of electrical machines to produce electrical impulses lead to the field of electrotherapeutics in the 19th century. By discovering that, it is possible to produce muscle contractions by a tetanic frequency of electrical impulses the field of electrogymnastics was born in the 19th century. From there on it lasts till the middle of the 20th century since the term FES was introduced. The first applications, around 1960, of FES were for grasping and for cardiac pacemaker. Since then FES was used in sports for additional training, as neuroprosthesis to restore impaired body functions and for rehabilitation [25]. Subsequently some selected examples for rehabilitation of the lower limps are explained.

FES-Rowing

Beside FESC, FES-Rowing (FESR) was developed to enhance cardiovascular fitness in people with SCI. An advantage of FESR is that the muscles of the arms and the upper body are voluntary activated additional to the artificial involuntary movement of the lower limps. This leads to an increase in VO2 uptake in comparison to exercises with either only movement of the arms or only movement of the legs [14].

For FESR stationary rowing ergometers are used. The ergometer main components are a moveable seat which slides along a rail, a foot fixation as support to produce the leg driving force, a braked flywheel to produce the resistance and a handle which is attached to the flywheel by a rope. Additional to these components ergometers used for FESR have to have foot fixations which allow also the fixation of the shank. The seat used for FESR has to be adapted to meet the requirements necessary for people with SCI. Therefore it has to take care that the seat has no regions with pressure peaks. A bucket seat with belts has to be used for fixation and stabilization of the trunk. A specially developed indoor rowing machine includes a seat brake which keeps the seat in position at the end of the driving phase. This can be necessary in case that the legs are not able to produce enough force to stay in this position.

For a rowing cycle the alternating stimulation of the musculus quadriceps femoris (MQF) and musculus biceps femoris (MBF) is necessary. A rowing cycle can be divided in following fife phases. The first phase is called the Catch-Phase. In this phase the seat is in frontal position, the legs are bend and the arms are stretched. In the second phase, the Drive-Phase, MQF of both legs is stimulated which produces a driving force. This leads to a backward movement of the seat. In the third, the Handle-Pull-Phase, the arms are pulled to the trunk while MQF, of both legs, is still stimulated to keep the seat in backward position. The fourth phase, the Finish-Phase, is achieved when the arms are pulled as close as possible to the trunk. Both MQF are still stimulated. In the Recovery-Phase MBF of both legs are stimulated and the stimulation of MQF stops. Additional

the arms are stretched again. This leads to a forward movement of the seat until the start position is reached [14],[26].

FES-Standing and Walking

In 1963 the first application of FES with a paraplegic person was reported. Erect standing was achieved for few minutes [27]. In 1973 a research group reported about experiments with patients about FES assisted lifting. They found out, that it is possible to lift a patient's body from sitting position with FES. Further, they summarized that FES is a more functional substitution for the orthopedical devices in those days and predicted FES as best hope for improved locomotion of paraplegic persons [28]. This led to the expectation that ambulation problems of paraplegic persons can be solved in near future. Further studies revealed that the potential of FES to restore ambulation is limited by high energy consumption, rapid muscle fatigue and very low ambulation velocities [29]. Nevertheless, in 1980 bipedal walking of a paraplegic patient was described for the first time [27]. In the eighties and at the beginning of the nineties research groups presented different approaches to bypass this problems. One approach was the combination of FES with leg-ortheses. Another was to implant electrodes surgically. None of these approaches was available as product on the market. The only system, achieving product stage was Parastep (Sigmedic/USA) [30]. It is actually the only available system for FES-waking available on the market. The system is distributed by the company Therapeutic Alliances. All these studies have in common that only patients with innervated muscles were chosen for the test trails.

In 2001 a European project named RISE was initiated with the aim to develop a rehabilitation method for persons with denervated muscles. As part of the project it was possible to prove that even with denervated muscles it is possible to stand-up. Three out of twenty patients were also able to walk for a short distance [31].

The Parastep system consists of a battery powered microprocessor controlled unit with six stimulation channels (Figure 13). The stimulation frequency is 24 Hz at a pulse with of 150 µs and with an amplitude range from 0-300 mA. A standard walker (Figure 12) is used for support. The walker includes buttons for controlling the stimulator. Two different functions are available, the walk function and a stand-sit function. For stimulation surface electrodes are used to stimulate the MQF and MBF. For triggering the stepping action the common peroneal nerve is stimulated. This activates a withdrawal reflex which is used to trigger the stepping action [29].

It is important to notice that the Parastep system is only designed as supplement to the wheel chair. The system is not capable to restore lost body functions for daily living. It can only be used as training device.

Figure 12 Parastep walker including switches (The picture is taken from [30])

Figure 13 Parastep stimulator (The picture is taken from [30])

Ancillary it has to be mentioned that it is not possible to start with one of the rehabilitation methods mentioned above. This is due to, that in many cases time periods up to several years are past between the start of the rehabilitation program and the event which lead to the SCI. This leads to partially severe atrophied muscle tissue. Therefore a training program to restore the muscle functionality and muscle mass has to be completed before.

3 Concept, Material and Methods

3.1 The Bicycle

The used bicycle called “Reha-Funtrike” from the company “OVG Marketing und Vertriebs GmbH” is a recumbent bicycle where the patient is able to sit in an upright position. It has three wheels, orientated in a triangle shape. Two wheels on the back side of the bicycle and one at the front. The steering of the bicycle takes place at the frontal wheel. The drive happens at the backward wheels, whereby only the left backward wheel, in driving direction, is driven by muscle power. The backward wheel on the right side can only be driven with the implemented electric motor. The motor is only intended as support, to assure that it is only used while driving by muscle force an inductive sensor is placed at the middle chain wheel to check the revolution of the wheel. Therefore it is only possible to use the engine while the bicycle is moving. The engine speed can be regulated via a turning handle at the right handlebar. A four speed gear box is available with the gear lever also at the right side of the handlebar. The speciality of the bike is, that it provides two different drivetrain possibilities. The first one is to drive the cycle, as usual for a bicycle, via pedalling, called “pedalling mode” (p-mode). The second one is to drive it with a linear movement, similar to a rowing movement here called ed-

mode. Therefore the pedal crank has to be fixated and the pedals have to be orientated in the same direction. The drive chain has to be clamped to the seat. This can easily be done with a lever placed underneath the seat. To allow the seat to slide along the guide rail (Figure 14), which is mounted on the bicycle frame, a second lever which fixes the seat has to be released. On this way the drive chain moves backward and forward according to the seat movement. To prevent a change in drive orientation while the seat moves in forward direction, the drive wheel was designed as a free-wheel.

Figure 14 Picture of the bicycle in extension drive mode with the seat in end position (left side) and forward position (right side) (Pictures taken from [32])

Bicycle Data:

Length, width, height [mm]	1985, 780, 1065
Weight (including battery) [kg]	48,2 (53,2)
Wheel dimension (ETRO)	28-406
Gear change	4-speed Shimano Nexus
Brakes front/back	Front: V-Break ShimanoRX100 Back: Rollerbrake Shimano Nexus
Accumulator Data: Nominal voltage [V] Capacity [mAh]	30 NiCd cells 36 5000
Electromotor Data: Nominal voltage [V] Type	Wheel hub motor 36 DC Electrically commutated

Table 2 Technical data of the Reha-Funtrike

3.2 System Concept

3.2.1 Safety

Injury

It has to take care that the patient does not get injured by the system. Neither while the stimulation process is active and works properly nor in case of a system malfunction.

Biomechanical safety

Since the bicycle is not intended to be used as FES-bicycle originally, it has to be taken care that biomechanical safety measures are considered. Particular joints and ligaments have to be prevented from to high loads. It is also important to avoid hyperextension of the knee.

Electric safety

Voluntary muscle contractions, of the locomotion system, as well as involuntary muscle contractions, like cardiac activity, are governed by electro chemical processes. Therefore they can be influenced by artificial current flow from an external source. Potential hazards, concerning low voltage, are ventricular fibrillation and apnoea, if the contact with the electrical circuit happens in the thoracic region. In all parts of the human body involuntarily muscle contraction can occur. This involuntarily muscle contractions can lead to secondary accidents.

To avoid such accidents it is important to know at which threshold currents start to be harmful for the human body. These thresholds have been found by experiments and are displayed in Figure 15. The first region is named DC-1 and is limited by the line “a” which displays the perceptibility limit. Therefore in DC-1 a human is not able to feel the current flow. Furthermore, current flow in this region does not lead to injuries. The second region DC-2 is limited by line “b” which marks the release threshold. Underneath this threshold it possible to voluntary release an object which carries current although involuntary muscle contraction occurs. For durations underneath 2 seconds, line “b” also marks the region where no permanent damages occur. Line “c” limits the third region DC-3 and marks the threshold until which the risk of ventricular fibrillation is acceptable. In DC-3 strong involuntary muscle contractions occur, they can lead to permanent or temporary injuries. In area DC-4, additional to the symptoms described for areas DC-1, DC-2 and DC-3, ventricular defibrillation is possible. The probability increases with raising contact current value and current flow duration.

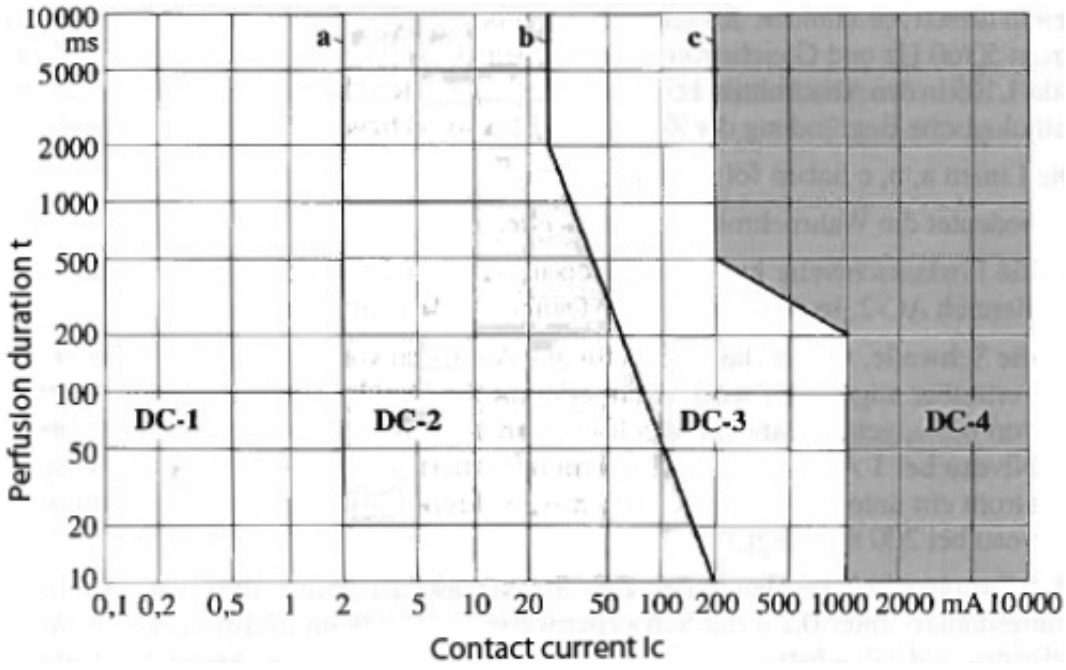

Figure 15 Simplified Time-Current-Regions DC-1, DC-2, DC-3 and DC-4 for electrophysiological effects displayed for direct current. (Figure adapted from [33])

Since the current flow varies depending on the body impedance and the voltage it is therefore complex to determine for practical purposes. The body impedance varies in a known range and the most safety hazards are voltage sources. Therefore voltage is used as safety criteria instead of current.

Experiments were made to determine a voltage threshold, at which no harm can occur. Four different current pathways and three different contact conditions were observed, at a voltage of 60V/50Hz AC. Results showed that for dry and wet contact conditions no risk of getting harmed exists. Even for the adverse case of contact between the hands and the trunk. Only for salty-wet contact conditions injuries can happen (Figure 16).

Current pathway	Hand - Hand (Hand-Foot)	Hand-Feed	Hands-Feed	Hands-Torso
Dry contact surfaces				
Z_B (50 %) (Ω)	11 080	8 310	5 540	2 770
I_B (mA)	5,5	7	11	22
Wet contact surfaces				
Z_B (50 %) (Ω)	6 870	5 150	3 435	1 717,5
I_B (mA)	8,5	11,5	17,5	35
Contact surfaces wet and salty				
Z_B (50 %) (Ω)	2 375	1 780	1 187,5	593,75
I_B (mA)	25	34	50	100

Figure 16 Body impedance and resulting contact currents. The Body impedance $Z_b(50\%)$ was measured at 50Hz alternating current and 60V contact voltage for different current pathways. The resulting contact currents I_b were measured for contact conditions dry, wet and salty-wet at medium sized contact surfaces. (Figure adapted from [33])

Since the body impedance is higher for direct voltage than for alternating voltage at regions < 200V, (Figure 17) this results are also valid for direct current. Therefore a contact voltage of 60V/DC can be assumed as safe. Contact voltage is defined as the voltage which occurs at a human body if conductive parts with different electrical potentials are touched [33].

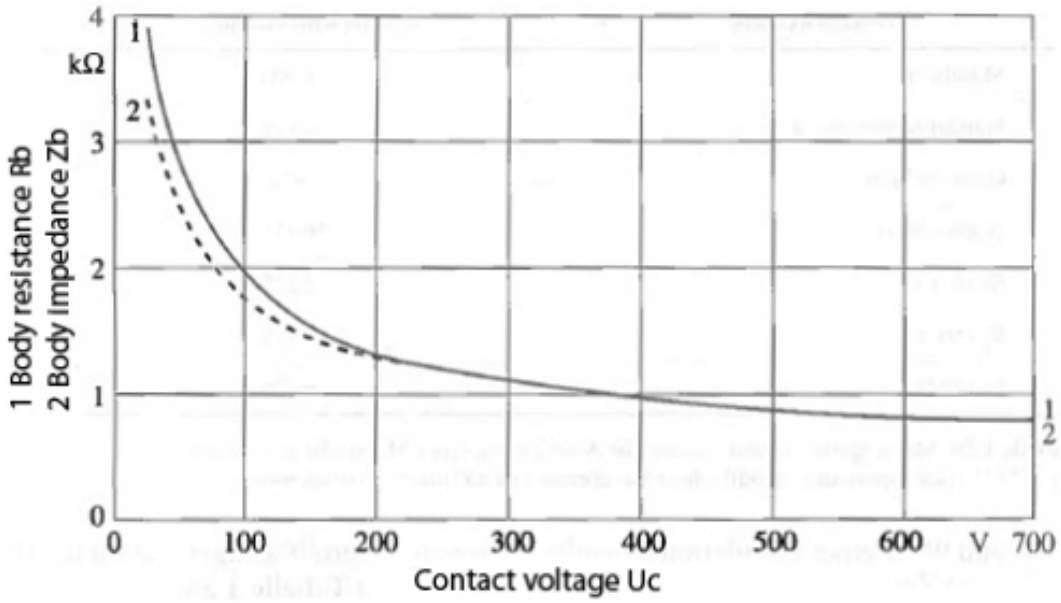

Figure 17 Body resistance at dry contact conditions. Body resistance R_b, for direct current and body impedance Z_b, for alternating current. At 50/60Hz, for a 50% population of living people, at the contact voltage U_C region from 25V to 700V. At dry contact conditions, large contact areas and hand-hand current pathway (Figure adapted from [33])

A further danger which has to be considered, concerning electro stimulation, is the electrolytic stress in the tissue around and underneath the stimulation electrodes. Electrolysis happens at the border between the stimulation electrodes and the human skin. In case of surface electrodes this leads to production of sodium hydroxide solution underneath the cathode while underneath the stimulation electrode muriatic acid is produced. Both, sodium hydroxide solution and muriatic acid lead to chemical burn of the skin and the tissue.

To avoid electrolysis it is to use biphasic pulse waves instead of direct current stimulation. The negative and the positive phase of the stimulation impulse have to have the same amplitude and phase duration to provide charge balancing. Despite the biphasic pulse wave it is important to limit the current density at the electrode contact surface. The current density is not allowed to exceed 2.0mA/cm². Above this threshold there is a risk of cauterization of the area underneath the electrodes [34].

Furthermore it has also to be guaranteed that the stimulation process can be aborted immediately in case of malfunction.

Stability

The whole system must be stable by itself and it must be impossible to overturn while driving or when the test person takes place on the bicycle.

3.2.2 Requirements

Functional Requirements

Drive Modes: The bicycle can be driven by two different modes (ed-mode, p-mode). It has to be guaranteed that both modes can be used by a person with paraplegia.

Bicycle Alteration: The mechanical and electrical alteration of the bicycle from one drive mode to the other should be easy and without use of many tools.

Stimulation: The stimulation triggering and the stimulation process have to be intuitive and easy to handle by the test person.

General Requirements

Bicycle Modifications: All modifications, which are necessary for this investigation, have to be non-destructive. This means that all parts added to the bicycle have to be removable and are not allowed to let traces as holes, slots or other in mechanical design usually used fixation elements.

Stimulator: The stimulator for this investigation has to be suitable for the stimulation of denervated muscles. Therefore it has to be able to generate longer impulses as well as to produce higher energy per pulse. The experimental four channel stimulator provided by the Center for Medical Physics and Biomedical Engineering is capable to fulfil these requirements and is used for this investigation. Since the stimulator is not designed for this investigation it needs to be adapted to work properly in combination with the controller.

Bicycle Service: Due to its age and previous investigations the bicycle needs to be repaired, maintained and restored to its originally state.

3.2.3 System Draft

The stability of the bicycle, while standing and driving, is already satisfying. A handbrake for fixation of the bicycle, while the test person is taking place on it, exists. Therefore there is no need to make alterations to the bicycles geometry or the fixation mechanism. From former investigations a tray on the back of the bicycle is available which can be used to carry the stimulator and the controller while driving with the bicycle. The stimulator button is placed on the handlebar. The voltage supply for the stimulator, the controller and the stimulator button is provided by the stimulators battery. To provide an opportunity to stop the stimulation process immediately, in case of an emergency, an emergency button is placed on the handlebar.

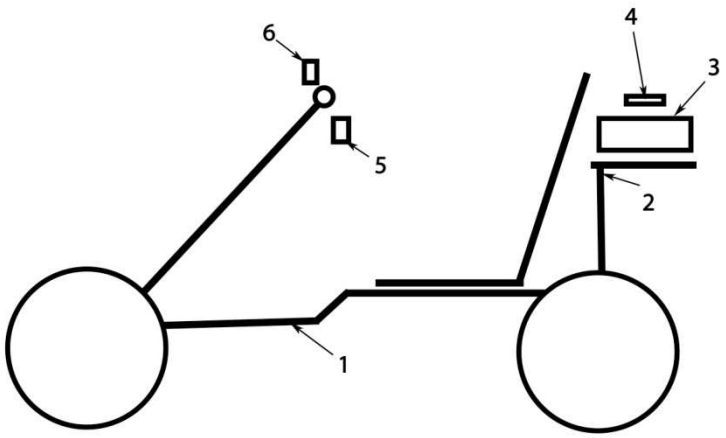

Figure 18 System Draft of the bicycle displaying the bicycle (1), the tray (2), the stimulator (3), the controller (4), the stimulator button (5) and the emergency button (6)

User Controller Interface Concept

A control panel (A), for the implemented electric engine, is part of the bicycle and needed to be fixated to it. The control panel possesses a clamp fixation but this fixation does not fit to the handlebar of the bicycle. To fulfill the requirement of doing no irreversible alterations to the bicycle a clamp able fixation was chosen. Because of the size of the control panel only a placement in the middle of the handlebar is possible. Also the length of the existing cables, leading to the control panel, had to be considered. Further limitations are , that it is not allowed to interfere with the driver's legs or to mask the drivers view while driving. Furthermore it has to take care that it does not interfere while taking place onto the bicycle. Thus these considerations the control panel mounting (CPM) (B) was placed on a lower position, in the middle of the handlebar, to enable a good overview on the control panel without masking the drivers view.

The position of the stimulator button casing needs to be good accessible by one of the test person's hands but is not allowed to interfere with the movement of the legs. It has also to be taken into account that the stimulation button has to be reached quickly and without interference, through other parts, by one of the fingers or the thumb. Since the driver is sitting in a low position on which he can only look close above the handlebar, in the final design, the casing (C) was placed subsequently to the left handle grip. The test person's left hand side had to be chosen since on the right side already the shifter for the gear box (E) is installed. Furthermore the activation through the thumb was chosen since this enables the possibility to use a shorter lever, which does not interfere with the driver´s legs.

The most important requirement concerning the position of the emergency button (D) was, that the button has to be accessible quickly and without interference, in case of an emergency. The best position therefore is near the handlebars handle since the test person's hands are already placed there. That is why a position slightly shifted from the

middle of the handlebar was chosen. The emergency button can be shifted along the connection pipe, in the middle of the handlebar, to adapt its position if a left-handed person drives the bicycle.

To give further information's about the driving condition and the stimulation process a bicycle computer (F) and a display (G) were attached to the handlebar (Figure 19).

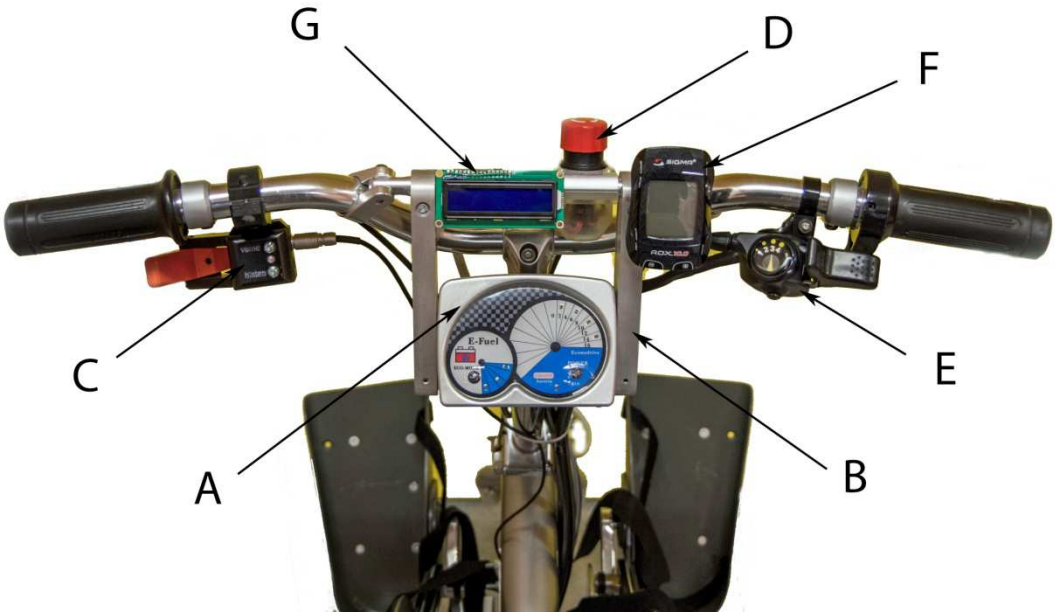

Figure 19 User controller interface. Position of the control panel (A), the control panel mounting (B), the stimulation button casing (C), the emergency button casing (D), the shifter of the gear box (E), the bicycle computer and the display (G) attached to the bicycles handlebar

Stimulator Button Casing Concept

The stimulation is voluntary triggered by the patient through the stimulation button. Therefore the design of the stimulation button casing obtains an important role in the design concept.

For better sensory feedback, while pressing the stimulator button, and therefore a more reliable stimulation by the test person the button should have a defined activation point. To increase the sensation of the activation point the leverage ratio needs to be designed that the needed activation force is slightly increased. To fulfil these requirements the button is placed on the back of the stimulator casing and is activated through a lever which is moved by the thumb.

For a better haptic sensation the lever of the stimulation button casing is slightly curved and all edges are rounded.

To provide additional feedback for the driver about the ongoing stimulation process light emitting diodes (LEDs) are implemented on the frontal plane of the casing. Two green LEDs, displaying the end positions of the seat, while using the ed-mode and one red LED to display an active stimulation process used in ed- and p-mode.

Stimulation Button - Leverage Ratio Calculation

The leverage ratio can be calculated outgoing from the equilibrium of moments with:

$$F_d * y = F_s * x$$

Solving the equation for F_s leads to:

$$F_d = F_s * \frac{x}{y}$$

With $x = 39mm$ and $y = 25mm$ follows:

$$F_d = 1{,}6 * F_s$$

This leads to a one and a half time higher needed activation force for the thumb and therefore to an increased sensory feedback.

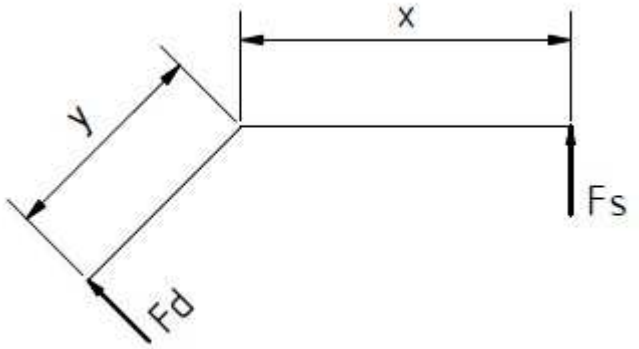

Figure 20 Stimulation lever force relationships. Sketch of the stimulation lever with the needed activation force (Fd), produced by the thumb, and the resulting force (Fs) acting on the stimulator casing button.

Electric Safety Concept

The electric engine of the bicycle is powered by a 36V DC accumulator. A 12V DC accumulator powers the stimulator, which also supplies the power for the controller. The controller transforms the received 12V DC to 5V DC for the angular encoder and to 3,3V DC for the limit switches and the stimulation button casing. Since none of these voltages exceeds 60V DC no particular precautions are necessary concerning the electric safety.

Voltages higher than 60V DC and 25V AC are only produced within the stimulator which has to be closed therefore. Alternating voltage higher than 25V appears at the stimulation electrodes. But this is wanted and necessary for transcutaneous electrical stimulation. Therefore the operator who is monitoring the stimulation process has to

take care that no unintended contact to the electrodes can happen while the stimulation process is active.

To avoid a short circuit or unintended contact with the electric circuit all cables have to be sealed, laid properly and provided with connectors. All housings of electrical devices have to be covered that their insides can't be touched accidently.

To fulfill the requirement to stop the stimulation process immediately in case of an emergency or if intended by the driver's choice an emergency button is necessary. The further tasks of the emergency button are, on the one hand to stop the stimulation process and on the other hand to disconnect the whole system from the voltage source. Therefore the emergency button is positioned direct after the stimulators battery, in the electric circuit. Thus the controller and the stimulator are without voltage supply when the emergency button is pressed.

The casing of the emergency button should be as small as possible to fit on the handlebar without interfering. But it has to be stable to withstand higher forces if the emergency button is pressed rapidly and strong in case of an emergency. A clamp was chosen for fixation. The rest of the casing design was adapted to the shape of the emergency switch and the required space for the connectors leading to the controller and the stimulator.

Stimulator Adaption Concept

The used four channel stimulator needs to be adapted and overhauled. Because of its age the battery of the stimulator needs to be replaced. The original used battery is a custom build model. To reduce costs a 10 cells, 4200mAh accumulator with a nominal voltage of 12V (Sub C/Conrad Electronic SE) (B) is used for replacement. Because of the bigger size of the new battery its position needs to be changed and therefore the fixation mechanism. The task of the fixation mechanism (A) is to keep the battery on its position while the stimulator is moved. Unintended movement of the battery could lead to a short circuit. The only existing fixation opportunities without need to drill through the stimulator housing are holes on the inner bottom of the stimulator. Therefore hook like clamps, called battery clamp (BC), were designed which are fixed to the stimulator housing (Figure 21).

For the control of the stimulator a new connector plug has to be implemented, since the original used type is not available anymore. Therefore a new 5 pin connector was placed underneath the old one and the control cables were also attached to the new connector.

Regarding the electrical concept the whole system is powered by the stimulators battery. Therefore a 3 pin connector was implemented on the backside of the stimulator housing therewith the controller is connected across the emergency switch.

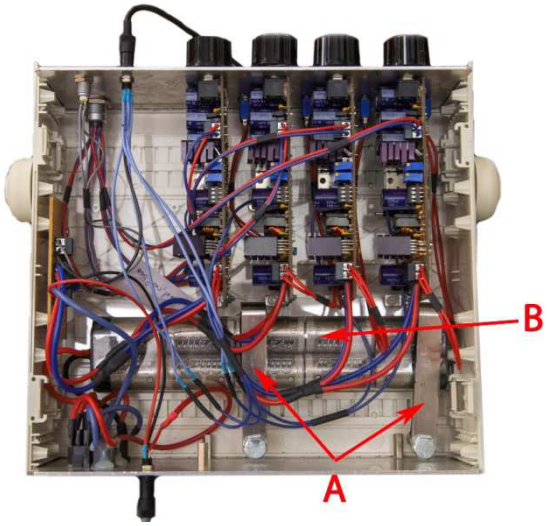

Figure 21 Position of the BC (A) and the battery (B) inside of the stimulator

Seat Position System Concept

To control the stimulation process and as visual feedback for the driver the position of the seat must be known. There was a choice of three different systems, a cable actuated position sensor, a magnetic tape sensor or a limit switch. At the final design two limit switches where chosen, for detecting only the end position of the seat, since there is no need to know its exact position. For controlling and as visual feedback it is sufficient to know the end positions of the seat. Other reasons for choosing the limit switch version are that a limit switch is small in size, the cheapest option and more easy to implement in the controller program than the actuated position sensor or the magnetic tape sensor.

The switches needed to be placed in a position where they do not collide with the moving seat. The most fitting place is the space among the bicycle frame, the sliding rails and the seat (Figure 22). To adapt the limit switch position to the body height of different drivers, the position of the limit switches needs to be adjustable in direction of the seat movement.

This leads to the final design of a rail with long slots on both ends where the limit switches are mounted. The rail is fixed to the bicycle frame with the same screws as the sliding rail to avoid destructive changes to the bicycle. As counterpart, for a defined activation of the limit switches, a fence is mounted to the bottom of the seat (Figure 23). The fence has a chamfer on both sides, to allow a smooth contact with the limit switches. To fixate the fence to the seat, the screws, which are used to mount the seat frame to the sliding frame, are used.

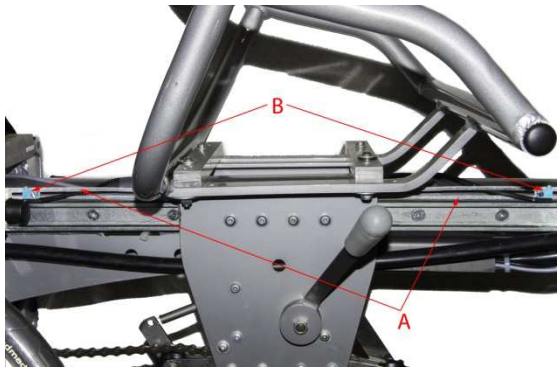

Figure 22 Position of the Limit Switch Mounting (A) including the Limit Switches (B)

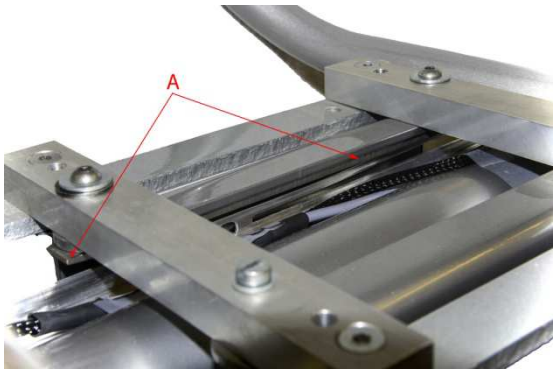

Figure 23 Placement of the Limit Switch Fence (A)

Concept of Mechanical Safety Measures

An important point of the systems concept is the safety of the test person. Since the bone density and the strength of the ligaments is strongly decreased at persons with paraplegia [35] it has to take care that no fractures can happen at the legs or the knees.

The first mechanical safety measure taken is that the wheel, which is driven by muscle force, is designed as freewheel. This assures that the test persons feed stop turning when the stimulation process is stopped, even when the bicycle is moving, in the p-mode. Without this measure the legs would be driven by the bicycles mass since they are directly linked to the drivetrain. This would lead to an uncontrolled movement of the legs and could easily lead to injuries of the knee or the legs. The used bicycle already fulfils this requirement.

The second safety measure is an adjustable end stop. The bicycle should be usable for persons with different heights. A taller person can use the whole length of the sliding rails without hyper extending its knee. A smaller persons knee would hyper extend before the end stop of the sliding rails is reached. This could lead to knee injuries, especially at paraplegic persons. Therefore a moveable ends stop needed to be designed, to limit the guide rails length. Since it has not been allowed to make any destructive changes to the bicycle a clamp design, with a quick release, was chosen. The end stop buffer, from the original design, can be mounted on the end stop clamp (ESC). The ESC is placed in the rails of the seat sleds guide rails (A). So it is guided by them and can be shifted along the guide rails (Figure 24).

Both pedals are able to rotate around their fixation shafts. This is a generally welcome behaviour, but it is undesirable at the end of the movement at ed-mode, when the seat has reached the backward end stop. Since when the seat is reaching the end stop it could happen that by a failure in the control program or the sensory equipment the stimulation does not stop and then the knee gets hyper extended. This can lead to an injury of the driver’s knee. One possibility to avoid this would be to reduce the possible travel of the

seat but this would lead to a reduced usable drive length of the seat. Therefore a mechanical pedal end stop (PES), which limits the angular movement, was designed (Figure 25). The guiding rail of the end stop is mounted to the pedals of the bicycle. The cylindrical end stop itself is mounted onto the rail and can be moved along the rail (A). Thus the rotation around the pedals axis can be limited. But it has to take care that this end stop is only used additional to the ESC because using only the rotational end stop could also lead to an injury of the knee or pressure sores at the region of musculus gastrocnemius.

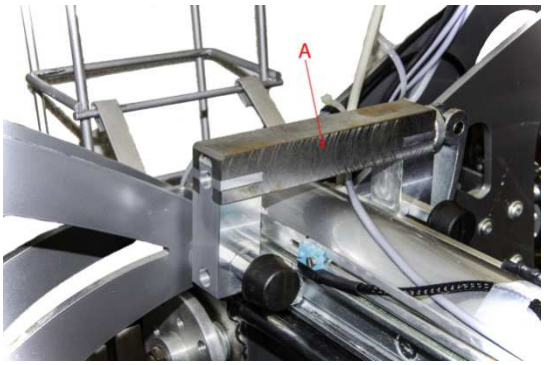

Figure 24 ESC (A), clamped onto the guide rails, in bottom position

Figure 25 Position of the PES (A) on the left side, in driving direction, in end position.

Controller Concept

The basic task of the controller is to receive sensor signals from the bicycle and control signals from the stimulation button. Then he has to send proper signals to the stimulator according to the actual situation. The sensors that are used are an angular encoder and two limit switches. A further task of the controller is to control a display and three LED´s as an optical feedback for the driver. Regarding to the electrical concept the controller possesses no own voltage source and is powered by the battery of the stimulator. Therefore the stimulator needs six connectors. As microcontroller a Fubarino Mini board was chosen because it is easy to use, cheap in price and it is based on the Arduino platform. Therefore it is like Arduino an open platform microcontroller. The Fubarion possesses two connectors for programming and energy supply, therefore the controller housing needs two additional connectors. The focus at designing the controller casing was to make it small in size and convenient to use. Therefore, the casing was produced by the institute’s 3D printer.

Necessary adaptations for the ed-Mode

For the extension drive, both pedal cranks needs to be aligned in the same direction. Therefore it is necessary to dismantle one of the pedal cranks and fix it in a 180° twisted position. Furthermore, they have to be fixed in their position to afford a stable platform for the legs. The bicycle already provided holes in the chain-guard and through the bicycle frame. The most convenient way was to use these holes for the fixation of the pedals to the bicycle frame (Figure 26). Therefore a crank fixation (A) needed to be designed. Since the dismantling of the bold should be easy and quick to handle on one side of the bold a handscrew was used for fixation. On the other side a slot was milled, broad enough to use a coin as counterpart while fixing the handscrew.

Figure 26 Position of the Crank Fixation (A)

Necessary adaptations for the p-Mode

For a previous investigation, gears (B) which are driving an angular encoder (C), were placed on the bottom bracket shaft (BBC) (A) (Figure 27). Since therefore the shaft was too short, pedal cranks with a thinner socket were installed instead of the original ones. For this investigation the original pedal cranks are necessary to fixate the patient's legs with the pedal´s orthesis. Therefore, the BBC needed to be extended. Furthermore the gear mounted to the BBC was only attached without further fixation. This could lead to unreliable measurement of the encoder because of slip between the gear and the BBC. Therefore a radial hole was drilled with a thread to fixate the gear with a setscrew.

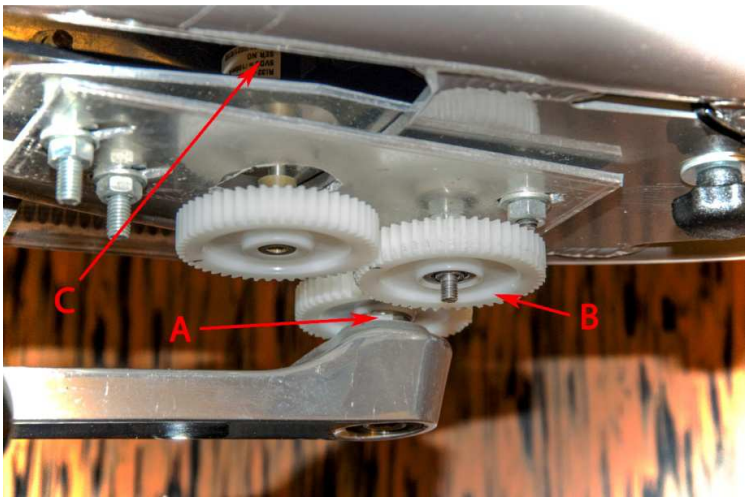

Figure 27 Position of the BBS (A), the installed gears (B) and the encoder (C)

For the pedalling movement an additional drive chain has to be mounted. This chain needs to be tensioned to provide a reliable force transmission without sliding. The existing chain tensioner is not able to fulfil this condition and allows the chain also to jump off the gear. Therefore, a new chain tensioner needed to be designed. To reduce the design effort an existing tensioner model (XLC/CR-A03) was chosen. Due to the required position it was not possible to fix the tesnioner directly to the bicycle frame. Therefore, an adapter had to be designed. The main objectives by designing the adapter where to prevent sufficient preloading to tension the chain, provide a possibility to slightly vary the preloading force to avoid a too high chain tension, keep the chain in line with the gear wheels and to be as small as possible to avoid a collision with surrounding parts. Furthermore existing fixation elements on the bicycle frame have to be used. The bicycle frame has a through-hole with a square shape on one side. This square shaped recess was fitting for a carriage bolt which was used for the fixation of the chain tensioner adapter (CTA) (Figure 28).

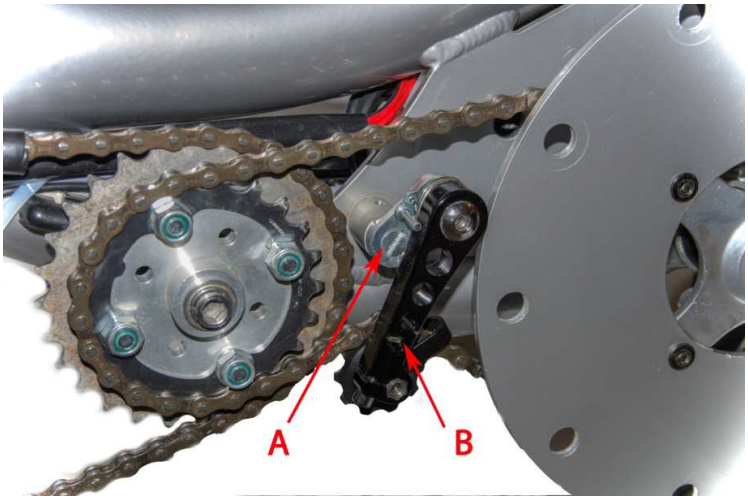

Figure 28 Position of the CTA (A) with the chain tensioner (B)

3.2.4 Resulting Concept

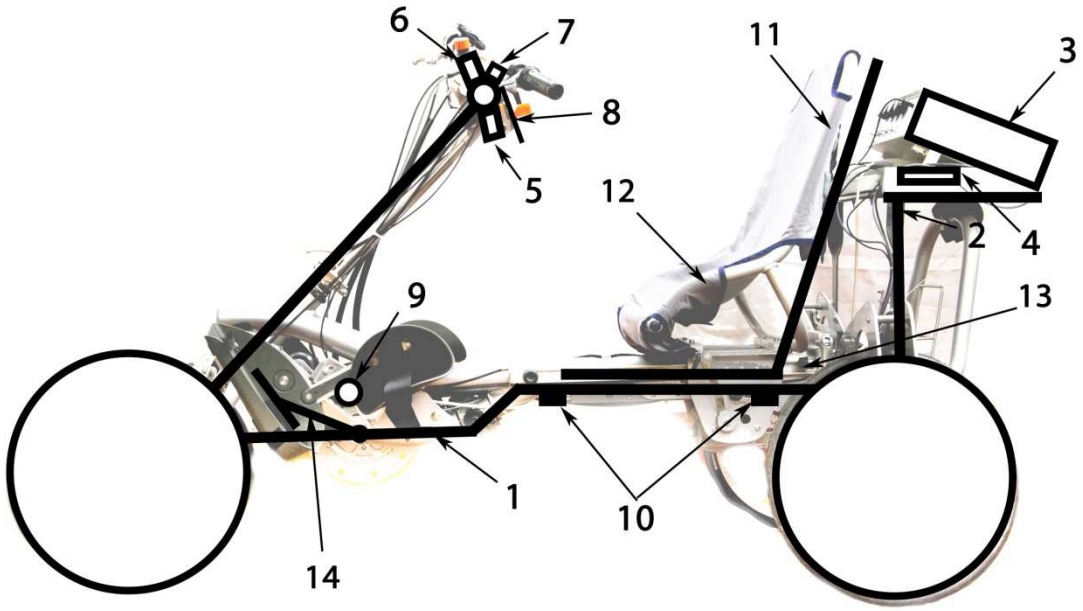

Figure 29 Sketch of the resulting system concept with the bicycle (1), the tray (2) for carrying the stimulator (3) and the controller (4). As sensory equipment the bicycle computer (7), the angular encoder (9) and the limit switches (10) are used. For observation of the stimulation process and the driving conditions the bicycle computer (7), the control panel, including the LCD (8) and the stimulation button (5) are used. To interrupt the stimulation process the emergency button (6) was implemented. The stimulation process is triggered by the stimulation button (5). To diminish the general injury risk belts (11) and a seat padding (12) were implemented. The hyperextension of the knee is avoided by the end stop clamp (13) and the pedal end stop (14).

3.3 Equipment

3.3.1 Stimulation Equipment

Stimulator

The stimulator used for this investigation is a four channel voltage controlled stimulator and has been adapted to the studies aim. The desired voltage amplitude can be set separately for each channel with four potentiometers in a range between ±2-75V. To limit the output current a voltage regulator, which is realized by controlling the voltage drop across an adjustable shunt, is used. The overall pulse width can be modified from 1 to 70 ms by binary coded switches. Whereas the overall pulse width includes the negative and the positive pulse phase. The duration between consecutive pulses can be set in a range from 1 to 250 ms. By combination of the pulse width and the delay between two

consecutive pulses the frequency can be adjusted in a range of 3-500 Hz. Every single channel can be turned on and off by a separate switch. The stimulation is triggered by an external on-off switch [36].

A voltage controlled stimulator was used since this stimulation type reduces the danger of skin burns if an electrode is not applied properly. This is even more important when stimulating persons with denervated muscles since therefore higher energy and longer impulses are needed.

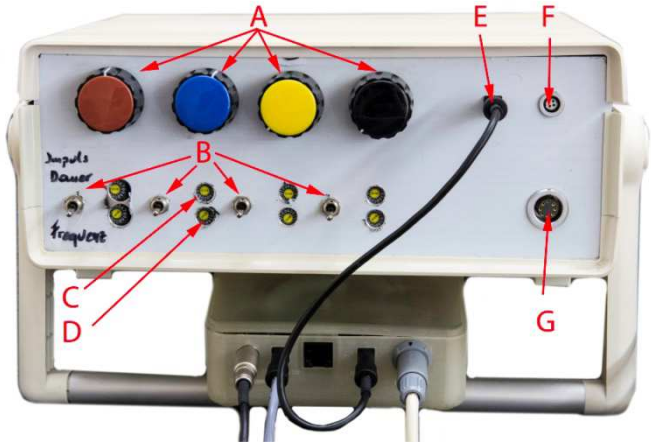

Figure 30 Image of the stimulator front panel with the connected controller underneath. On the top side of the panel the four potentiometers (A) for setting the voltage amplitude are mounted. Directly underneath, for every single channel, on-off switches (B) are placed. At the right side of the on-off switches the binary coded switches for setting the impulse duration (C) and the delay between the impulses (D) can be found. The new trigger input (E), implemented for this investigation, is placed next to the potentiometers near the original trigger input (F). The output connector for the stimulation electrodes (G) is placed at the right bottom corner.

Stimulator Data:

Supply Voltage [V] (Accumulator)	12 DC
Accumulator Capacity [mAh]	4200
Stimulation Voltage Range [V]	±2-75
Stimulation Frequency [Hz]	3-500
Pulse With [ms] (biphasic)	1-70
Interruption between impulse [ms]	1-250

Table 3 Technical data of the used stimulator

Controller

The controller was designed specifically for this investigation. As core of the controller a Fubarino Mini V15 board with an implemented PIC32 microcontroller is implemented. With the controller it is possible to control four stimulation channels separately.

The controller has two sensory inputs, one three pin connector for the limit switches and one six pin connector for the encoder. A further six pin connector is implemented for the stimulator button input. As output, for the control signals, a five pin connector is implemented. For the power supply a four pin connector is installed. As additional voltage supply while programming the microcontroller, a recess is made on the back of the casing, to have access to the microcontrollers USB connector. This is needed when the controller is not connected to the power supply of the stimulator. On the front side of the casing a RJ11 connector is implemented for programming. All connectors are labelled and have different forms to avoid unintended wrong connection of cables.

Further details concerning the used components are given in chapter “4 - Bicycle Modifications”. A circuit diagram can be found in the appendix.

Controller Data:

Dimensions [mm]	120x90x44
Supply Voltage [V]	9 – 18 DC

Table 4 Technical data of the controller

Electrodes

For transcutanious electrical stimulation surface electrodes are used. There are two possible types of surface electrodes which are suitable for this investigation, self-adhesive electrodes and surface safety electrodes.

Self-adhesive electrodes (Figure 31) are built in a multi layers configuration. The upper side consists of a non conductive layer, to avoid getting in contact with the current circuit involuntarily. A conductive layer with an imbedded wiring, for connection to the stimulator, is attached to the non conductive layer. Nowadays carbon is the most often used material for the conductive layer. A hydro gel layer with relative high peel strength and a low resistance is applied next to the conductive layer followed by the skin contacting hydro gel layer which has also a low resistance. To remove the electrode easier the skin contact layer has a relatively low peel of strength.

Safety electrodes (Figure 32) consist of two layers. The conductive layer is made of polyurethane loaded with electrical conductive particles. To insulate the conductive layer a silicone layer surrounds the conductive layer on all sides except the skin contact side. On the upper side connection holes are drilled, at which the stimulator cable can be connected to the electrodes. As contact medium between the conductive layer and the skin, electrode gel or a wet sponge can be used. The special feature of the safety electrodes is that the edges of the conductive layer are surrounded by a thick silicone bead.

The bead unloads the edge-skin contact and decreases therefore the current density in this region. Another advantage is that the bead avoids loss of contact medium and therefore skin burns over the conductive surface and at the electrode edges.

Figure 31 Picture of self adhesive electrodes for transcutaneous electric stimulation (Taken from [37])

Figure 32 Safety electrodes with conductive layer pointing upward. On this picture electrode gel is used as conductive medium (Taken from [34])

3.3.2 Sensory and Measurement Equipment

Limit Switches

Limit switches are used for registering and displaying the seat end positions in ed-mode. Two, single pole single throw-normally open (SPST-NO), stroke switches (ASQ10230/Panasonic) were used. With single pole single throw a simple on-off switch is meant. There is only one lever which is either connected to the other pole or not. If it is not connected to the other pole in default condition the switch is called normally open (Figure 33).The limit switch is triggered by a pin plunger which is mounted perpendicular to the upper side of the limit switch.

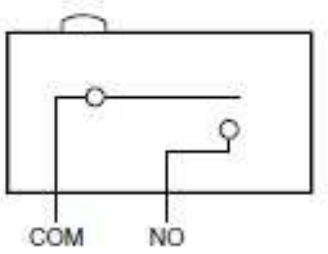

Figure 33 Circuit diagram of the SPST-NO switch in initial condition, with the schematic displayed pin plunger on the upper side (Taken from [38])

Limit Switch Data:

Max. Operating Force [N]	1,5
Max. Operating cycle rate [cycle per minute]	120
Rated Voltage [V]	5 – 30 DC
Rated Current [mA]	1 – 100 DC

Table 5 Technical data of the implemented limit switches

Bicycle Computer (BC)

A BC (ROX10.0GPS/SIGMA) is used for recording the bicycle velocity which is used to calculate the mean power while driving. The BC has plenty of different functions, which were not necessary to use in this investigation. Here only the used functions are explained.

The velocity is measured with the velocity sensor of the BC which is connected wireless to the computer. A magnet is fixed to a spoke of the bicycle rim and passes the sensor every revolution. This produces a signal which is transmitted to the computer. The perimeter of the bicycle wheel has to be programmed into the computer. In this way he computes the velocity according to the number of revolutions.

One of the biggest disadvantages of the computer is that the minimal sample rate for the velocity recording is 1 second. This leads to inaccuracy at the recorded velocity, specifically at lower velocities. A further limitation is that the lowest possible measurable velocity is 2,2 km/h. The recorded data are stored on the BC´s memory. With a sample rate of 1 sec., 8 hours and 12 minutes can be recorded and be stored as up to 50 different recordings.

The transmission of the recorded data from the BC to a computer is done with a USB cable and the companies own software, called Sigma Data Center 3.3. With the program it is possible to import, display and edit recorded data. Recorded data can also be exported to other programs.

The BC and the sensor can be fixed to the bicycle with rubber bands. The BC is powered by a non-replaceable lithium ions accumulator.

Selected BC Data:

Actual velocity [km/h]	2,2 – 199,8
Possible sample rate [sec.]	1,2,5,10,20,30
Possible recording duration [h, min]	8h 12min – 246h 24min
Power source	Lithium ion accumulator
Data transmission	Wireless

Table 6 Selected technical data of the BC

Incremental Angular Encoder

For controlling the stimulation timing in p-mode an incremental angular encoder (RI32/Hengstler) is used. The encoder is connected to the bottom bracket shaft through

gears. It possesses three output channels, called channel A, B and N. Channel A and B submitting a rectangular shaped signal with a phase shift of 90° between each other. By counting the edges of the signal the travelled angle can be determined. Therefore different possibilities are available. Counting only the rising edges of e.g. channel A is called single evaluation and provides the least angle resolution. Counting the rising and falling edges of channel A is called double evaluation and will double also the angular resolution. When the rising and falling edges of channel A and B are counted the evaluation is called quadruple evaluation. This will provide the highest resolution which is doubled again, regarding the double evaluation (Figure 34). With the method of the quadruple evaluation a resolution of 360° can be achieved for the used encoder type.

The channel N is sending one impulse with a rectangular shape every revolution and can therefore be used as reference point.

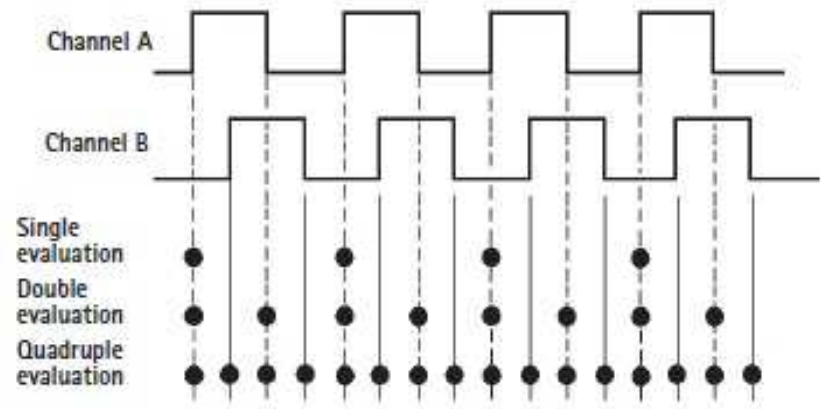

Figure 34 Possible evaluation methods of the angular encoder. Displayed are the output signals A (upper rectangular curve) and signal B (lower rectangular curve) and the resulting possible evaluation methods. Every black dot, in horizontal direction, means that the rising or falling edge is counted for evaluation [39].

Encoder Data:

Supply Voltage [V]	5 DC
Lines per revolution	360
Max. current consumption [mA]	40
Output signal shape	rectangular
Output signal amplitude [V]	5
Output signal current [mA]	30

Table 7 Selected technical data of the shaft encoder

Liquid Crystal Display (LCD)

The LCD (Hitachi/HD44780U) is used to give information about the stimulation process as well as to give instructions to increase the usability of the bicycle. During the developing process the display can also be used to give valuable sensory information. The LCD is able to display up to 8 characters per line whereby a maximum of two lines is possible. The display is illuminated to provide sufficient legibility even in situations with unfavourable light conditions.

LCD Data:

Supply Voltage [V]	2,7 – 5,5 DC
Lines	1 - 2
Characters per line	8
Possible character sizes	5x8 dots 5x10 dots

Table 8 Selected technical data of the LCD

3.4 Stimulation Concepts

For the two different drive modes, the ed-mode and the p-mode different stimulation concepts are necessary. The basic difference at these two modes is that for each mode different muscle groups have to be stimulated as well as different trigger timings are required. For the ed-mode only two stimulation channels are required and for the p-mode all four channels are necessary. Furthermore the ed-mode stimulation concept is easier to realise because it is only triggered by two limit switches. Whereas the sensory feedback for the p-mode has to be provided by an angular encoder because the stimulation has to takes place in angular regions.

3.4.1 Extension Drive Mode

The ed-mode is very similar to rowing movement. At the start position both legs are bent and the seat is in forward position. Then both legs extend while the seat moves backward. Therefore only the stimulation of the left and the right legs MQF is necessary. MQF is a muscle group positioned on the frontal side of the femur and consists of musculus vastus lateralis,musculus. vastus medialis, musculus rectus femoris.

The aim of the stimulation concept is to provide a fluent stimulation procedure as well as to interrupt the stimulation process when necessary. The stimulation process is started by pushing the stimulation trigger. Next the controller has to check the seat position. This is realized by observing the limit switch activation. If the backward limit

switch is activated, the seat is in backward position. Then, the controller has to wait till the forward limit switch is activated. If the forward limit switch is activated, the seat is in forward position and the legs are bent. Now the controller is allowed to activate stimulation channel 1 and 2 and to start the stimulation after a short time delay. If the stimulation trigger is still pressed, the stimulation is active till the backward limit switch is activated. When the backward limit switch is activated the stimulation process is stopped. Now the seat has to be moved in forward position, this is achieved by pulling with the test person's arms. Then again the forward limit switch is activated and if the stimulation button is still pressed the stimulation process starts after a small time delay. The time delay, after reaching the forward position, is implemented that the movement of the legs and the upper body is completed. On this way higher load to the knee joints, ligaments and bones of the legs are avoided by eliminating kinetic energies.

If the stimulation trigger is released, while the stimulation process is active, channel 1 and 2 are stopping the stimulation immediately. Is the stimulation trigger pushed again the controller has to check the position of the seat. When the forward limit switch was activated before, stimulation starts again. In case the backward limit switch was activated before, the controller has to wait till the forward limit switch is activated. Then again the stimulation is allowed to start.

In case the emergency button is pressed all channel have to stop stimulating immediately. When the emergency button is deactivated mechanically the stimulation trigger can be pressed again. But the controller has to wait till the forward limit switch is activated. Then again stimulation channel 1 and 2 are activated and after a small time delay the stimulation process starts (Figure 35).

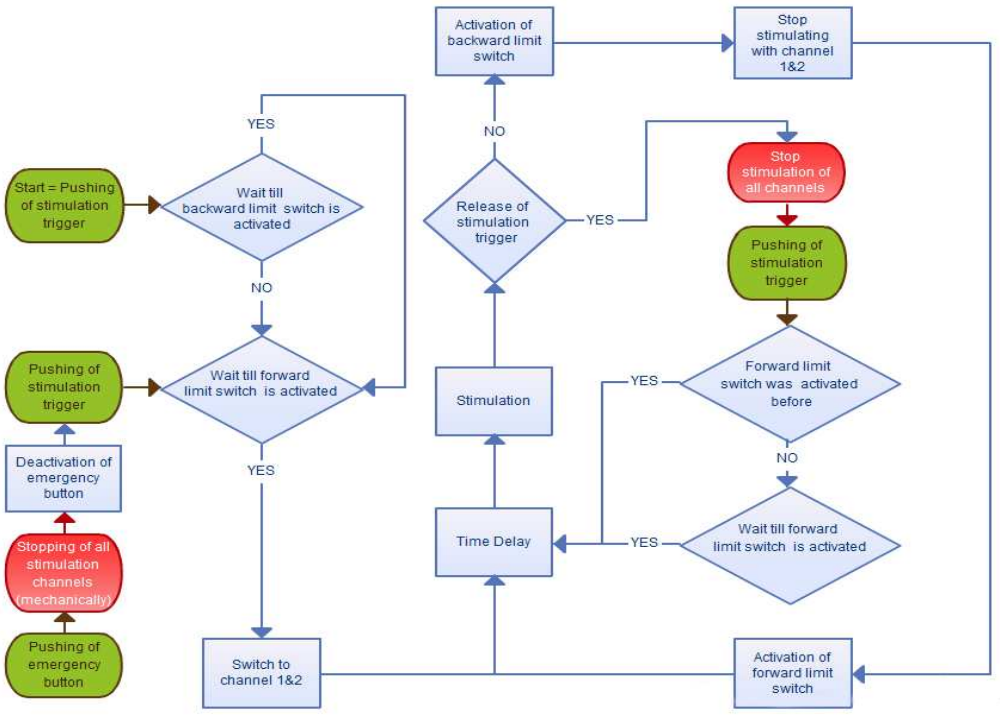

Figure 35 Flowchart, displaying the sequences and possibilities of the stimulation program for the ed-mode.

3.4.2 Pedalling-Mode

The movement patterns for the pedalling movement are the same as by a usually bicycle. For the start a pedal position has to be chosen at which enough torque can be produced. Two potential pedal positions are available for the start. The first is when the right crank arm points upward, the second position is 180° shifted. Then the left crank arm points downward. The directions left and right are defined as the drivers left and right side while looking in driving direction. For the pedalling movement MQF is needed to produce the main driving force. Since MQF can only produce driving force in a certain angle range an addition muscle is needed to achieve a rotational movement. Therefore MBF or musculus gluteus maximus can be used to produce additional driving force in angle regions where MQF is not able to provide it.

The p-mode stimulation concept has to enable a smooth circular movement and provide the possibility to interrupt the stimulation process if intended. At the beginning of the stimulation process the pedal crank has to be rotated 360° to initialise the angular encoder. If then the stimulation trigger is pressed the controller has to retrieve the crank position and velocity. Dependent on the angle region of the pedal crank the stimulation starts with stimulation channel 1,2,3 or 4. If e.g. the stimulation starts with channel 1 as next step the crank position and velocity have to be retrieved permanently by the controller. When the angle region of channel 2 is reached, it has to start with the stimulation with a short delay. This delay is the result of the time that is needed to activate the muscles on one hand and the time the microcontroller needs for computing on the other hand. Therefore the pedal crank velocity was retrieved before to compensate the travelled angle while the delay. This sequence is the same for channel 3 and channel 4. When channel 1 starts with the stimulation again a full rotation of the pedal crank was performed.

In case the driver of the bicycle decides to release the stimulation button the stimulation process of all channels has to stop immediately. If the trigger is pressed again the controller has to retrieve the crank position and velocity. Then again, dependent on the crank position, channel 1,2,3 or 4 starts with the stimulation.

If the emergency button is pressed the controller and the stimulator are powerless and the stimulation of all channels stops immediately. After deactivating the emergency button the angular encoder needs to be initialized again by rotating the pedal crank about 360°. Then the stimulation process can be started by pushing the stimulator button. The controller retrieves crank position and velocity and starts with fitting the stimulation channel according to the angle region (Figure 36).

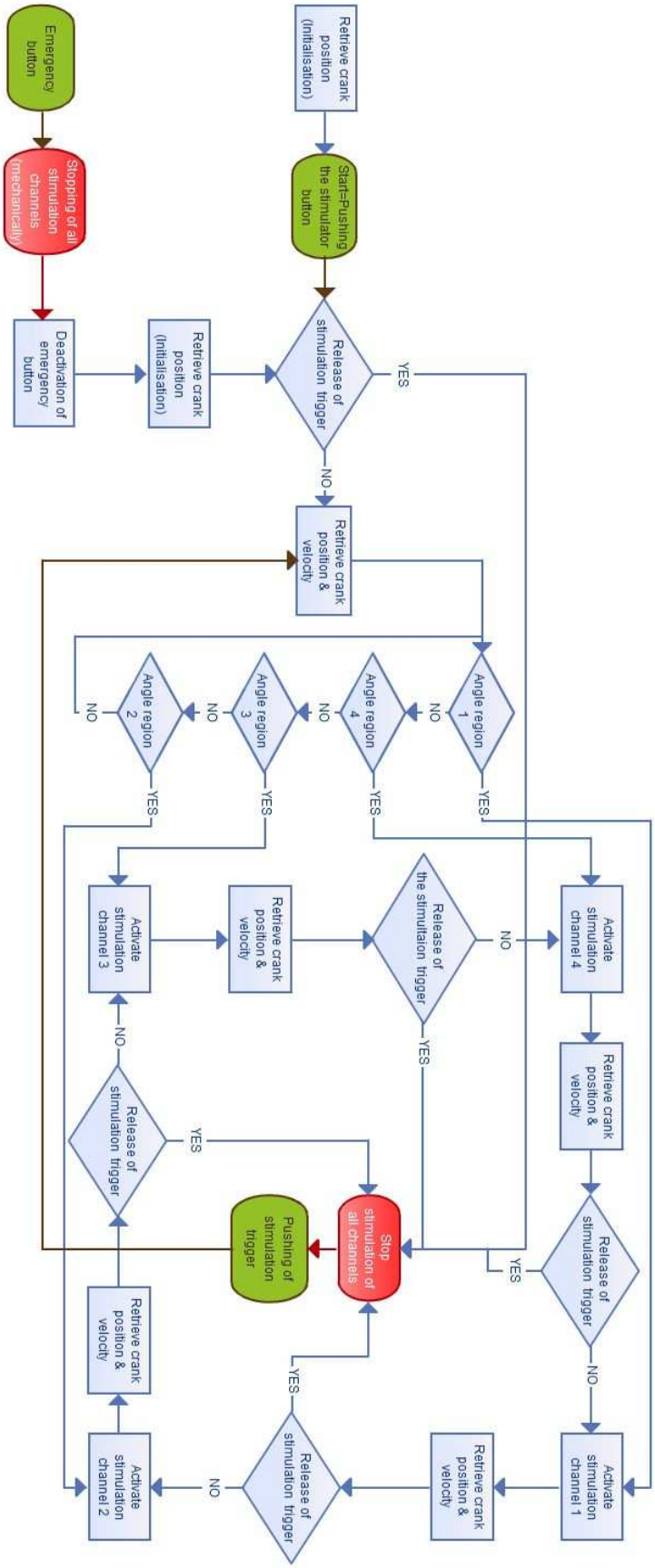

Figure 36 Flowchart, displaying the sequences and possibilities of the stimulation program for the pedalling movement of one leg

3.5 Stimulation Program

The stimulation programs for the ed-mode and the p-mode are based on the stimulation concepts described in 4.3. For writing, the program (PMLAB X/Microchip) was used. The coding language was “C”. The programming of the controller was part of a separate diploma thesis. More detailed information as well as the detailed program code can be found there [1].

3.6 Calculations

To assess different drive modes and to evaluate various trials it is necessary to calculate a parameter which can be used as comparative value. Therefore the power and mean power which are produced while driving a defined test track are calculated.

To calculate the achieved power it is necessary to determine the occurring forces which are present while the bicycle is driving (Figure 37). The forces, acting on a bicycle while driving, can be split up into two groups, the driving forces and the bicycle resistance forces F_{BR}. The driving forces can further be differentiated into inertia force F_I, the drag force F_D and the potential force F_P .Whereby the inertia force can further be divided into translational inertia forces F_{IT} and rotational inertia forces F_{IR}. The bicycle resistance forces F_{BR} can be differentiated into bicycle friction forces of rotating parts, oscillation forces and forces produced by the rolling resistance. The rolling resistance can furthermore be differentiated into flexing resistance and roll-off resistance. The potential force is neglected in this calculation because the test trails took place on a plain surface (Figure 38, case B). If not quoted else all calculations are based on basic mechanic knowledge [40].

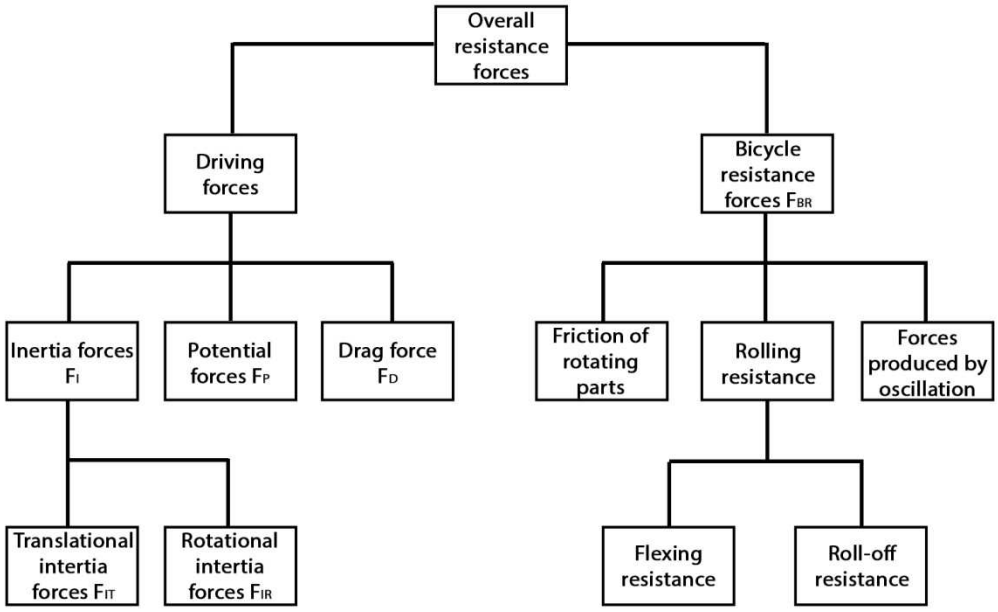

Figure 37 Diagram of forces acting on a bicycle while driving. (Adapted from [41])

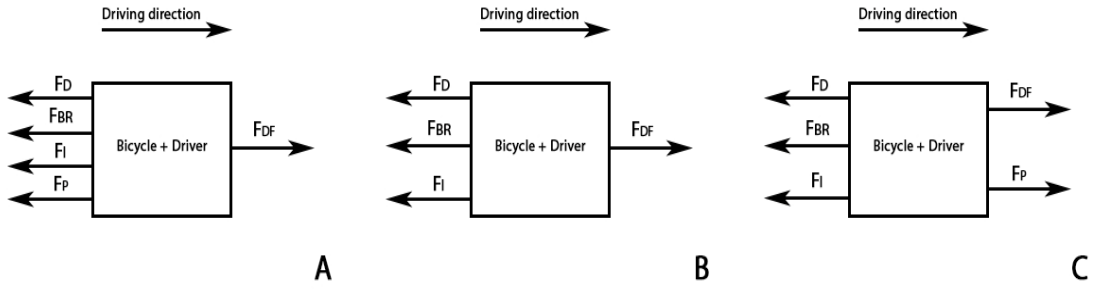

Figure 38 Symbolic depiction of the bicycle including driver, the occurring forces and their effective direction while driving. With F_{DF} as driving force, F_I as inertia force, F_D as drag force, F_P as force resulting of the potential energy and F_{BR} as force produced by the bicycle resistance. The left picture (A) displays the case when the bicycle is accelerating uphill, the middle picture (B) depicts acceleration on a plain and the right picture (C) displays the case when the bicycle is accelerating downhill.

3.6.1 Calculation of the Drag Force (F_D)

For calculating the drag force the afforded work, which is necessary to overcome the air resistance, can be set equal to the kinetic energy of the air mass.

$$F_D * s = \frac{1}{2} * cw * \rho * A * v^2 * s$$

By reducing "s", the drag force can be calculated by

$$F_D = \frac{1}{2} * cw * \rho * A * v^2$$

Whereby c_w is the drag coefficient, ρ the air density, "A" the air contact surface, "s" the travelled path and "v" the velocity.

The unit less drag coefficient c_w has to be determined experimentally and is not constant. For this work the value has been set to $c_w = 0.77$. This value is suggested for recumbent bicycles and is only valid for a frontal upstream flow [41]. This condition is fulfilled since the tests trials have been made in closed rooms without air flow.

The air density ρ is calculated by

$$\rho = \frac{p}{R * T}$$

Whereby "p" is the absolute air pressure, "R" is the specific gas constant and "T" is the absolute temperature. The specific gas constant for dry air is $R = 287.058 \frac{J}{kg*K}$. And the room temperature at the test trail is kept constant at T=293.15 K.

The absolute air pressure is calculated by the international barometric height formula

$$p(h) = p_0 * (1 - \frac{0.0065 \frac{K}{m} * h}{T_0})^{5.255}$$

T_0 is the reference temperature at sea level, p_0 the reference air pressure at sea level and 0.0065 is the temperature gradient per 100 m. The reference values are defined by the international standard atmosphere. And these parameters are set to $p_0 = 1013.25\ hPa$ and to $T_0 = 288.15\ K$ [42].

To determine the wind contact surface "A" a frontal view picture (Figure 39) has been taken from the bicycle with driver. The picture has to contain a yardstick. First the photo has to be cropped with a photo editing software that only the area of the bicycle and the driver is left. As next step the pixel number of the resulting picture has to be determined. Now the yardstick is used to achieve a correlation between the pixels and the area of the picture. This area now can be taken as wind contact surface "A".

The driving velocity "v" is measured with the bicycle computer.

Figure 39 Cropped picture used to determine the wind contact surface. The picture includes a yardstick (1) to achieve a correlation between pixel number and surface area.

3.6.2 Calculation of the Translational Inertial Force (F_{IT})

The translational inertia force F_{IT} is calculated by

$$F_{IT} = m_O * a$$

Whereby, m_O is the overall mass of the bicycle which is compound of m_B as the mass of the bicycle and m_D as the mass of the driver. The variable "a" is the acceleration and is derived from the measured velocity. This leads to the formula

$$F_{IT} = (m_B + m_D) * a$$

3.6.3 Calculation of the Rotational Inertial Forces (F_{IR})

To achieve the inertial forces of the bicycle, the moments of inertia have to be calculated before. The moments of inertia which have to be considered are these of the bicycle wheels. For the frontal wheel I_F and the wheel at the left rear side I_{RL}, the moment of inertia can be calculated by

$$I_F = I_{RL} = m_F * \frac{{r_O}^2 + {r_I}^2}{2}$$

Whereby, m_F is the mass of the wheel, r_o is the radius from the rotation axis to the tread and r_i is the radius from the rotation axis to the inner side of the rim. The backward wheel on the right side contains a wheel hub motor, which has to be considered in the calculation. Therefore the moment of inertia I_{RR}, of the wheel on the rear right side, is calculated by

$$I_{RR} = m_F * \frac{{r_o}^2 + {r_i}^2}{2} + (m_{RR} - m_F) * r^2$$

Here m_{RR} is the mass of the right rear wheel with rim hub motor and "r" is the radius from the rotation axis to the outer side of the rim hub motor. The first term of the equation is the moment of inertia of the wheel with rim and outer tyre, the second term is the moment of inertia of the wheel hub motor.

The resulting moments for the front wheel and the left rear wheel, produced by the moments of inertia, are calculated by

$$M_{IF} = M_{IRL} = I_F * \dot{\omega}$$

And for the right rear wheel by

$$M_{IRR} = I_{RR} * \dot{\omega}$$

Whereby $\dot{\omega}$ is the angular acceleration of the wheels and is achieved by calculating the angular velocity first with

$$\omega = \frac{v}{r_O}$$

And furthermore derivate the angular velocity ω with respect to the time "t"

$$\dot{\omega} = \frac{1}{r_O} * \frac{dv}{dt}$$

As last step the inertia force for the front wheel and the left rear wheel, at the tread, is calculated by

$$F_{IF} = F_{IRL} = \frac{M_{IF}}{r_O}$$

And for the right rear wheel by

$$F_{IRR} = \frac{M_{IRR}}{r_O}$$

The overall rotational inertia force F_{IO} of the bicycle is compound of the front wheel inertia force F_{IF}, the right rear wheel inertia force F_{IRR} and the left backward wheel inertia force F_{IRL}.

$$F_{IR} = F_{IF} + F_{IRL} + F_{IRR}$$

3.6.4 Calculation of the Bicycle Resistance Forces (F_{BR})

The bicycle resistance force is compound of friction force of rotating parts, oscillation force and the force produced by rolling resistance force (Figure 37).

Friction forces are produced in bearings of rotating parts when the bushing rubs on the bearing ring. The thus produced friction is diminished by lubricant which is normally

put between bushing and ring. Dependent on the rotation velocity more or less lubricant is dragged into the gap between bushing and ring. Therefore the rotational friction forces are velocity dependent.

When a bicycle is moved by a driver, oscillations are produced by the inertia forces of the human body, irregularities of the surface or imbalances of rotating parts like the wheels. This oscillations lead to elastic deformations of the bicycle. Although every elastic deformed part is set back to its originally shape, energy losses are produced while this deformation through friction within the material. On this way kinetic energy is transformed into thermal energy, which is released into the surrounding atmosphere.

The rolling resistance force can be divided into a force produced by flexing resistance and one produced by the roll-off resistance. The flexing resistance is based on energy losses while elastic deformation of the bicycle tyres. When the tyres are deformed within the rubber frictions happens. Again, kinetic energy is transformed into thermal energy by friction. The roll-off resistance is based on a breaking force produced when the wheel is deformed [41].

Since the friction forces, the oscillation losses and the rolling resistance force are complex to calculate or determine another approach was needed to determine the bicycle resistance force. Therefore a test trail was made before the experiment took place. Based on this trail the bicycle resistance force can be calculated.

Test trail to determine the Bicycle Resistance Force

To ensure that the measurements are usable for the calculation of the mean power, the test trail took place on the same test track as the driving tests will afterwards.

Test trail restrictions:

– The same wheel pressure, of 8 bar, was used on both tests.
– The driver had to sit on the bicycle.
– The test took place on an even surface

The test procedure was to accelerate the bicycle to a certain velocity. Then the front wheel had to be kept in line to drive in straight direction and it was not allowed to break. The bicycle had to roll out till it stopped by its own. Thus the forces acting on the bicycle where reduced to the translational and rotational inertia forces, the drag force, the potential force and the bicycle resistance force. The potential force could be neglected because of the even surface. Under these conditions the inertia forces act as driving force whereby the drag force and the bicycle resistance force are retarding forces (Figure 40).

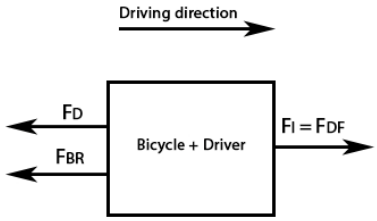

Figure 40 Draft of the occurring forces and their effective direction while the test trial to determine the bicycle resistance force.

Since the drag force and the inertia forces are known, the bicycle resistance force can be calculated by calculating the translational inertia force

$$F_{IT} = m_O * a$$

The rotational inertia force

$$F_{IR} = F_{IF} + F_{IRL} + F_{IRR}$$

And the drag force

$$F_D = \frac{1}{2} * cw * \rho * A * v^2$$

With the equilibrium of forces the bicycle resistance force is achieved

$$F_{BR} = F_{IT} + F_{IR} + F_D$$

The translational force, rotational force and drag force are calculated on the same way as described in 4.6.1, 4.6.2 and 4.6.3

3.6.5 Power Calculation

Power is defined as the performed work per time unit. The performed work is calculated by

$$W = F * s$$

This equation is only valid if the force “F” and the distance “s” are acting in the same direction. Than the power is calculated by

$$P = \frac{W}{t}$$

Whereby “t” is the time for which the work is performed. These terms can be simplified to

$$P = \frac{F * s}{t}$$

The term $\frac{s}{t}$ is the velocity “v”, by which the performed power can be calculated by

$$P = F * v$$

To calculate the achieved power at the test trail, the performed power of the drag force, the inertia force and the bicycle resistance force have to be calculated by

$$P_D = F_D * v$$

$$P_I = (F_{IR} + F_{IT}) * v$$

$$P_{BR} = F_{BR} * v$$

and summed up to the overall power P

$$P = P_D + P_I + P_{BR}$$

The mean power P_M is calculated by

$$P_M = \frac{1}{n} * \sum_{i=0}^{n} P_i$$

4 Bicycle Modifications

This chapter is about the necessary modifications of the bicycle, to make it possible to use it as a FES bicycle and to fulfil requirements necessary for people with paralysis. The single parts and all decisions concerning their design and chosen elements are explained in this chapter. For designing the mechanical elements the 3D-drawing software “AUTOCAD Inventor 2014” was used. The calculation of the stress analysis where done with “Mathcad 15” based on basic mechanic knowledge [40]. The software “AUTOCAD Inventor 2014” was also used for validation of the “Mathcad 15” calculations as well as to optimize the pressure distribution for the “End Stop Clamp” via Finite Element Method (FEM). To design the electrical circuits and produce the circuit diagrams “EAGLE 6.5.0” was used regarding the basic electronic knowledge [43], [44]. The technical drawings and circuit diagrams can be found in the appendix.

4.1 Construction of the Control Panel Mounting (CPM)

As construction material aluminium was chosen to keep the overall weight low and no high loads have to be absorbed. To save further weight the clamp bar for the control panel was accomplished as a pipe. The control panel mounting (Figure 41) consists of fife parts, four square shaped bars for fixation on the handlebar, numbers (1-4), and one pipe (5) for fixation of the control panel. To fixate the position of the pipe grooves were lathed at both ends that setscrews can be screwed in for fixation. The clamp mechanism on the handlebar is designed that only two screws are needed for clamping and assembling of the control panel mounting. To ensure that enough clamp force can be produced, the diameter of the clamping surface was fitted to the diameter of the handlebar whereas the centre of the diameter, on each side, was shifted slightly towards each other.

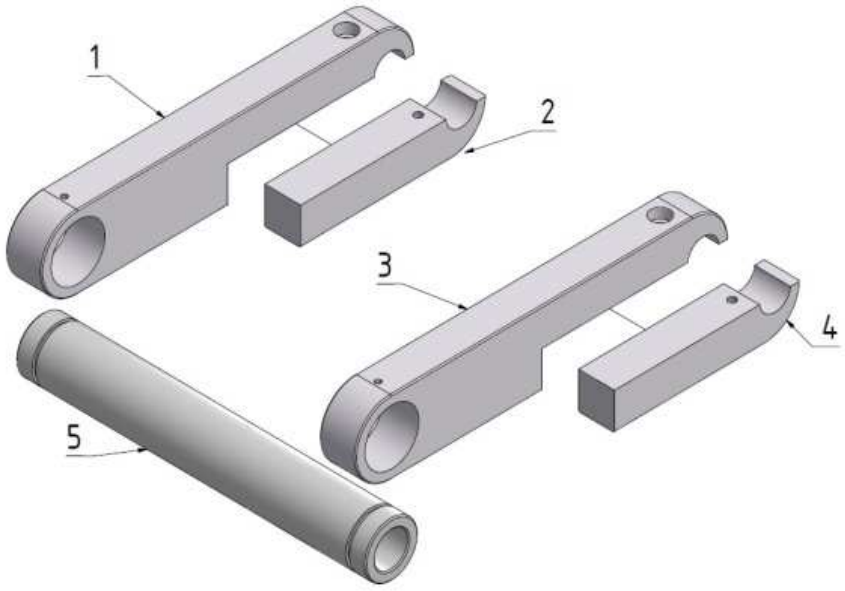

Figure 41 Exploded drawing of the CPM

4.2 Construction of the Crank Fixation

As construction material steel was chosen to provide more stability against bending and shear forces and since the part is small in size it does not contribute much to the overall weight of the bicycle. The crank fixation (Figure 42) consists of a lathed bold (1), a washer, suitable to a M4 thread (2), and a handscrew (3). For the washer and the handscrew, standard parts were used. The handscrew is made of plastic with a metal bit. The metal bit possesses a M4 thread for fixation. The length of the bolt is 101.5mm and the fixation diameter 12.8mm. The dimensions were chosen that the bolt protrudes as less as possible at the bicycle frame and that there is as less clearance, in diameter, as possible. One end has a M4 thread, for the handscrew fixation. On the other side a 2.1mm

slot was made. The slot was designed that a coin may be used to fixate the bolt while mounting the handscrew.

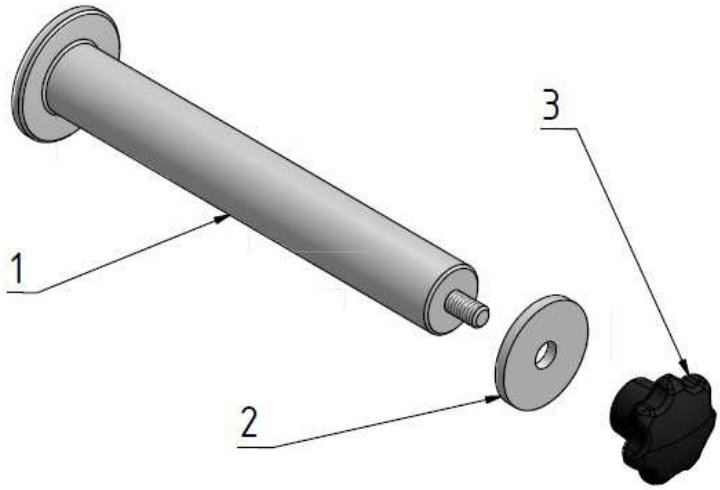

Figure 42 Exploded drawing of the Crank Fixation

4.3 Construction of the Bottom Bracket Shaft (BBS)

For the BBS (Figure 43) (1), steel was chosen as construction material to ensure a durable surface in the regions of the bearings. The dimensions were kept the same as the original ones except the length of the square section on which the gear (2) is installed, has been elongated about 8.5 mm. On one surface of the square section a cone with a diameter of 3 mm was drilled for the fixation of the gear with a M3 setscrew. Since the transmitted force is very little, a M3 thread has been drilled radial into the gear for fixation with the setscrew.

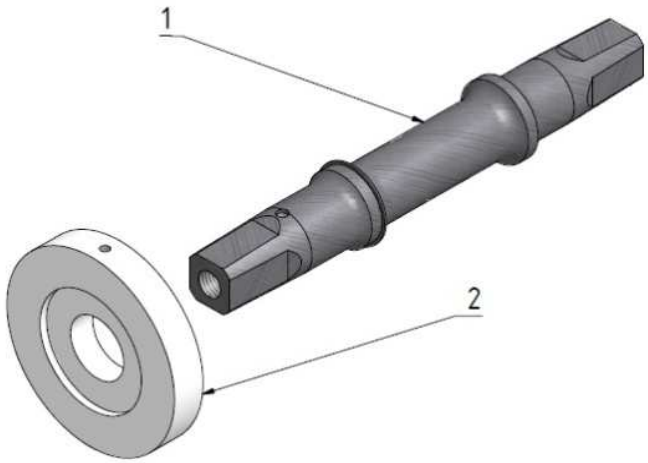

Figure 43 Exploded drawing of the BBS and the encoder gear

4.4 Construction of the Limit Switch Mounting

4.4.1 Mechanical Design

An angular rail (Figure 44) (1), made of aluminium, was designed for this purpose. Aluminium was chosen because the rail has to carry only the weight of the limit switches and the lower resulting weight of the rail itself. The rail was mounted with the same holes and screws, used for the sliding rails of the seat. On both ends of the rail long slots were milled to allow the shifting of the limit switches. To fixate the switches screws with nuts were used.

4.4.2 Electrical Design

As already mentioned for limit switches two SPST-NO stroke switches (ASQ10230/Panasonic) (2,3) (Figure 44) where used. Every single positive connection side of the switches is attached to the 3.3 V power supply of the controller, while both negative poles are connected to the same ground of the controller.

4.4.3 Electrical Functional Description

In initial state the limit switches are open, and therefore the circuit is interrupted. In this case, a permanent 3.3 V signal is send to the controller. When a limit switch is activated, the circuit is closed and therefore connected to the ground. Now a 0 V signal is send to the controller.

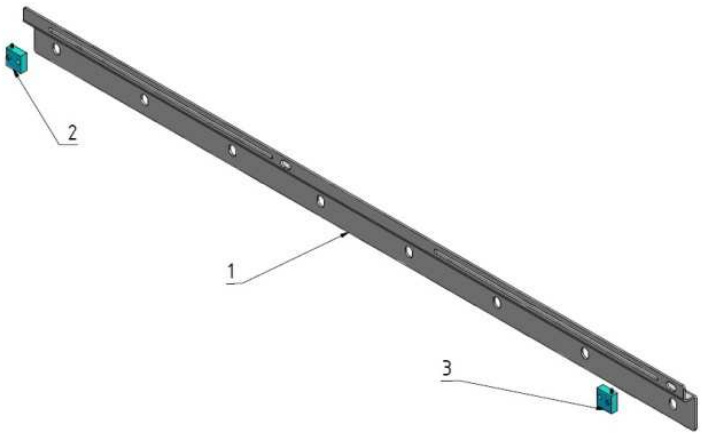

Figure 44 Exploded drawing of the Limit Switch Mounting

4.5 Limit Switch Fence

As construction material aluminium was chosen to reduce the weight and since there is no need to provide a tougher surface because the limit switches tapped is made of plastic. The limit switch fence (Figure 45) consists of an aluminium bar (1) with a chamfer on both sides. Since the space between the sliding frame and the limit switches has been only few millimetres the fence was made slim. For fixation a M6 thread was tapered into the fence, but it was not possible to drill a blind hole because of the slim shape of it. Therefore, clearance holes were drilled. To cover the holes on the sliding surface a thin metal sheet (2) was glued to the fence surface.

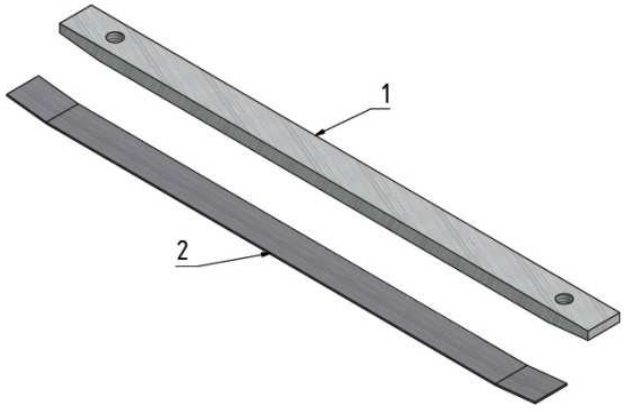

Figure 45 Exploded drawing of the Limit Switch Fence

4.6 Construction of the Stimulation Button Casing (SBC)

4.6.1 Mechanical Design

The SBC (Figure 46) consists of a main body (2) on which a leaver (1) is mounted. A spring, which can be preloaded through a setscrew, was placed between the stimulation lever and the main body of the casing, to ensure that the lever and the stimulation button are in contact at any time. The two parts where connected through a bold (3) with a thread on one side and a slot for a screwdriver on the other side. The fixation of the casing was realised through two clamping pieces (4) (5). The pieces where adapted to the radius of the handle bar, while the radiuses centre, of the clamping surfaces, of each part was shifted towards each other. This ensures a small cleft, which is necessary for the production of the clamping force. The frontal side of the casing was designed as a lid (6) with three circular recesses for the fixation of light emitting diodes (LED). In the main body of the casing two recesses were made. On the right side for connection plugs and on the backward side one recess was made for the stimulation button. Parts of the casing were produced by the institutes own 3D-printer. A polypropylene like material

(DurusWhite RGD430/Objet) was used because it provides sufficient stability for this prototype. Because of the brittleness of the material, mechanically higher stressed regions had to be designed with a larger wall thickness. All edges where rounded to reduce the mechanical stresses in this areas. Due to material behaviour it was not possible to cut threads directly into the parts for fixation. Therefore recesses in which a M3 nut can be placed and glued where used instead for fixation.

4.6.2 Electrical Design

The stimulation switch is the central element of the casings electrical design. A single pole double throw (SPDT) (C&K/8121) (7) switch with a defined activation point was chosen. The SPDT switch has three connection terminals. Two green LEDs (8,9), with diameters of 5 mm, indicate the end positions of the seat, one red LED (10), with a diameter of 3 mm, indicates that the stimulation process is active. To connect the stimulation switch and the LEDs with the controller a six pole plug (HR10/Hirose) (11) was used (Figure 46).

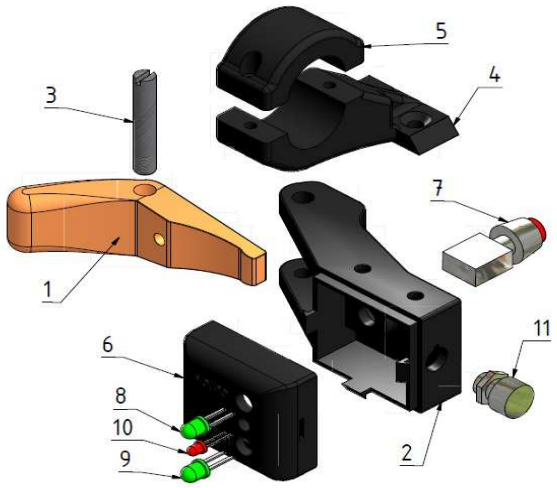

Figure 46 Exploded drawing of the Stimulation Button Casing

4.6.3 Electrical Functional Description

The SBC contains the mechanical switch to trigger the stimulation voluntary and three LEDs as optical feedback. The switch has three connection terminals. One terminal of the switch is connected directly to one of the FBs 3.3 V power supply pins. Another is directly connected to an input pin of the ST and the third one to the ground. In the initial state a constant 3.3 V signal is send to the ST input. When the switch is activated the circuit is shifted to the ground. This leads to an input signal of 0 V at the ST. The three LEDs are connected separately to three different outputs of the FB, on one side, and to the ground on the other side. On this way every single electrode can be controlled by the

FB separately. The green electrodes are activated when the frontal or backward limit switch is activated. The red LED is activated while the stimulation process is ongoing.

4.7 Construction of the Controller

4.7.1 Mechanical Design

The controller housing (Figure 47) consists of two parts. The main body (1) with the recesses for the connectors and fixation holes for the circuit board and the lid (2), for fast access to the electrical components. On the frontal side, of the main body, the recesses for the stimulation trigger-, the limit switch-, encoder- and the stimulation output connectors as well as the recess suitable to a RJ11 connector, for programming the FB, were located. On the backward the recess for the connector of the power supply and a slot to connect a micro USB cable to the FB were made. The casing was produced by the institutes own 3D-printer and a polypropylene like material (DurusWhite RGD430/Objet) was used.

4.7.2 Electrical Design

The electrical design of the controller casing board was planned outgoing from the microcontroller. As microcontroller a Fubarino Mini v15 board (FB) (1) was chosen. The FB Mini is an Arduino compatible Application Programming Interface (API) board with a PIC32MX250 microcontroller. Further features are a USB connector for power, programming and connection to a PC and an In Circuit Serial Programming (ICSP) connector for hardware programming. The chosen board, for the controller circuit, had the dimension of 110x67 mm with a 2.54 mm hole grid. The controller was chosen to be powered directly by the battery of the stimulator. Since the battery of the stimulator supplies a mean voltage of 12 V, but the allowed input voltage of the FB Mini is at maximum 5 V, the voltage had to be reduced. Therefore, a DC/DC (Traco Power/TEL 5-1211) converter (2) was implemented. The converter provides a constant output voltage of 5 V by a maximum output current of 1000 mA. Other reasons for choosing a DC/DC converter, instead of decreasing the supply voltage by a voltage divider, were that the input voltage for the FB Mini would decrease regarding the charging level of the stimulator battery and that the resistors of a voltage divider would get hot since the electrical energy is transformed into heat by mechanical processes. To guarantee a defined input signal at the FB input pins a six-times Smith Trigger (ST) (Texas Instruments/SN74HC14N) (3) was implemented. Another reason for implementing a ST is to prevent the FB from being damaged through too high input voltage at the input pins. Three inputs, two for the end limit switches and one for the stimulation trigger, of the ST were equipped with 1k Ω resistors to limit the current flow. The other three inputs

were directly connected to the angular encoder and needed no current limitation. To trigger the stimulator, an on semiconductor based analogue quadruple bilateral switch (Philips/HEF4016B) (4), was implemented. The analogue switch (AS) can easily be triggered by the microcontroller with minimal power consumption. A further advantage is that there is no mechanical wear due to the semiconductor technology. A 100 Ω resistor, for the red LED, and two 56 Ω resistors, for the green LEDs, of the SBC were positioned between the FB output pins and the wire to board connector (WTB) leading to the SBC. The resistors were necessary to ensure the appropriate voltage value for the LED´s and for current limitation. To connect the controller board devices with the casings connectors, WTB connectors (Wurth Elektronik) were used (5-9). The controller and the angular encoder where connected with a six-pole connector (Lemo) (10), the power supply and the connection to the stimulation trigger were realized with a three-pole and a six-pole connector (HR10/Hirose) (11,12), whereas the limits switches and the stimulator were connected with a three-pole and a five-pole connector (Series 719/Binder) (13,14). To provide an interface, for programming the microcontroller without removing the FB board, an additional connector was implemented (RJ11/Wurth Elektronik) (15). All explained components are illustrated in Figure 48.

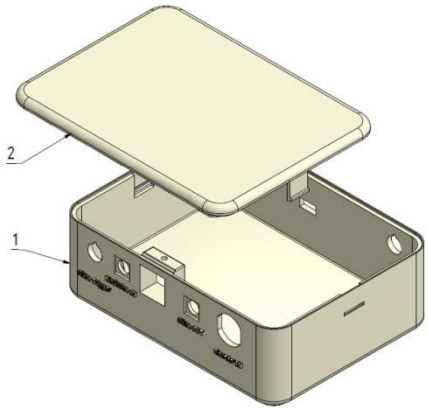

Figure 47 Controller housing with the main body (1) and the lid (2)

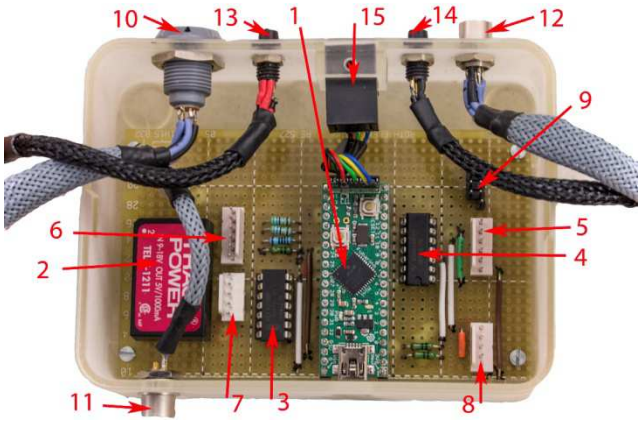

Figure 48 View into the controllers inside, with the microcontroller (1), DC/DC converter (2), smith trigger (3), analogue switch (4), wire to board connectors (5-9), plugs (10-15)

4.7.3 Electrical Functional Description

The purpose of the controller is to provide a connection between the sensors like the angular encoder and the limit end switches, to control the stimulation timing and forward these signals to the stimulator. A further task of the controller is to transform the electrical energy from the stimulator battery and to distribute it between the connected devices. The FB is powered by 5 V and it is able to supply 5 V and 3.3 V trough three power output pins. The ST is directly powered by one of the FBs 3.3 V power supply pins. The same output pin is connected to two 1k Ω resistors which further leading to two inputs of the ST and to the limit end switches. Therefore, these two inputs of the ST

receive as long a 3.3 V signal as no limit switch is activated. When a switch is activated, this circuit is connected to the ground and no signal is present at the ST input. The ST is a special variation of a differential amplifier and can switch between two different states. If the input voltage of the ST is lower than approximately 1.35 V the input is “low”, then the output is set to “high” which means that an output signal is produced. If the input voltage is higher than 3.15 V, the input is “high” and the output is set to “low” and no output signal is produced. Due to this behaviour the ST is named an inverting differential amplifier. Therefore, the ST transmits a “high” signal to the input pins when a limit end switch is activated. The FB receives this signal, at one of its input pins, and activates or deactivates, according to its programming, an output pin which leads to the AS. The AS is powered by the FBs 5 V power supply. The task of the AS is to interrupt or connect the control circuit of the stimulator, and thereby, to stop or start the stimulation. Therefore, every single switch has three terminals. One input and one output pin, for the control circuit of the stimulator, and an enable input pin. If the enable input is supplied by minimal 3.5 V the switch is in the ON condition. This leads to a low resistance between the input and output of the stimulator control circuit. If the enable input is supplied with a voltage underneath 1.5 V the switch is turned OFF and a high resistance occurs between the input and the output of the controller circuit. At a low resistance, at the control circuit of the stimulator, the device starts to stimulate. At a high resistance it stops the stimulation. One 3.3 V supply pin of the FB leads to a resistor and further to the stimulation trigger switch. From the stimulation trigger switch this conduit leads back to one input of the ST. The circuit and processing principle is the same as at the limit end switches before. The only difference is that the signal amplitude of 3.3 V is produced by the FB, regarding the programming of the microchip. Three output lines of the angular encoder are connected to three inputs pins of the ST. The input signals generated by the angular encoder show a rectangular shape with amplitudes of 5 V, starting by 0 V. These signals are processed on the same way, by the ST and the AS, as the signals of the mechanical switches before. Three output pins of the FB are connected to separate resistors, leading to the LED´s of the stimulation trigger casing. On this way the LED´s can be controlled according to the programming of the FB.

4.8 Construction of the Emergency Button Casing (EBC)

4.8.1 Mechanical Design

The casing (Figure 49) consists of two parts, an upper plate (1) with a hole for the emergency switch fixation and a lower housing (2) which includes the recesses for the connectors, leading to the controller. These two parts are connected to each other with two vertical bolted M3 screws and one horizontal bolted M3 screw. With the vertical screws the casing is fixated to the handlebar of the bicycle. For stability reasons the upper plate was made of aluminum and the lower housing was produced by 3D printing

out of a material similar to polypropylene (DurusWhite RGD430/Objet). All sharp edges of the lower housing where rounded to avoid stress pikes in these regions which can lead to fractures. Since the 3D printer material is brittle no threads were cut into the lower housing. Instead of threads nuts are embedded in it.

4.8.2 Electrical Design

As switch type an emergency stop button (CE3T10R11/ABB) (3) was chosen (Figure 49). This type was selected because of its small dimensions and the option to use it as normally closed- and as normally open switch. As connector, coming from the controller, a four-pole connector (HR10/Hirose) (4) was chosen. For the connection from the EBC back to the controller a four-pole connector (Series 719/Binder) (5) was selected.

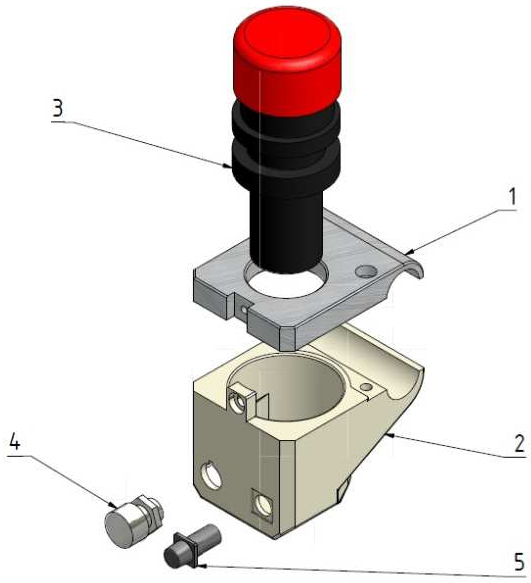

Figure 49 Exploded drawing of the EBC

4.8.3 Electrical Functional Description

In working mode the emergency switch is closed. On one terminal, of the emergency stop button, the power supply, coming from the stimulator, is connected. On the other terminal two wires are fixed, one leading back to the stimulator, the other one leads to the controller for its power supply. A separate wire connects the ground of the stimulator directly to the ground of the controller. If now the emergency button is activated the switch opens the circuit and thus the stimulator and the controller are powerless.

4.9 Construction of the Pedal End Stop (PES)

The PES (Figure 50) consists of fife elements. The main element is a bar (1) with the dimensions 262x30x7 mm, made of steel. The bar has a hole for fixation to the pedals and a long slot, in its middle, for sliding the end stop in it. The end stop (2) itself has a cylindrical shape with a radial groove on one side and a thread on the other side. On the same side as the thread, a groove for an open-end wrench with a rim with of 15mm is milled. Steel was used as construction material for the end stop. In the radial groove two rubber seals (3,4) are fixated to ensure a damped contact, to avoid damages to the pedal crank and for noise reduction, between the end stop and the pedal crank. The end stop is mounted to the bar by a pilot pin (5), made of steel, with a M4 thread on one side. This design makes is possible to station the end stop in a fitting position.

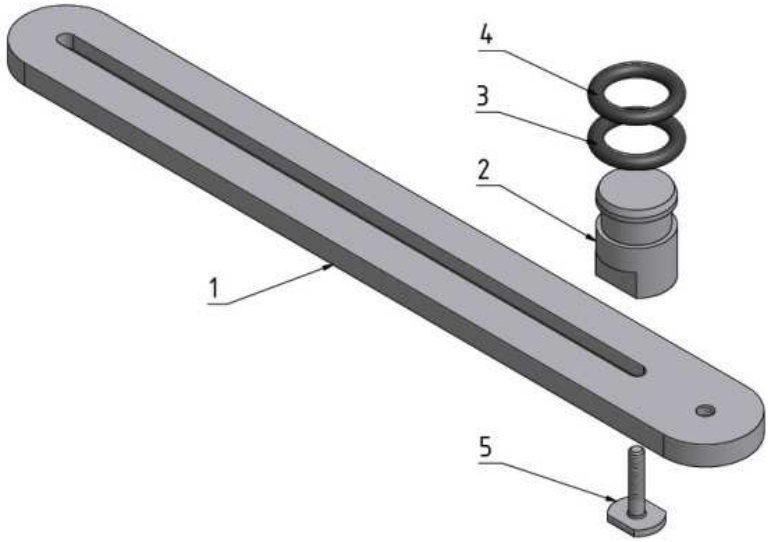

Figure 50 Exploded drawing of the PES

4.10 Construction of the End Stop Clamp (ESC)

4.10.1 Mechanical Design

The ESC (Figure 51) consists of a horizontal beam (1), with a M5 thread on one side and a M6 thread on the other side. Guideways were milled on both front sides for fixation of the vertical beams. The horizontal beam is made of steel to avoid high deformations especially at the small cross sections of the guideways. Two vertical beams (2,3), made of aluminium, are attached to the horizontal beam. On both vertical beams on one end a guideway, fitting to the horizontal beams guideway, was milled. On the same side holes were drilled for fixation to the horizontal beam. On the opposite side of both vertical beams a socket was milled. The socket is used as guideway and for fixation of the

clamping jaws. The thread in the middle of the socked is used to adjust the distance between the two clamping jaws by a M8 setscrew. Aluminium was used to reduce the overall weight of the ESC. This was possible because of the smaller length of the vertical beams and therefore a lower resulting bending moment. The vertical beams are mounted with a screw to the horizontal beam on one side and a quick release (Elesa+Ganter/GN927.3) (8) on the other side. The clamping jaws (4,5) were made of aluminium to avoid damages at the guide rails in case of too high contact pressures. The clamping jaws were fixed to the vertical beams with two M2,5 screws in a way that a movement toward each other is possible when adjusted by the M8 setscrew. The rubber buffers (9,10) are fixed to spacers (6,7) Which are furthermore mounted to the vertical beams with setscrews. The clamping jaws length was extended so that tilting torques can be absorbed. After calculating the deflection of the beams FEM was used to control the calculations results. Also the stress distribution and the contact pressure, between the clamping jaws and the guide rails, have been simulated and optimized by FEM.

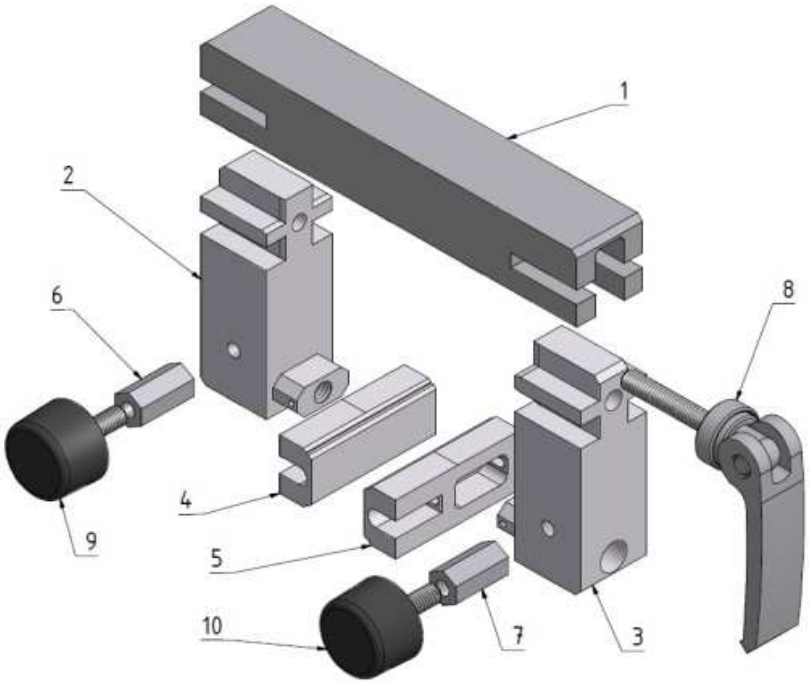

Figure 51 Exploited drawing of the ESC

4.10.2 Finite Element Analysis (FEM)

The Finite Element Analysis was performed in two separate steps. In the first step only the horizontal beam and in the second step the whole system, except the rubber buffers, were analyzed.

4.10.2.1 FEM Analysis of the Horizontal Beam

To control the calculated deflection of the horizontal beam an analysis of the single beam was realized.

Mesh

As general mesh preferences the default values of the program were chosen. They were for the average element size 0.1, for the minimum element size 0.2. For the grading factor 1.5 and for the maximum turning angle 60°. The average element size specifies the element size relative to the model size. The minimum element size allows an automatically net refinement and is related to the average element size. The grading factor controls the transition from a larger net element to a smaller one. The factor 1.5 e.g. limits an element edge length to 1.5 the length of a adjacent element. The maximum turning angle affects the number of elements on curved surfaces, smaller angles result in more elements [45]. At the guideways, where higher stresses were suspected, a local mesh with a constant element size of 0.5 mm was chosen (Figure 52).

Constraints

The constraints “fixed” were applied on the surfaces (A) (Figure 52). If an element is fixed, all its degrees of freedom are removed and it is impossible to deform the element [44]. Although this does not coincide with the real situation and would therefore lead to altered results in the middle of the beam, this type was chosen since the section between the two surfaces (A) was designed with sufficient stability. A development calculation of this section resulted in a deflection of 0.114 mm at the middle of the beam. Therefore it is not of interest for this investigation. The sections of interest where the guide rails which can be considered as cantilever beams. And, for this purpose, the chosen constrains where applicable.

Loads

As loads, forces where applied on the bottom surface of each cantilever beam perpendicular to the surface (Figure 52). Force magnitudes of 4360 N, the same values as used for the calculation, were chosen. The same magnitude was applied on each cantilever beam since a consistent force distribution was assumed.

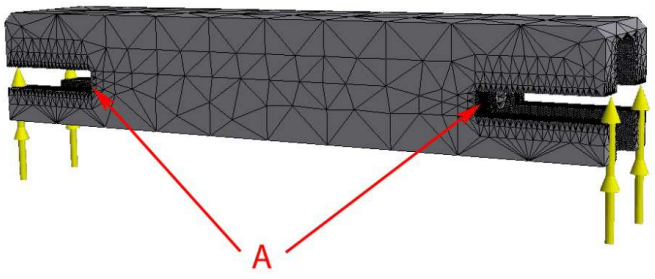

Figure 52 Picture of the applied mesh, position of the fixed surfaces (A) and the applied loads (yellow arrows)

Results

The result of the analysis showed a maximal displacement of 0.1232 mm at the outer end of the cantilever beams, in vertical direction (Z-coordinate) (Figure 53). But this maximum value is not meaningful because it represents only very small deformation areas at the force application site. At none deformed areas the displacement was about 0.08 mm. The control calculation resulted in a displacement of 0.022 mm. Although these results differ quantitatively, this difference is only small in magnitude and allows therefore a qualitative conclusion. Therefore the chosen cross section and material, as described in 4.10.1, were classified as sufficient and used for production of the horizontal beam.

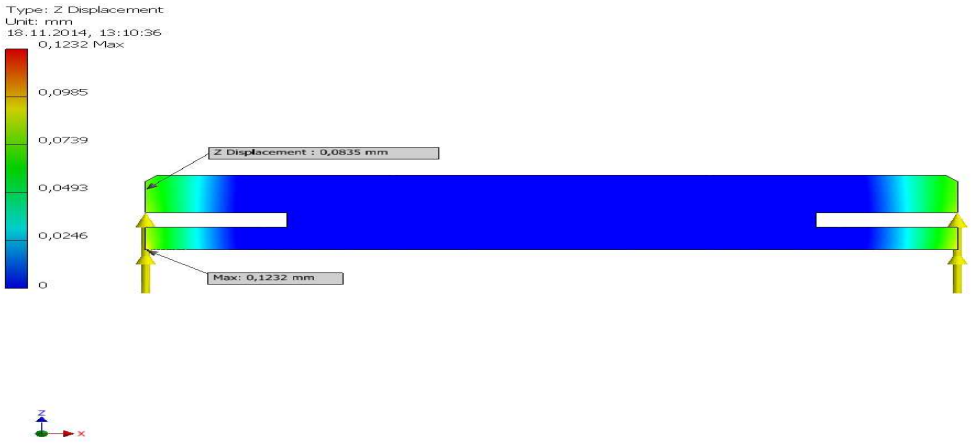

Figure 53 Analysis results of the horizontal beam, in vertical direction (Z-coordinate)

4.10.2 FEM Analysis of the Clamping Jaws

Model Variations

The aim of the analysis was to decide between two design variations of the clamping jaws to reduce the local contact pressure between clamping jaws and guide rails. Therefore, one clamping jaw with a rectangular shape (Figure 54) was designed and a second version with a 0.5° chamfer (Figure 55) the contact surfaces.

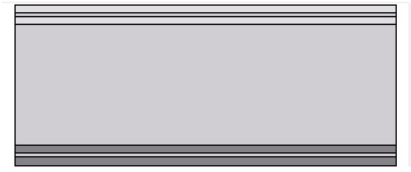

Figure 54 Picture of the rectangular version of one clamping jaw

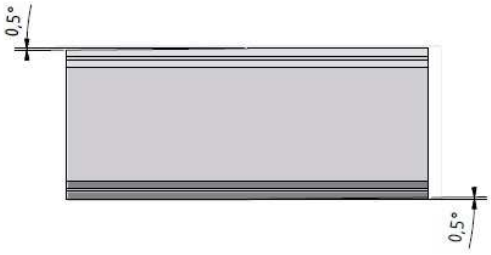

Figure 55 Picture of one clamping jaw version with 0.5° chamfer

Mesh

For the analysis of the clamp jaws the whole model, excluding the rubber buffer and the quick release, of the ESC was used. For the horizontal beam, the same mesh preferences as described at 4.10.2.1 where applied. For the other parts, the default preferences for the element sizes and the grading factor, as described at 4.10.2.1, where used (Figure 56).

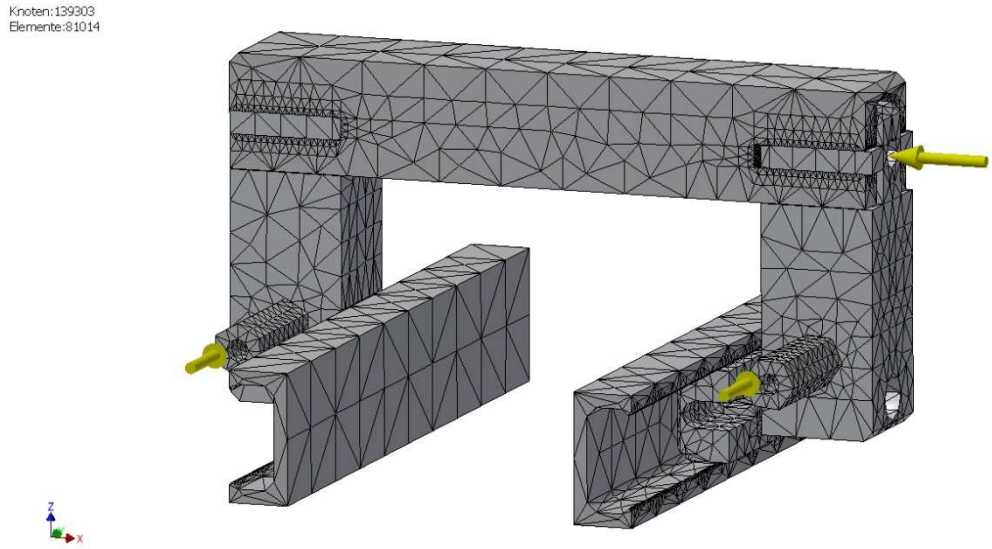

Figure 56 Depiction of the mesh applied to the ESC model.

Constraints and Contact Conditions

Fixed constraints were placed on surface (Figure 57) (A) of the guide rail dummies (1), which were designed for this analysis. Since for the optimization of the clamping jaws the whole model of the ESC was used, also contact conditions needed to be defined. Between the clamping surface of the clamping jaws and the inner surface (B) of the guide rail dummies the contact condition “sliding/no separation” was applied. This condition allows a relative movement between the elements, but prohibits separation. At the surfaces on the upper and lower side of the clamping jaws (C), which are in contact with the guide rails, the contact condition “Separation” was used. This contact type allows separation between parts, but prohibits penetration. At the inner surfaces (D) of the clamping jaws, which are in contact with the vertical beams, also the contact type “Separation” was applied. Between the spacers and the vertical beams (E) the contact type “Separation” was used. On the side where the horizontal beam is fixed to the vertical beam with a screw, the contact condition “Bonded” was applied to the surfaces (F). On the other side, where the quick release system is used the contact condition “Separated” was used between the surfaces (G). The condition “bonded” simulates rigid bonding between surfaces [45]. At the surfaces (H) between the horizontal and the vertical beam the condition “separated” was used and at the surfaces (I) “Sliding/No Separation” was applied.

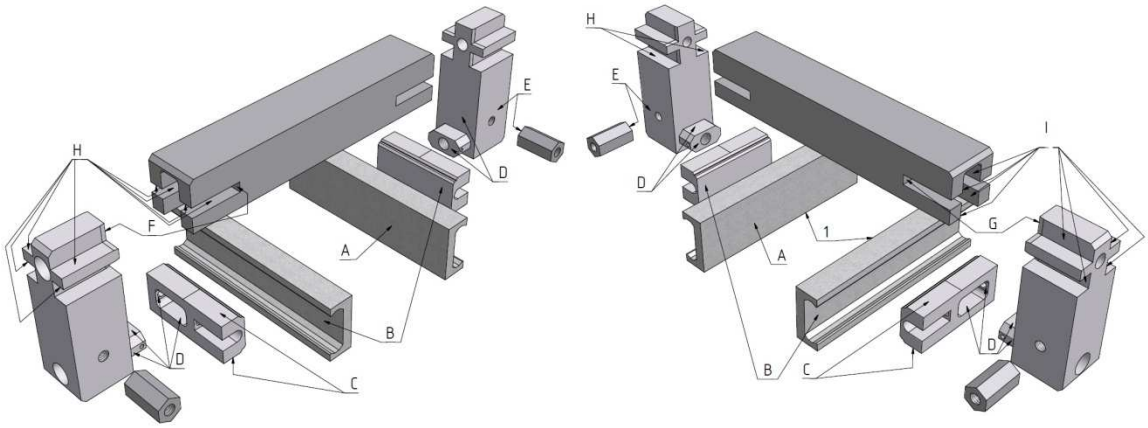

Figure 57 Depiction of the ESC surfaces and their applied contact conditions and constraints. The surfaces “H”, only depicted on the left picture are also valid for the right picture. The surfaces “I”, only depicted on the right picture are also valid for the left picture.

Loads

Since it was not possible to apply friction between the surfaces of the clamping jaws and the guide rails, forces F1 where applied to the clamping surfaces oriented parallel to the surfaces. The magnitude of the forces was 4000N per element. To simulate the impact of the seat, forces F2 with the magnitude of 4000N and an opposite direction as the forces F1 were applied to the spacers on which normally the rubber buffers are mounted. The quick release was simulated by two forces F3 and F4 acting on the outer surface of the vertical beam and the fixation thread for the quick release on the horizontal beam. The magnitude of both forces is 8000N but their orientation is opposed (Figure 58).

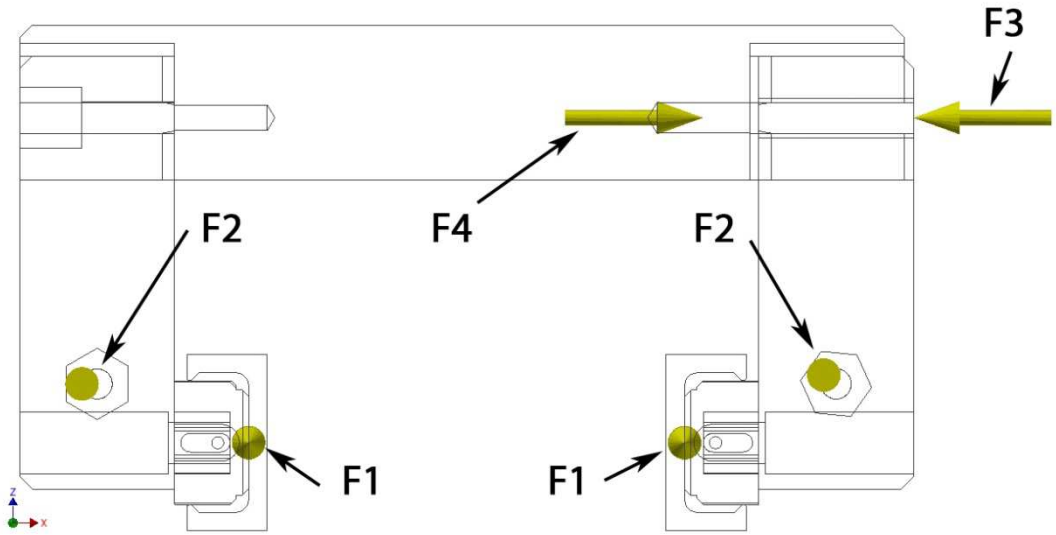

Figure 58 ESC model with applied forces (yellow arrows). F3 and F4 represent the clamping force. F1 represents the adhering force and F2 the impact force of the seat with driver

Results

Figure 59 displays a section of the seat guide rail including a clamping jaw of the ESC. In the following pictures the clamping jaw is hidden to allow observing the contact pressure distribution between clamping jaw and guide rail. The version with a 0.5° chamfer (Figure 61) showed a more distributed contact pressure in comparison to the rectangular version (Figure 60) and leads only to a slight tilting of the ESC. By evaluating the two different designs, it has also to be considered that elastic deformations are not taken into account in a FEM analysis. In the real system the regions with high contact pressures, displayed as red areas in Figure 60 and Figure 61, will be attenuated and the pressure will be more distributed. As result of this simulation, the design with the 0.5° chamfer was chosen for production.

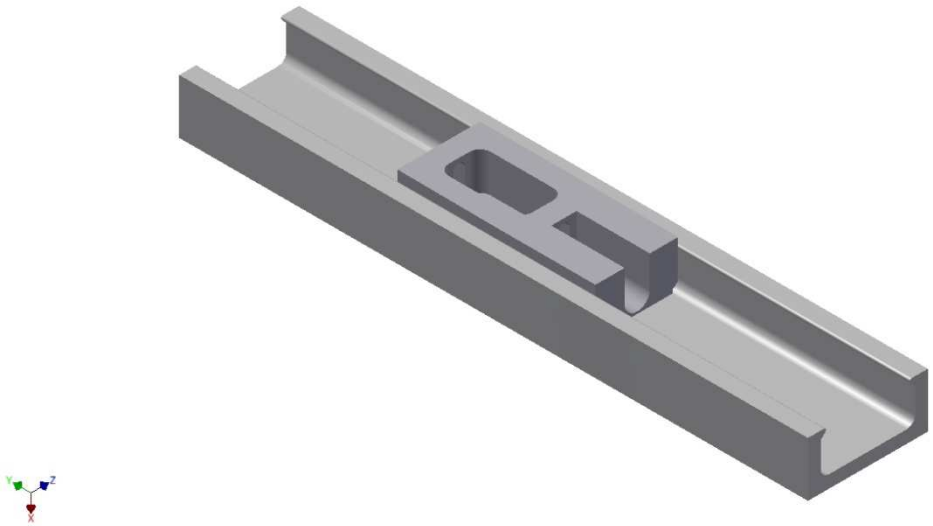

Figure 59 Picture of a guide rail section with clamping jaw.

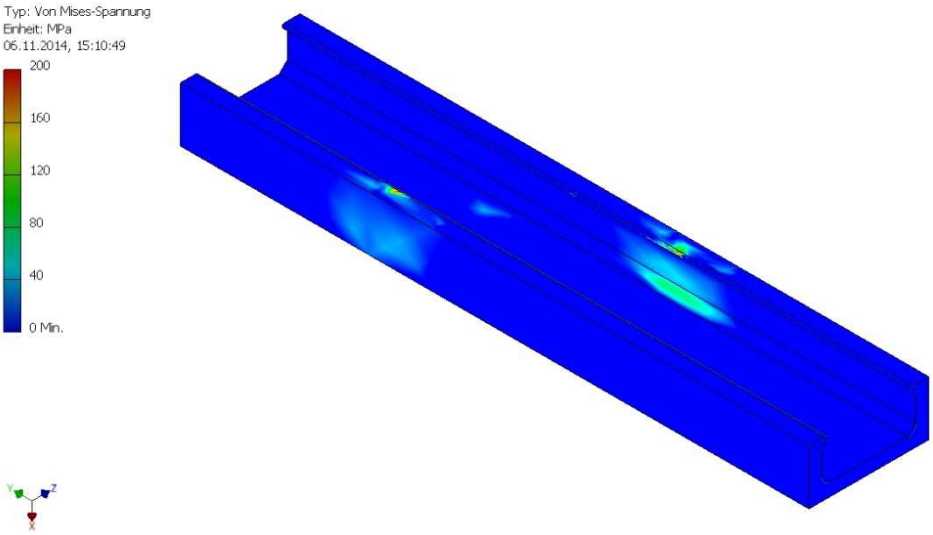

Figure 60 Guide rail section without clamping jaw. The clamping jaw was hidden to display the contact pressure distribution of the rectangular clamping jaw version.

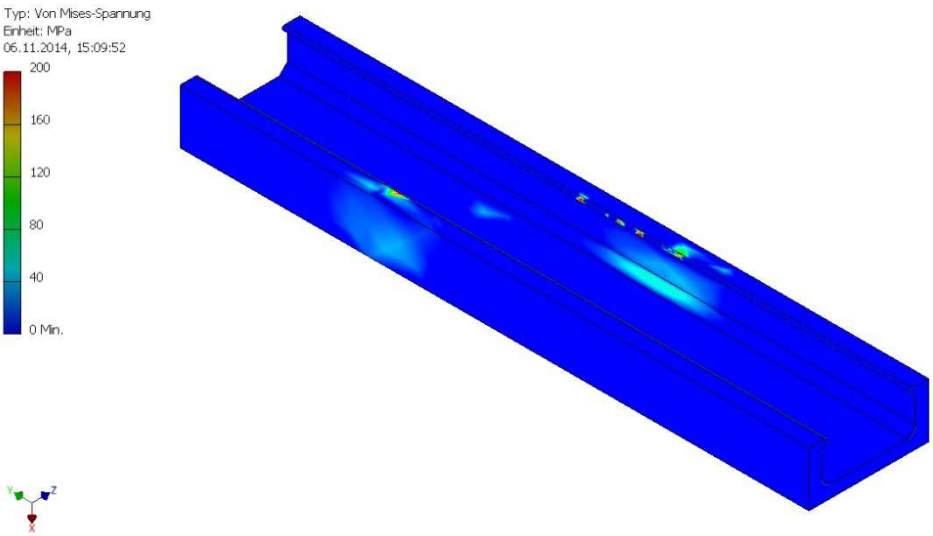

Figure 61 Guide rail section without clamping jaw. The clamping jaw was hidden to display the contact pressure distribution of the clamping jaw version with a 0.5° chamfer

4.11 Construction of the Battery Clamp (BC)

The fixation mechanism (Figure 62) has a hook like shape and consists of two parts. A cylinder (2), made of aluminium, for fixation to the stimulator housing and as fixation for the clamping hook. And the clamp hook (1), made of steel, for fixation of the battery. On the straight side of the hook a hole is drilled, for fixation to the cylinder. The cylinder is produced hollow. On one side there is threaded a M8 thread, on the other side the inner radius is widened relative to the core drilling. This is made because the stimulator housing possesses cylindrical trunnions where the cylinder can be placed and fixated to. First the cylinder is bolted with M3 screws, to the stimulator housing, than the hook is bolted with M8 screws to the cylinder. Two of such clamps where used for fixation.

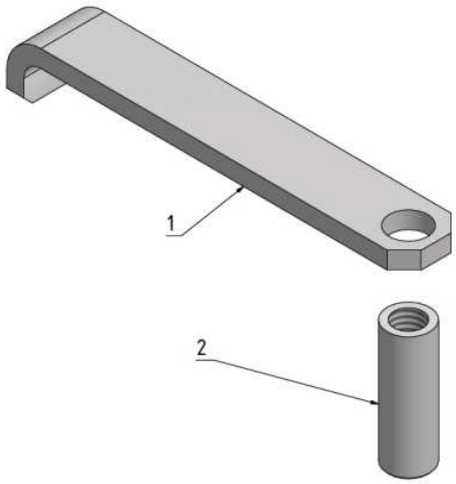

Figure 62 Exploded drawing of the BC

4.12 Construction of the Chain Tensioner Adapter (CTA)

The CTA (Figure 63) consists of three elements. A fixation pin (1) made of steel, with a round cap as end stop and a square guide to prevent against rotation on one side and a radial drilled hole on the other side. A hollow cylinder (2) made of aluminium, which serves as distance piece and as connection between the two other parts. Further, a plate (3) also made of aluminium, on which the chain tensioner is mounted. It has three holes with a diameter of 3.5 mm, which serve as end stop for the chain tensioner. The holes are placed on the same radius, but shifted by an angle of 23° that the chain tensioner can be rotated and therefore the preload can be changed. The fixation pin is put through the bicycle frame while the cylinder is put on the pin and is fixed with a M4 set screw. The plate is mounted with a M6 screw to the cylinder while the chain tensioner is fixed directly to the plate.

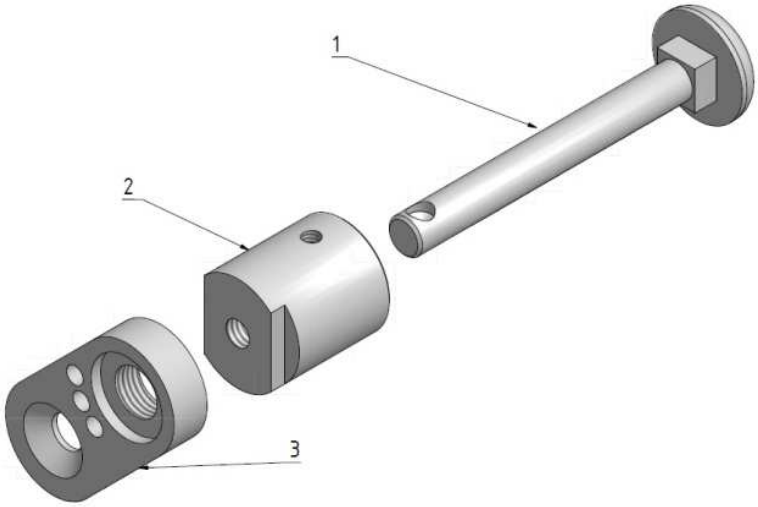

Figure 63 Exploded drawing of the CTA

5 Development Accompanying Function Tests

The development accompanying function tests were performed in cooperation with Christoph Kast [1].

5.1 Investigation of the Bicycle Resistance Force (BRF)

As described in chapter 3.6 the BRF is composed of the rolling resistance, resistance produced by oscillation forces and the friction of rotating parts. Since most of this resistance forces are hard to determine an approach to access the overall BRF was needed.

5.1.1 Measurement of the BRF

The BRF can theoretically be measured while the bicycle moves with constant velocity on an even surface, at an area without air movement. To allow neglecting the drag force the measurement has to be performed at a velocity slow enough that the drag force has almost no influence on the BRF. If this requirements are fulfilled the only forces acting on the bicycle are the driving force and the BRF (Figure 64).

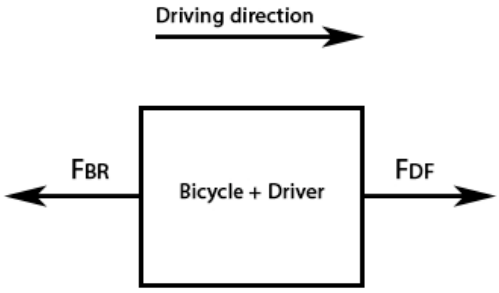

Figure 64 Sketch of the forces acting on the bicycle if the potential force, the inertia force and the drag force are neglected. Then the only forces acting on the bicycle are the driving force F_{DF} and the BRF F_{BR}.

5.1.2 Measurement of the BRF - Test Setup and Calculations

The test trial took place in a workshop room of the Center for Medical Physics and Biomedical Engineering. Therefore the area is wind shielded and the surface on which the trial was performed was even. The driving force was produced by a lathe. Therefore a round-bar, with a diameter of 50 mm, made of steel, was clamped in the three-jaw chuck. A metal wire was fixed to the round-bar on one side. On the other side the wire was fixed to a spring scale. The spring scale was fixed directly to the bicycle.

The lathe velocity was set to 50 revolutions per minute. Therefore the resulting drive velocity for the bicycle can be calculated by

$$v = \omega * r$$

With ω as angular velocity and "r" as radius of the round-bar

The angular velocity can further be expressed as

$$\omega = 2 * \pi * n$$

With "n" as revolutions per minute

Which further leads to the formula for the driving velocity of the bicycle

$$v = 2 * \pi * n * r$$

To control if the influence of the drag force can be neglected, it can be calculated by

$$F_D = \frac{1}{2} * cw * \rho * A * v^2$$

The formula for the drag force F_D and the used variables are given in 3.6.1. The values used at the test trial were:

cw=0,77, ρ=1,17 Pa, A=0,48 m², n=50 1/min, r=0,025 m

The resulting drag force is

$$F_D = 0{,}0036\ N$$

The calculation result confirms that the drag force can be neglected for determine the BEF.

Conclusion

With this method it was not possible to access the BRF because it was impossible to achieve a constant driving velocity of the bicycle. The system showed high oscillation potential and therefore it was not possible to access a constant value at the spring scale. As next step the spring scale was replaces by an electronic spring scale to eliminate the elastic properties of the spring. But even with the electronic version the system showed too much oscillation potential and it was not possible to achieve a constant force. The main oscillation potential was produced by the metal wire which was used as connection between the spring scale and the lathe. So it was decided to look for another possibility to access the drag force.

5.1.3 Calculation of the BRF

Another approach to determine the BRF is to calculating it. As mentioned above, if the potential energy, acceleration forces and additional wind forces can be neglected, only inertial forces, the BRF and the drag force are acting to the bicycle. The inertia forces and the drag force are known and therefore the BRF can be calculated. This method was used for this investigation. Further details and explanations are given in chapter 3.6.4.

5.2 Extension Drive Mode-Function Test

A function tests was performed, to assess the functionality of the controller program as well as the mechanical and the electrical devices. To achieve a meaningful test trial the same protocol which was intended to be used for the final test trial with a test person was used. The protocol template can be found in the appendix.

5.2.1 Test Preparations

Following data were collected by using the protocol template.

Subject data:

Weight:	76 kg
Age:	37 Years
Sex:	male
Kind of injury:	healthy
Injury since:	/
FES training since:	/

Test trail conditions:

Slope:	0°
Trail surface:	smooth/plastic coating
Wind condition:	no wind

Electrodes:

Electrode type:	self-adhesive electrodes
Electrode size:	80x130mm
Conductive material:	adhesive gel

Assessment of the wind contact area:

A picture (Figure 39) was taken to assess the wind contact surface by means of a photo editing software.

Resulting wind contact surface:	0,48m²

Bicycle Adjustments

For the ed-mode the pedal cranks were orientated in the same direction. Therefore one crank was dismantled and mounted again rotated about 180°. To provide a stable platform for the feed both pedals were fixated with the crank fixation bolt. The test person's legs were fixated to the orthesis, mounted to the pedals, with Velcro belts. The short driving chain, which connects the driving gear with the middle gear, was removed. The seat was clamped to the longer driving chain with the clamping lever, positioned on the

right side underneath the seat. To enable the seat to slide along the guide rails, the fixation bolt was released. To prevent the knees of getting hyperextended the ESC was adjusted that the seat stops when the knee arrives at an angle of approximately 60° (Figure 65). The PES was adjusted subsequently according to the ESC position and the resulting knee angle.

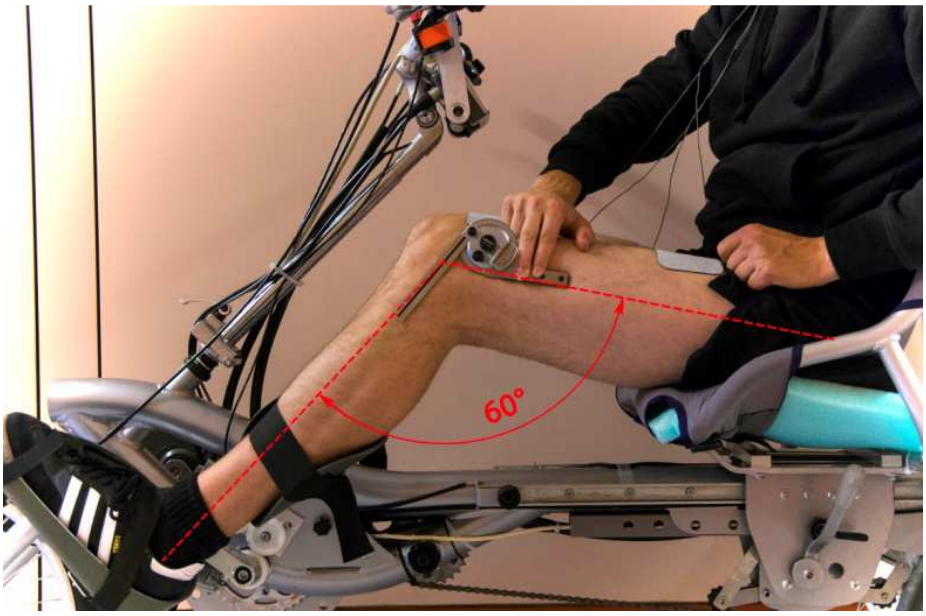

Figure 65 Adjusted knee angle in end position.

Sensors Application

The limit switches, which are needed to register the forward and the backward position of the seat, are fixed to the bicycle. The limit switch output cable was connected to the controller. The BC was fixed to the handle bar. The speed sensor of the bicycle computer was fixed to the bicycle fork. Two magnets were mounted to the spokes of the frontal rim for speed detection. The velocity sensor of the BC is fixed at the bicycle fork with only little clearance to the magnets. Each time a magnet passes the BCs velocity sensor triggers a signal. The magnets were positioned opposite each other. This leads to a theoretically bisection of the wheel circumference and therefore to a better detection of lower velocities.

Electrode Application

For the ed-mode two channels are necessary to stimulate the MQF. Therefore, on both legs, one electrode was placed anterior on the femur 4 cm proximal from the patella. The second electrode was also placed anterior on the femur 27 cm proximal from the patella (Figure 66). As electrodes self adhesive gel electrodes were used. The electrode cables were connected to the stimulator and to the electrodes. To avoid the cables of getting caught they were fixed to the driver, but with enough length to allow the seat to move forward and backward.

Figure 66 Position of the stimulation electrodes on the left femur. On the right femur the same position was chosen.

Controller Program

Before starting the stimulation the ed-mode stimulation program was stored on the controller's microchip. A function test was performed to assure a proper performance.

Stimulator Settings

Only channel 1 and 2 were activated. Channel 3 and 4 were deactivated and for safety reasons the potentiometer were reduced to minimal output for these channels. For the first trial the potentiometers of channel 1 and 2 were adjusted to a quarter of the maximum possible adjustable amplitude. The resulting voltage at this setting was 17 V for both channels. From there the amplitude was raised up to 25 V for the final trial. The stimulation frequency was set to 32 Hz for every trial.

5.2.2 Documentation of the Test Setup:

Seat fence position:	rearmost position
Knee angle in rear position:	120°
Knee angle in forward position:	63°
Electrode position (from Patella end to electrode outset):	proximal = 40mm
	proximal = 270mm
Adjusted stimulator amplitude:	trial1 = 22V
	trial2 = 25V
Stimulation signal shape	biphasic
Adjusted stimulator frequency:	32Hz
Adjusted pulse width:	1ms (both phases)
Adjusted pulse pause:	31ms

5.2.3 Test Data

Data to Determine the BRF

To calculate the BRF test trials were performed. The procedure was the same for every trial. First the recording of the bicycle computer was started and then the bicycle was accelerated with the implemented electrical engine till a constant velocity was achieved. At a defined mark at the ground the engine was turned off and the bicycle was driven only by inertia forces. It was not allowed to break or steer till the bicycle stopped by itself. Then the recording of the bicycle computer was stopped.

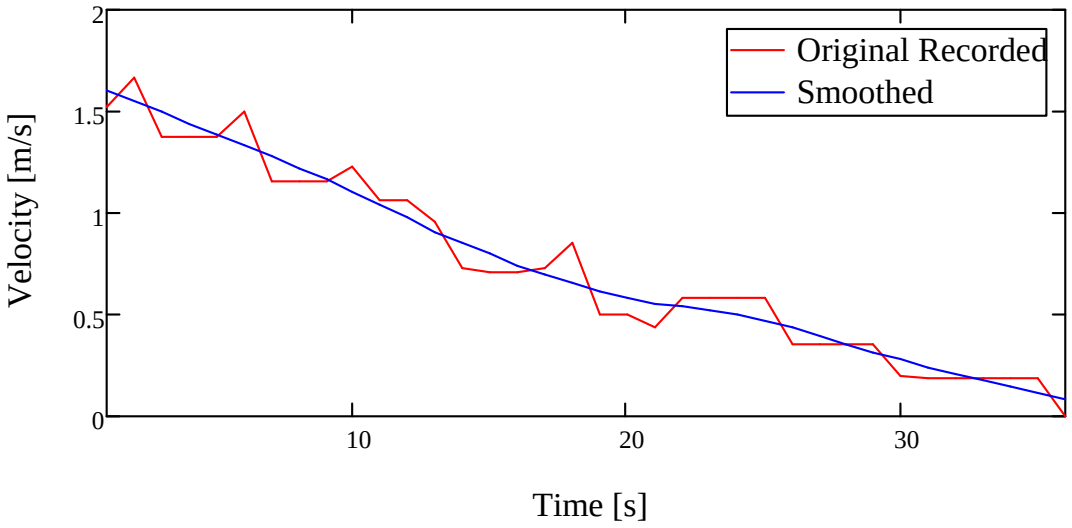

Figure 67 Velocity of the first test trial. The red line depicts the original recorded velocity whereas the blue line was smoothed

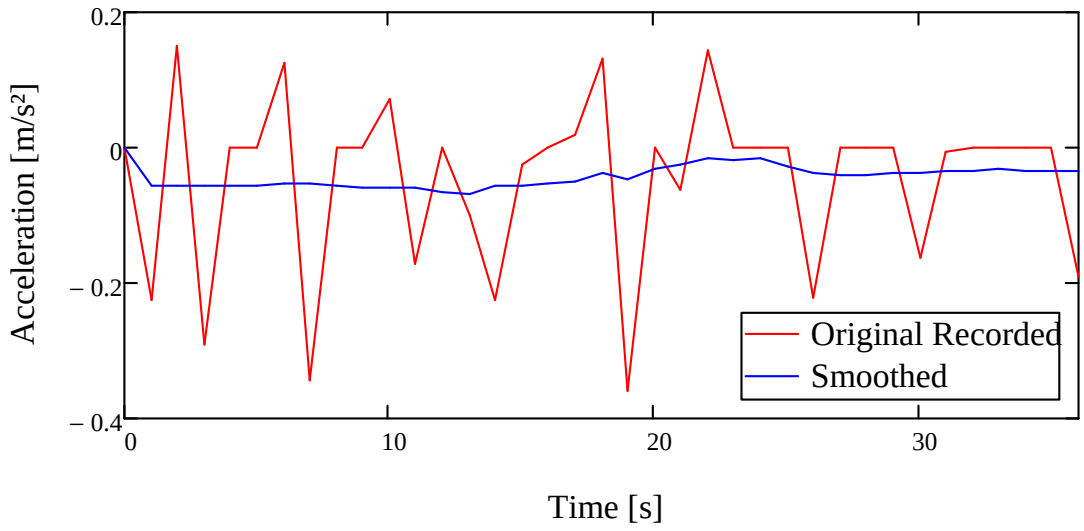

Figure 68 Acceleration of the first test trial calculated on the basis of the recorded velocity. The red line depicts the acceleration based on the original recorded data whereas the blue line represents the acceleration based on the smoothed velocity.

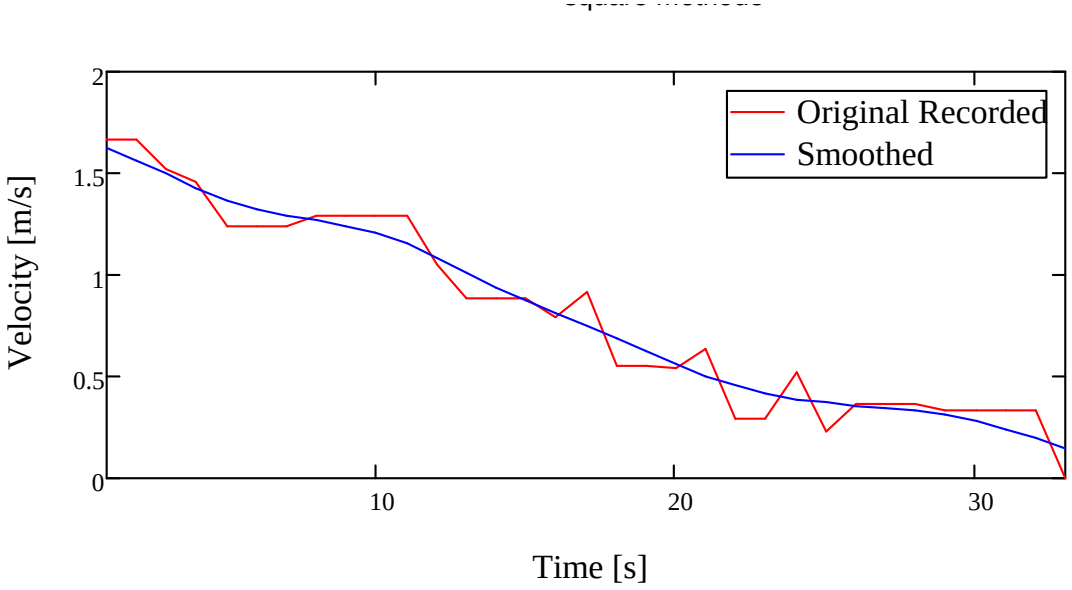

Figure 69 Velocity of the second test trial. The red line depicts the original recorded velocity whereas the blue line was smoothed.

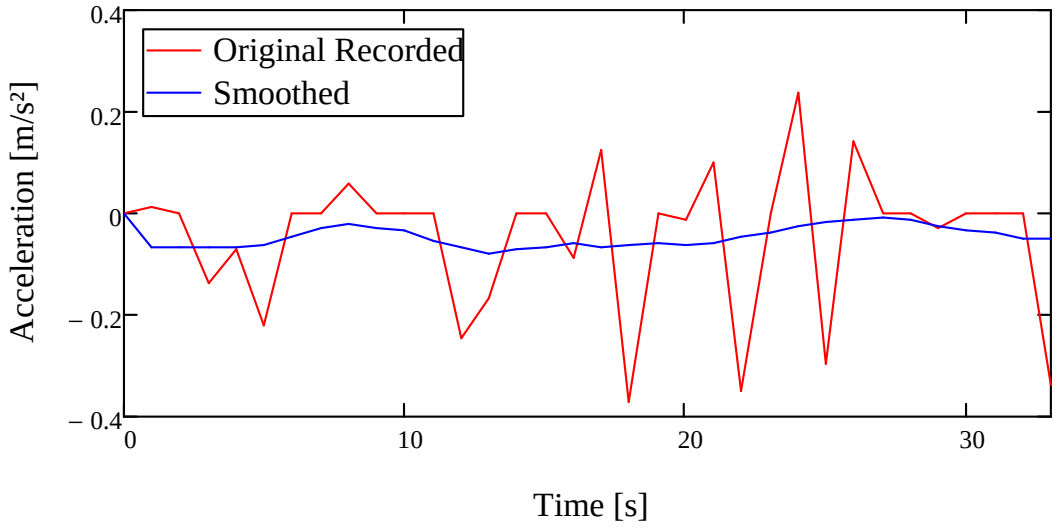

Figure 70 Acceleration of the second test trial calculated on the basis of the recorded velocity. The red line depicts the acceleration based on the original recorded data whereas the blue line represents the acceleration based on the smoothed velocity.

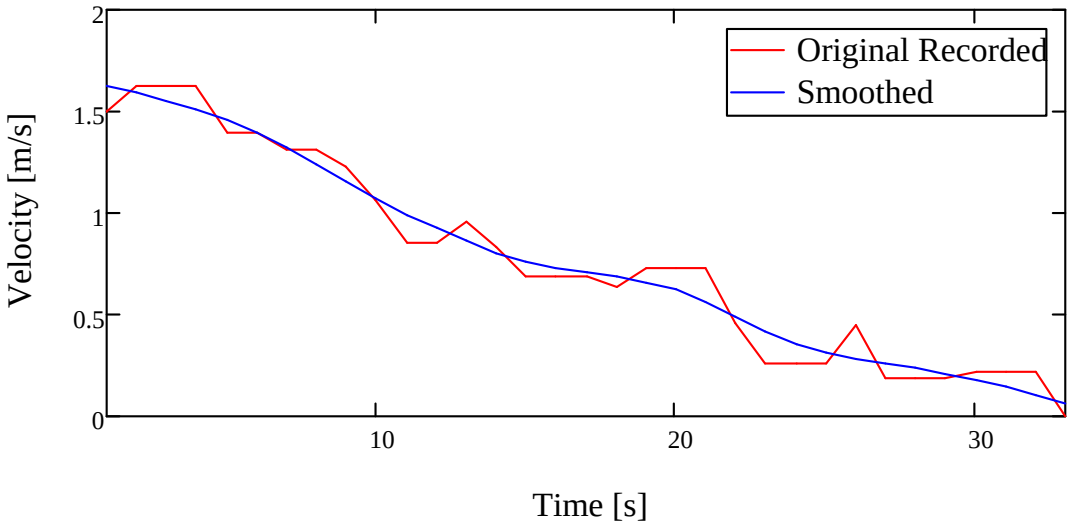

Figure 71 Velocity of the third test trial. The red line depicts the original recorded velocity whereas the blue line was smoothed.

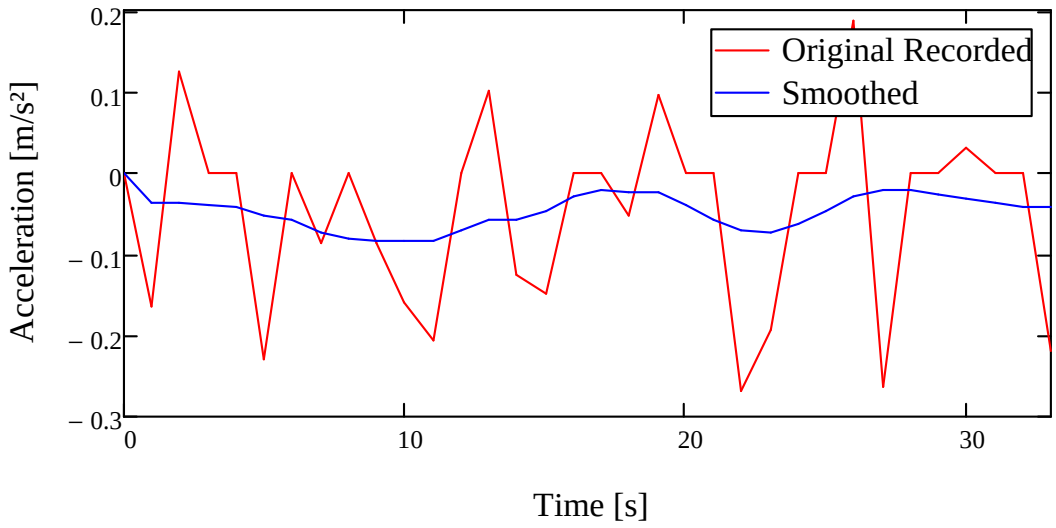

Figure 72 Acceleration of the third test trial calculated on the basis of the recorded velocity. The red line depicts the acceleration based on the original recorded data whereas the blue line represents the acceleration based on the smoothed velocity.

Test Trial Data

For the test trial a route was defined by choosing a start-mark and an end-mark. The bicycle was positioned at the start-mark and the driver also was told to take start position. Before starting the test trial the recording of the bicycle computer was initiated. Then the driver was allowed to start the stimulation and to accelerate till the end-mark is arrived. The driver was told to accelerate as much as possible. When the end-mark was arrived the driver had to brake till the bicycle stops. Coincident with stopping the bicycle the recording ended.

Three acceleration test trials were performed, one after another, without breaks between each trial. The recorded data can be found at Figure 73 - Figure 78.

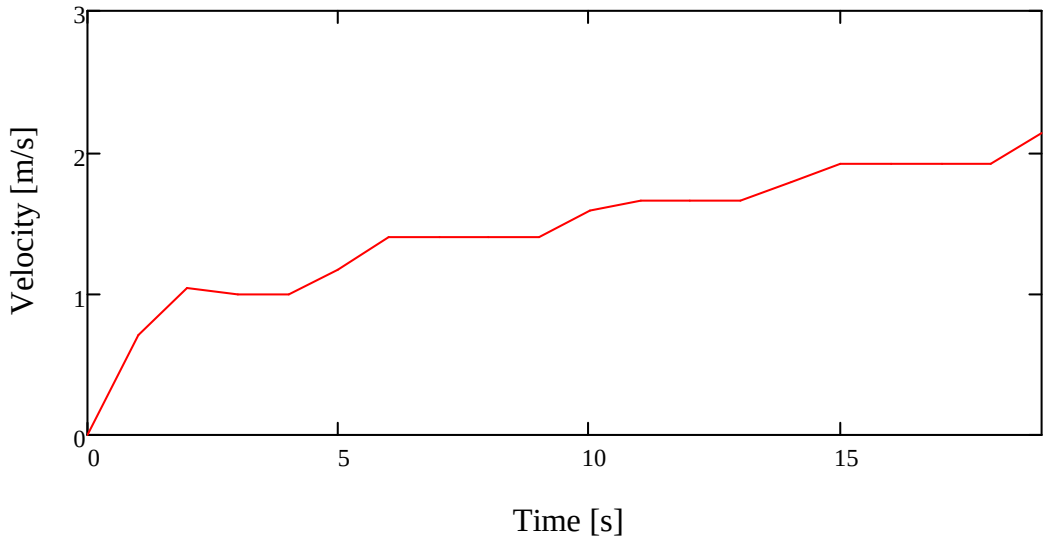

Figure 73 Recorded velocity of the first test trial in dependence of the driven time.

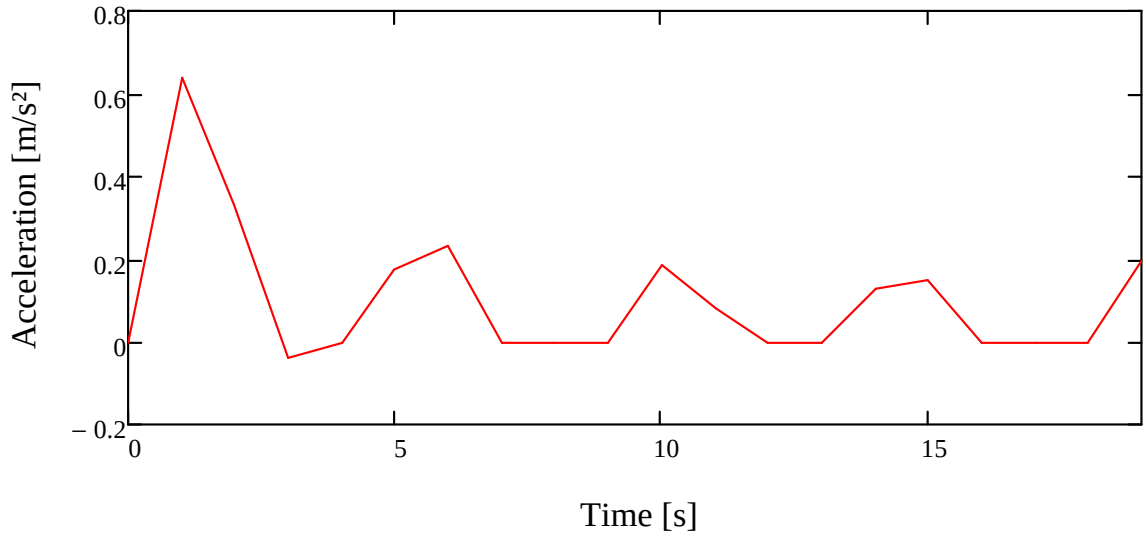

Figure 74 Resulting acceleration of the first test trial in dependence of the driven time.

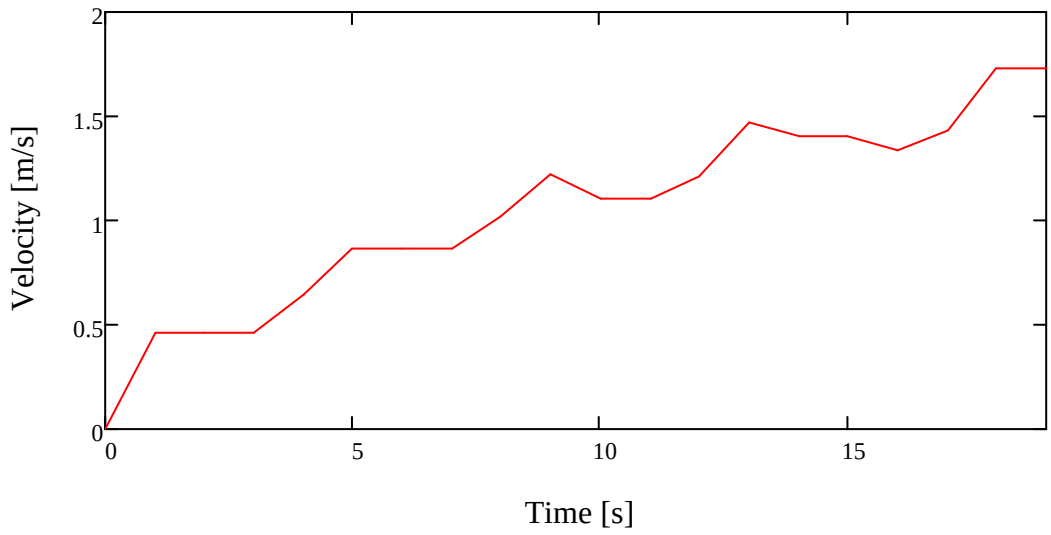

Figure 75 Recorded velocity of the second test trial in dependence of the driven time.

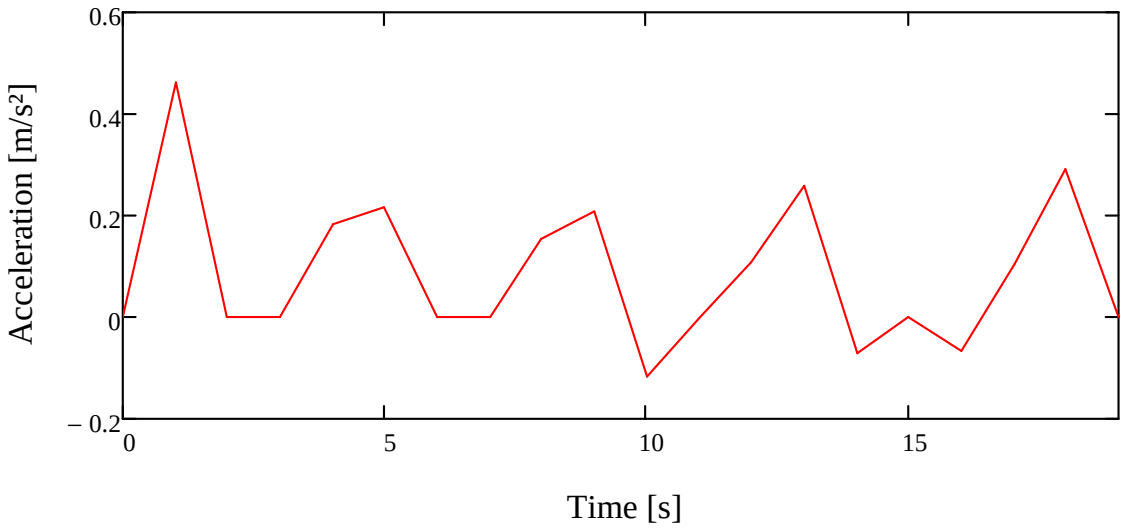

Figure 76 Resulting acceleration of the second test trial in dependence of the driven time.

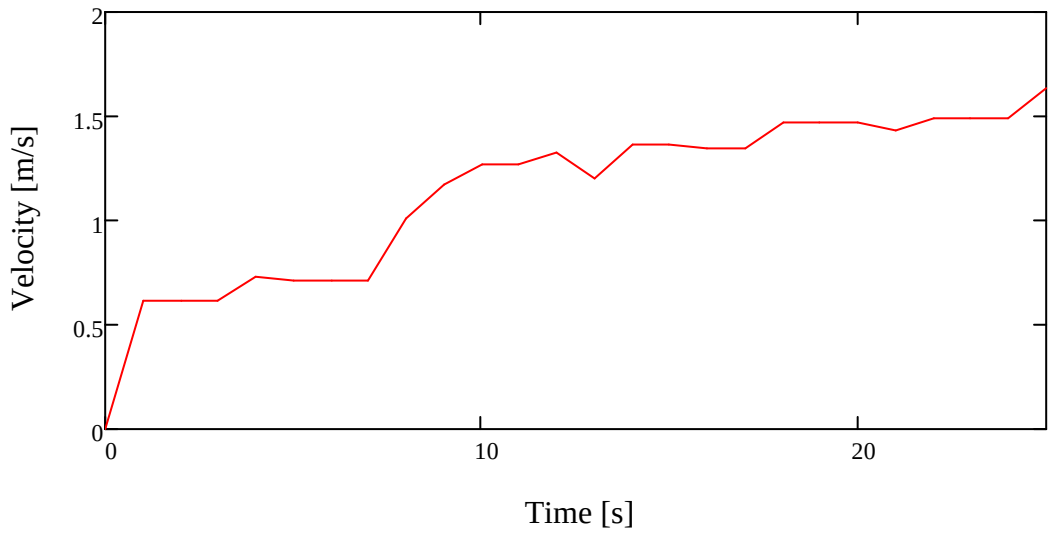

Figure 77 Recorded velocity of the third test trial in dependence of the driven time.

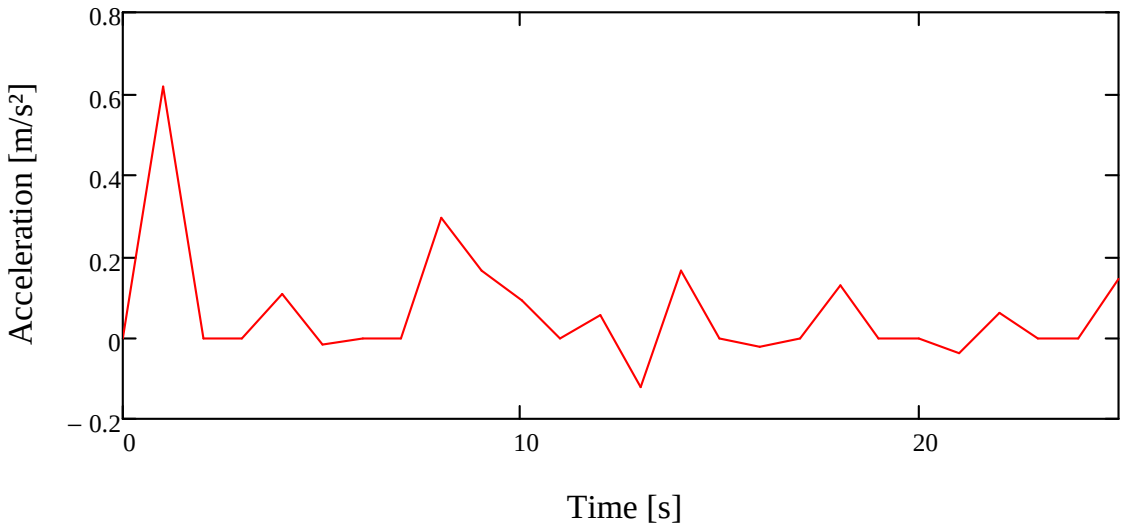

Figure 78 Resulting acceleration of the third test trial in dependence of the driven time.

5.2.4 Test Results

BRF Results

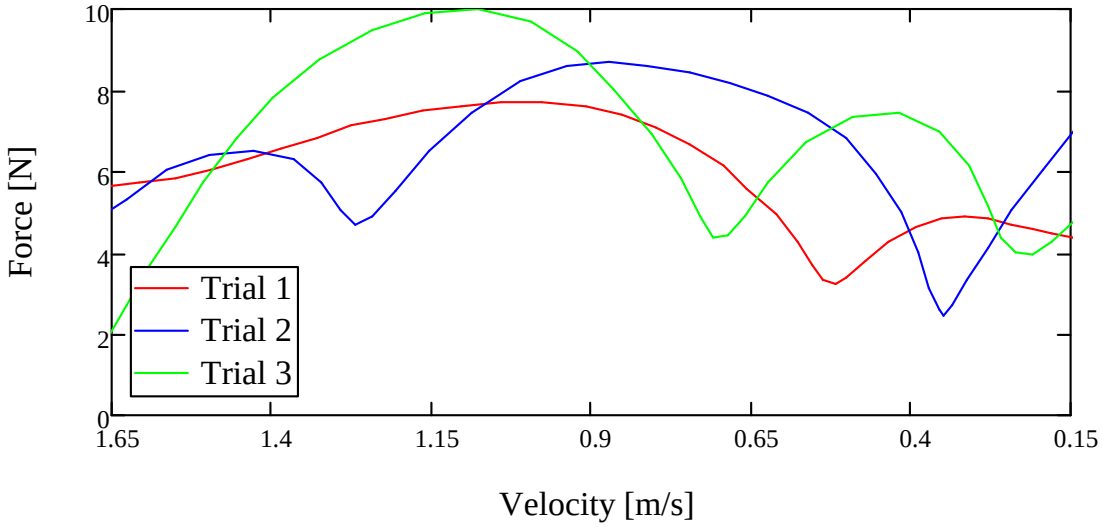

Figure 79 Diagram of the BRF in dependence of the driving velocity. The red line depicted the BRF of the first test trial, the blue line of the second test trial and the green line depicts the third trial.

All three test trials were performed under the same conditions as described in chapter 5.2.3 and resulted in a mean BRF of

$$BRF=5.8\ [N]$$

Test Trial Results

For every single trial the resulting forces, the power which was achieved as well as the mean power were computed and are displayed at Figure 80 - Figure 85.

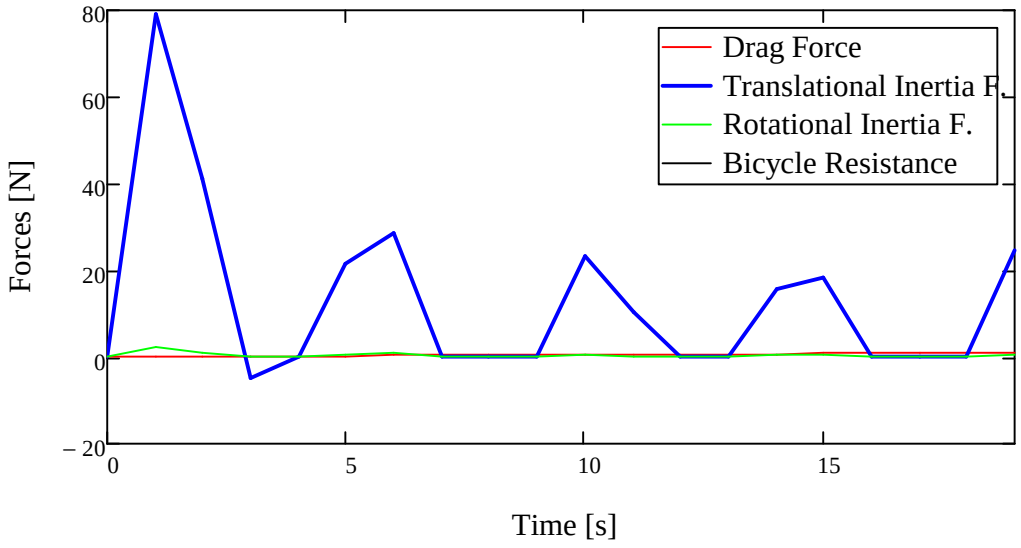

Figure 80 Diagram of the forces acting to the bicycle while accelerating in dependence of the driven time displayed for the first test trial.

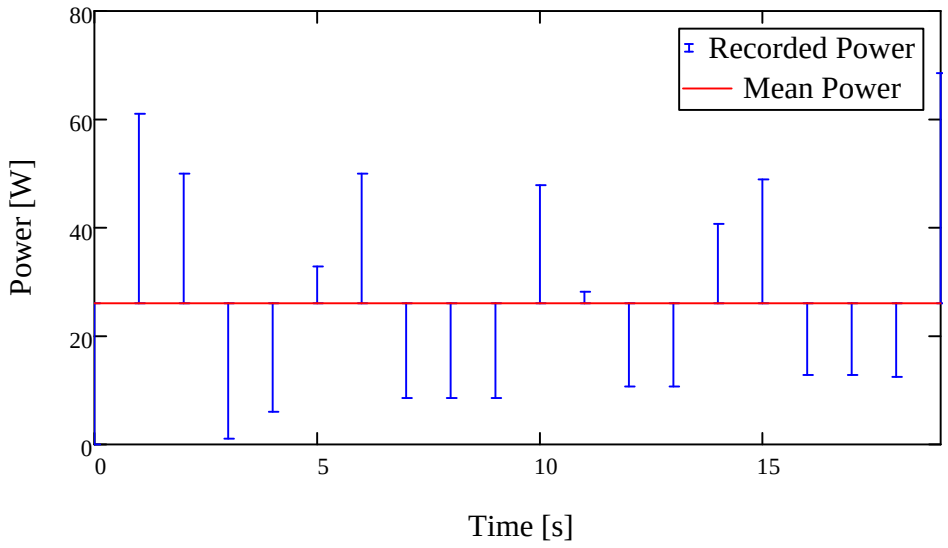

Figure 81 Diagram of the achieved power, depicted as blue bars, and the mean power, depicted as red line, in dependence of the driven time. Both processes are displayed for the first trial.

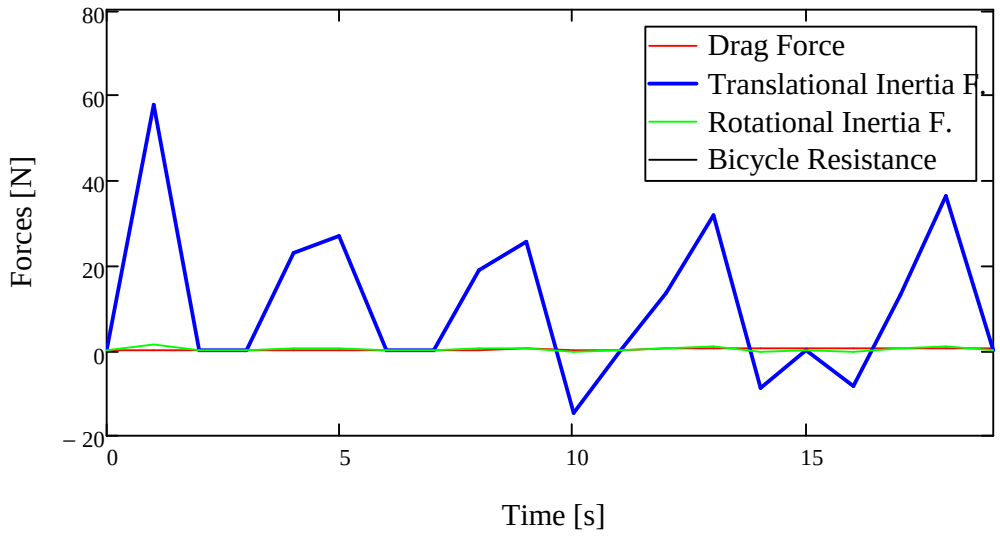

Figure 82 Diagram of the forces acting to the bicycle while accelerating in dependence of the driven time displayed for the second test trial.

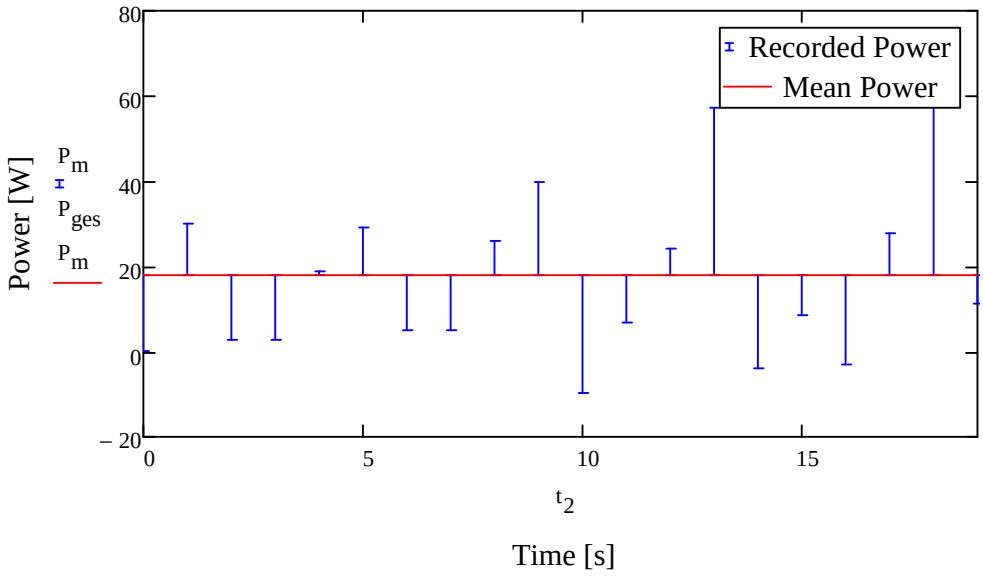

Figure 83 Diagram of the achieved power, depicted as blue bars, and the mean power, depicted as red line, in dependence of the driven time. Both processes are displayed for the second trial.

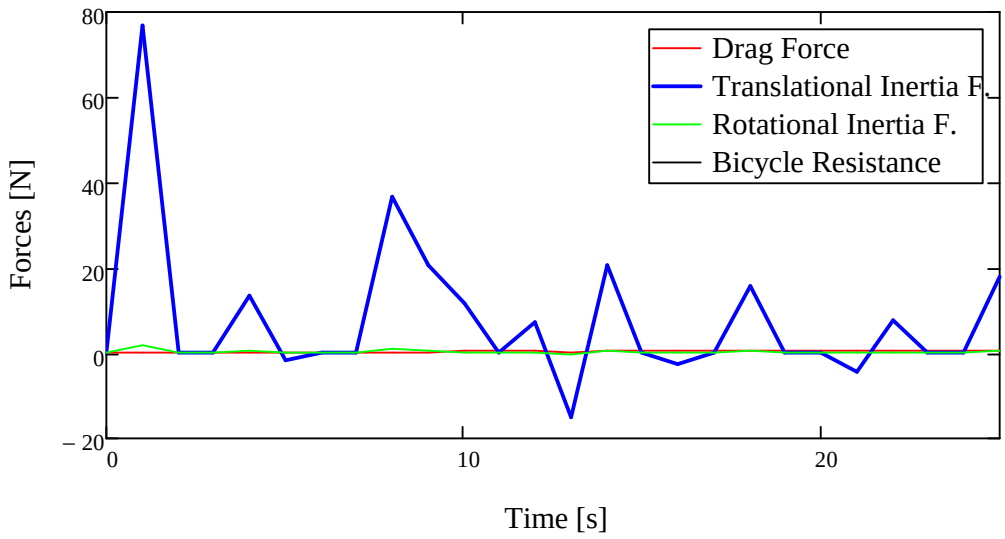

Figure 84 Diagram of the forces acting to the bicycle while accelerating in dependence of the driven time displayed for the third test trial.

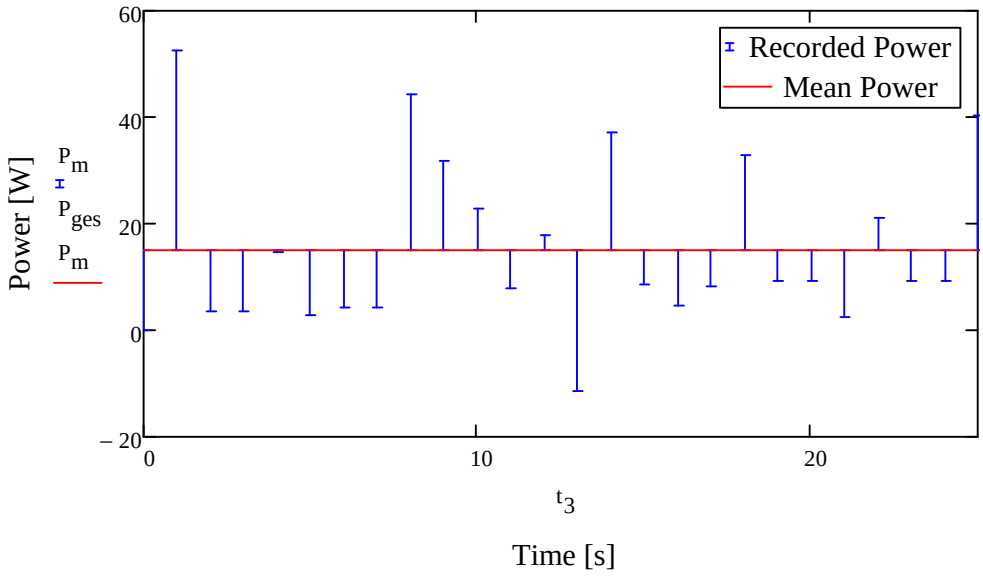

Figure 85 Diagram of the achieved power, depicted as blue bars, and the mean power, depicted as red line, in dependence of the driven time. Both processes are displayed for the third trial.

The achieved mean power was:

P1=26 [W] for the first trial

P2=17.7 [W] for the second trial

P3=15 [W] for the third trial

5.2.5 Assessment of the Designed Bicycle Components

As part of the function test also the designed components were assessed regarding their functionality. Also future improvements which can be done are mentioned.

Crank Fixation

As intended the crank fixation is easy to use and can be mounted in approximately 30 seconds. The chosen diameter is large enough to withstand the loads produced while the extension movement.

It would be an improvement to drill some additional fixation holes for the crank fixation into the chain guide of the pedal crank. This would make it possible to adjust the pedal position in smaller steps. Furthermore this would lead to an improved usage of the available guide rail length in combination with the space underneath the handle bar for different body heights.

Pedal End Stop

The Pedal End Stop was intended to avoid hyperextension of the knees. When it is adjusted correct it fulfils this requirement. While the test trials it was observed that it is important to adjust the ESC first taking into account that the knee is not already extended. Then PES can be adjusted. This order is important to follow because when the PES is adjusted first it can happen that it blocks the seat movement before the ESC is reached. This would lead furthermore to high loads at the tibia and the fibula of both legs. Particular in case of persons with paraplegia this can lead to bone fractures.

Steel was chosen as construction material for the ESC. While the test trials it was observed that this was not necessary and that it would be better to use aluminium to save weight instead. Another improvement would be to reduce the diameter of the fence itself and to implement a fixation mechanism which needs no tools.

Limit Switch Mounting and Fence

The Limit Switch Mounting and the Limit Switch Fence did operate as intended without incidence. Furthermore it is possible to adjust the limit switch position to different body heights in a few minutes.

To improve the usability when adjusting the limit switches a quick release would be more comfortable than the now used fixation by screw and nut.

End Stop Clamp

The ESC has to be adjusted when the used range of the sliding rails needs to be adapted to the body height. This can easily be done by opening the quick release. When fixated, the ESC has a good clamping behaviour and does not change position. The design is stable enough to withstand the occurring loads without showing plastic or larger elastic

deformations. As demanded the ESC does not damage the sliding rails when it is clamped to it.

Due to the little clearance, between the clamping jaws and the guiding rail, the ESC is sometimes hard to slide, without loosening the quick release further than only open the clamping lever. This could be improved by increasing the clearance. But this should be done in small steps because too much clearance would lead to rotational movement of the ESC. A further improvement would be to reduce the overall weight of the ESC by optimizing the profile of the horizontal and vertical beams as well as the guidance of the horizontal beam.

Battery Clamp

The battery clamp is able to keep the battery in position while the test trials. Whereas the BC would properly not be able to fixate the battery under extreme conditions like in case that the stimulator would drop to the ground.

To avoid destructive changes to the stimulator housing already available fixation holes were used. This fixation holes only consist of plastic like the stimulator housing and are a weak fixation possibility. To achieve a more stable fixation, destructive changes to the stimulator housing would be necessary.

Control Panel Mounting

The CPM fulfils all criteria which were claimed. The clamping to the handle bar is strong enough to avoid sliding. The position is chosen well so that the CPM does not interfere.

At the moment there is no need to recommend any changes to the CPM.

Controller

While the function test phase the controller did work without any malfunctions. The design is small enough to place the controller underneath the stimulator. Also the connectors for the cables are placed well and enable a good usability.

The controller housing is produced by 3D printing. It has shown that the thin walls of the housing, especially of the housing lid, are prone to deformation. Therefore it would be necessary to reinforce the walls with stiffening elements.

Stimulator Button Casing

The SBC did work as intended without any malfunctions. The used button, to trigger the stimulation, had the demanded pressure point. This made it possible to obvious feel when stimulation impulses are triggered. The stimulation lever showed a good accessibility and the implemented LEDs were a supportive indicator if the seat reliable reaches the limit switches and if the stimulation process is active.

When adjusting the bicycle to the driver it has to be taken care if there is enough clearance between the driver's knee and the SBC in narrow turns. A further task could be to search for positions of the SBC where this collision possibility is minimized.

Emergency Button Casing

It was not necessary to use the emergency button while the test trials because no malfunctions did occur. Nevertheless the emergency button was used several times to test its reliability. As intended the system was shut down immediately. It was found that the chosen position in the middle of the handle bar was placed well and that it is quick to reach. Also the clamping fixation did work well and hindered the EBC from sliding or tilting.

At this moment there is no need to give any improvement recommendations concerning the EBC.

5.3 Pedalling Mode – Function Test

5.3.1 Test Preparations

Like for the ed-mode a function test, to assess the functionality of the controller program and the designed mechanical- and electrical devices, was performed. For the p-mode two different tests were made. The first one took place on a test device and the second one took place on the test track.

For both tests the same test person who took part at the ed-mode tests was performing the p-mode tests. Therefore the personal data can be found in chapter 5.2.1.

Bicycle Adjustments

For the pedalling movement the pedal cranks needed to be mounted in a position 180° shifted to each other. The crank fixation bolt was removed to allow the cranks to spin. The short frontal drive chain was mounted to provide a connection to the drive wheel. The clamping device which fixates the seat to the long drive chain was loosened. The seat was placed and fixated in a position where the driver is able to sit comfortable without hyperextending his knees (Figure 86). The legs were fixated to the orthesis by belts.

Figure 86 Adjusted seat position for the p-mode. The picture shows a bend knee in the position where the leg is stretched most to avoid hyperextension.

Sensors Application

The incremental angular encoder which is needed for the p-mode is fixed to the bicycle. The output cable, of the encoder, was connected to the controller. The bicycle computer was fixed to the handle bar. Two magnets were mounted to the spokes of the frontal rim for speed detection. The velocity sensor of the BC is fixed at the bicycle fork with only little clearance to the magnets. Each time a magnet passes the BCs velocity sensor triggers a signal. The magnets were positioned towards each other. This leads to a theoretically bisection of the wheel circumference and therefore to a better detection of lower velocities.

Electrode Application

As already mentined for the p-mode four channels are necessary to stimulate the MQF and MBF. For the stimulation of the MBF on both legs, one electrode was placed anterior on the femur 4 cm proximal from the patella. The second electrode was also placed anterior on the femur 27 cm proximal from the patella. To stimulate the MBF the electrode positions were chosen according to the best muscle activation response while stimulation. The position can be found at Figure 87.

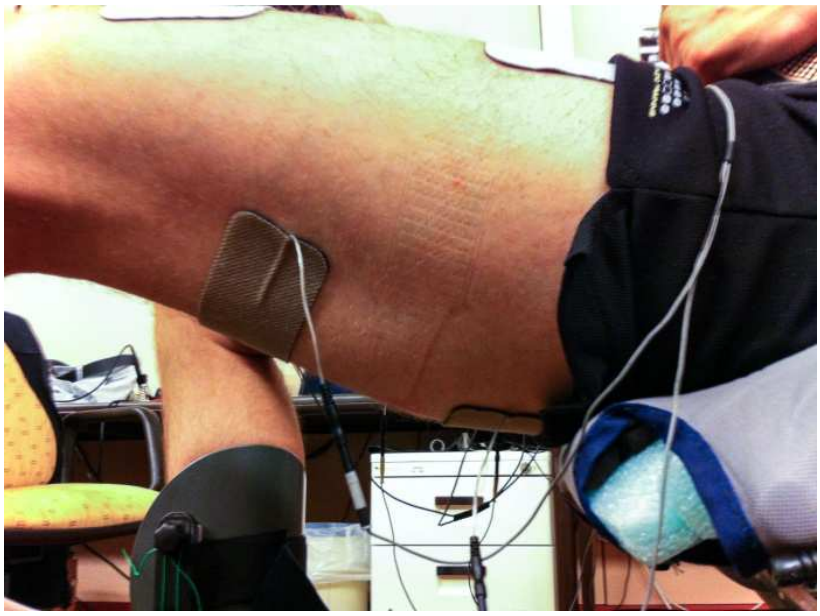

Figure 87 Position of the dorsal femural surface electrodes used to activate the BF muscle group

Controller Program

Before starting the stimulation the p-mode stimulation program was stored on the controller's microchip. A function test was performed to assure a proper performance.

5.3.2 Test device – Function Test

The test device is a frame made of steel on which the bicycle can be placed with the rear part of the bicycle frame. When placed on the device both backward wheels are without ground contact. Furthermore the bicycle is not able to move in any direction.

The test, on the test device, was performed to assess the angular stimulation regions on which the muscle groups have to be stimulated. Therefore the test person did pedal voluntarily first and the muscle activations which are necessary to achieve the movement were observed optically by the test administrator. Then the observed regions were used as basic angular stimulation regions. Following the regions were adapted regarding to the test person's feedback to achieve a pedalling movement.

The stimulation regions depicted in Figure 88 were found to produce the best results. But even there the best result which could be achieved was about two full revolutions before the movement stopped. The reason for this behaviour was that it is not possible to produce a positive driving moment for a whole revolution when only the QF and the BF muscle groups are stimulated. At the transition region between BF and QF occurs a gap without driving moment. The observed two revolutions could only be produced at high stimulation amplitudes and resulting high accelerations of the legs. In this case the force produced by the acceleration and the moment of inertia of the legs and the pedal cranks was sufficient enough to bridge the gap. But the high velocities lead to a highly

imbalanced movement which furthermore lead to the stopping of the pedalling movement.

To increase the moment of inertia a weight, with a mass of 3 kg, was placed on each pedal. With this additional, in total 6 kg, it was possible to produce a pedalling movement as long as the stimulation was active. Also the stimulation amplitude could be reduced which lead to a more balanced movement.

5.3.3 Test Track – Function Test

The same setup, which was determined at the test device before, was used at the test track. But with this setup it was not possible to achieve a full revolution neither from resting position nor from an already driving condition. The reason therefore is that only low braking forces occur on the test device. These braking forces are produced by the mass inertia of the legs, the pedal cranks and the driving wheel on one hand and by friction forces, of the drive train and the wheel bearing on the other hand. Therefore only short activation regions were necessary to produce sufficient driving force. On the test track much higher additional forces act to the bicycle, produced by the rolling resistance and mass inertia of the bicycle. Therefore the angular stimulation regions had to be adapted to broader stimulation regions (Figure 88). It was also necessary to remove the additional added 6 kg weight because of the braking moment they produce. At the test track this braking moment has more influence then the driving moment produced by it.

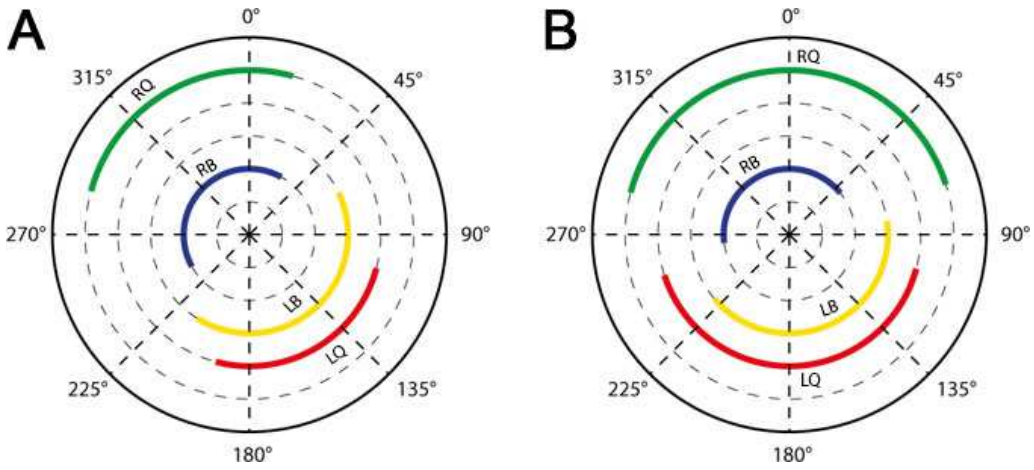

Figure 88 Angular stimulation regions with the best results to produce a pedal movement. Picture A represents the determined angular stimulation regions at the test device. Picture B displays the regions determined at the test track. The stimulated muscle groups are RQ = quadriceps femoris of the right leg, RB = biceps femoris of the right leg, LQ = quadriceps femoris of the left leg and LB = biceps femoris of the left leg. (adapted from [1])

But even by adapting the stimulation regions it was not possible to achieve a pedalling movement, neither from standing nor from already driving condition. This was due to

the driving moment gap in the region between MQF and MBF on one hand and the weak produced force by MBF on the other hand.

5.3.4 Assessment of the Designed Bicycle Components

Chain Tensioner (CT)

The CT was able to keep the chain in line and produced sufficient preload to avoid a loss of the driving chain.

A further improvement would be to use steel as construction material instead of aluminium for the adapter to guarantee more stability. Also the clearance between the CT and the pedal should be increased by slightly remove material from the pedal. This was not possible in this work because of the requirements.

6 Conclusion and Outlook

Modifications were realised to enable the recumbent bicycle to be used for an investigation of FES-cycling with persons suffering of flaccid paraplegia. As demanded this modifications were done non destructive which allows to remove all added devices without residues. The modifications included mechanical parts and devices which were necessary to enable the required functionality on one hand and to increase the safety on the other hand. Electrical devices were designed to serve as link between the stimulator, the bicycle and the test person as well as to provide the necessary electrical safety measures.

Tests with healthy persons were performed for the ed-mode and the p-mode to assess the modifications and the functionality of the bicycle in general. The function test of the ed-mode could be accomplished successfully. It was possible to drive with the bicycle as intended without any support sole by electrical stimulation. The designed parts and elements did perform as intended. Concerning the original design it was observed that the chain clamping device, which links the seat to the driving chain, does not work properly. When high driving forces were produced it sometimes happened that the chain did slide and produce cracking sounds. Also the guidance of the seat was found to be designed incorrect because both bearing sides are designed as solid bearing. This lead to the destruction of one bearing while the test phase.

The p-mode test could not be accomplished successfully. It was not possible to achieve a pedalling movement while driving neither from standing position nor from already driving position. This was not possible because of a lack of driving torque in the angular region between MBF and MQF. But it was possible to achieve a pedalling movement when the load was reduced at the driving wheel and additional weight was fixed to the

pedals. But like before at the ed-mode test the designed components could be tested and did work as intended.

A further task is to enable the p-mode. Therefore the problem of the driving torque gap has to be solved. In FES-bicycles without gear box this can easily be done by removing the freewheel and therefore fix the driving chain to the driving wheel. This is no option in this case since the bicycle needs a free wheel to enable the ED-mode. Therefore one possibility would be to fix a flywheel with sufficient moment of inertia to the pedal cranks. This moment of inertia would produce the missing driving torque in the gap between MBF and MQF. The advantage of this probability is that it does not need any controlling, power supply or additional supply devices. The disadvantages are that due to the needed mass the resulting dimensions of the flywheel would it make critical to implement. Furthermore it would increase the bicycles overall mass. Another disadvantage would be that the increased mass also leads to an increased moment of inertial when accelerating the bicycle. This would result in to high resistances especially in case of starting from standing position and when driving uphill. Another possibility is to link the driving gear with an electrical engine. This engine would produce the needed driving torque. One possibility would be to produce a constant driving torque with the engine high enough to overcome the resistance at the driving torque gap. Another possibility is to control the electric engine and to activate it only in the gap region. The advantage of the second possibility is that the electric engine does not provide much mass to the overall mass of the bicycle and does therefore lead to a much higher moment of inertia. Depending on the chosen version it would also be possible to control the produced torque and adapt it to the driving situation and for example increase the produced torque when starting from standing position. The disadvantage of using an electric engine is that the electrical and the mechanical implementations are more complex. Especially in the case of a controlled electric engine.

Another further task is to perform driving tests with a test person suffering of flaccid paraplegia. This can already be done for the ed-mode which works at healthy persons and for which it is expected to work also for persons with flaccid paraplegia. To perform a p-mode test one of the modifications mentioned before has to be done prior.

Bibliography

[1]. **Christoph, Kast.** Control Electronics for Cycling with FES Activated Denervated Muscles. 2014.

[2]. *Spektrum der Wissenschaft.* **Jesper L Andersen, Peter Schjerling, Bengt Saltin.** März 2001, S. 70-75.

[3]. **Adolf Faller, Michael Schünke, Gabriele Schünke.** *Der Körper des Menschen.* 15. Auflage. s.l. : Thieme, 2008.

[4]. **St. Silbernagl, A. Despopoulos.** *Tschenatlas der Physiologie.* 7. s.l. : Thieme, 2007.

[5]. **Helmut Kern, MD, Katia Rossini, DBiol, Ugo Carraro, MD, Winfried Mayr, PhD, Michael Vogelauer, MD, Ursula Hoellwarth, MD, Christian Hofer, DEng.** Muscle biopsies show that FES of denervated muscles reverses human muscle degeneration from permanent spinal motorneuron lesion. *JRRD - Journal of Rehabilitation Research & Development.* May/June 2005, Vol. 42, pp. 43-54.

[6]. **Simona Boncompagni, Helmut Kern, Katia Rossini, Christian Hofer, Winfried Mayr, Ugo Carraro and Feliciano Prostasi.** Structural differentiation of skeletal muscle fibres in the absence of innervation in humans. *PNAS - Proceedings of the National Academy of Sciences.* December 2007, Vol. 104, S. 19339-19344.

[7]. **H Kern, C Hofer, M Mödlin, W Mayr, V Vindigni, S Zampieri, S Boncompagni, F Protasi, U Carraro.** Stable muscle atrophy in long-term paraplegics with complete upper motor neuron lesion from 3- to 20 year SCI. *Spinal Cord.* 2008, 46, pp. 293 - 304.

[8]. **Helmut Kern, Christian Hofer, Winfried Mayr, Simona Bancompagni, Ugo Carraro, Feliciano Protasi, Michaela Mödlin, Claudia Straub, Michael Vogelbauer, Stefan Löfler.** Elektrostimulation komplett denervierter Muskulatur. [Buchverf.] Veronika Fialka-Moser. *Kompendium Physikalische Medizin und Rehabilitationstechnik.* s.l. : Springer, 2013.

[9]. **D.Bader, C. Bouten, D. Colin, C. Oomens.** *Pressure Ulcer Reserch.* s.l. : Springer, 2005.

[10]. **Marca L. Sipski, MD, Joel A. Delisa, MD, and Due Schweer, PT.** Functional Electrical Stimulation Bicycle Ergometry: Patient Perceptions. *American Journal of Physical Medicine & Rehabilitation.* June 1989, Vol. 68, pp. 147-149.

[11]. **Chih-Wei Peng, Shihi-Ching Chen, Chien-Hung Lai, Chao-Jung Chen, Chien-Chih Chen, Joseph Mizrahi, Yasunobu Handa.** Reviwe: Clinical Benefits of Functional Electrical Stimulation Cycling Exercise for Subjects with Central Neurological Impairments. *Journal of Medical and Biological Engineering.* 2011, 31.

[12]. **Jerrold S. Petrofsky, Roger M. Glaser.** *Vehicle for the Paralyzed.* USA, 20. December 1983.

[13]. **Glaser RM, Gruner JA, Feinberg SD, Collins SR.** Locomotion via Paralyzed Leg Muscle: Feasibility Study for a Leg-Propelled Vehicle (Abstract). *Journal of Rehabilitation Research&Development.* 1983, Bd. 20, S. 87-92.

[14]. **J J Laskin, E A Ashley, L M Oenik, R Burnham, D C Cumming, R D Steadward, G D Wheeler.** Electric Stimulation Assisted Rowing Exercise in SPinal Cord Injuried People. A Pilot Study. *Internation Medial Society of Paraplegia.* 1993, 31, S. 534-541.

[15]. **EJ, Kennedy.** *Spinal Cord Injury: Facts and Figures.* Birmingham : University of Alabama Press, 1986.

[16]. **Edwards BG, Marsolais EB.** Metabolic responses to arm ergometry and functional neuromuscular stimulation. *Journal of Rehabilitation Research and Development.* 1990, 27, S. 107-114.

[17]. **Hooker SP, Figoni SF, Rodgers MM, Glaser RM, Mathews T, Suryaprasad AG et al.** Metabolic and Hemodynamic Responses to concurrent Voluntary Arm Crank and Electrical Stimulation Excersise in Quadriplegic. *Journal of Rehabilitation Research and Development.* 1992, 29, S. 1-11.

[18]. Therapeutic Alliances Inc. [Online] [Zitat vom: 22. 09 2014.] http://www.musclepower.com/.

[19]. Restorative Therapies. [Online] [Zitat vom: 22. 09 2014.] http://www.restorative-therapies.com/.

[20]. HASOMED. [Online] [Zitat vom: 22. 09 2014.] http://www.hasomed.de/de/home.html.

[21]. BERKEL BIKE. [Online] [Zitat vom: 22. 09 2014.] http://www.berkelbike.de/.

[22]. MOTOmed. [Online] [Zitat vom: 22. 09 2014.] http://www.motomed.com/en.html.

[23]. Thera Trainer. [Online] [Zitat vom: 2014. 09 22.] http://www.thera-trainer.de/cms/.

[24]. HASE BIKES. [Online] [Zitat vom: 22. 09 2014.] http://hasebikes.com/12-0-Startseite.html.

[25]. **Kern, Helmut.** Funktionelle Elektrostimulation paraplegischer Patienten. *European Journal of Translational Myology.* 2014, S. 75-157.

[26]. **Rahman Davoodi, Brian J. Andrews, Garry D. Wheeler, Robert Lederer.** Development of an Indoor Rowing Machine With Manuak FES Controll for Total Body Exercise in Paraplegia. *IEEE Transactions on Neural Systems and Rehabilitation Engineering.* September 2002, Bd. No. 3, Vol. 10.

[27]. **Alojz R. Kralj, Tadej Bajd.** *Functional Electrical Stimulation: Standing and Walking After Spinal Cord Injury.* s.l. : CRC Press Inc, 1989.

[28]. **Alojz Kralj, Slobodan Grobelnik.** Functional Electrical Stimulation - A New Hope for Paraplegic Patients? *Bulletin of Prosthetics Research.* 1973.

[29]. **K. John Klose, Patrick L. Jacobs, James G. Broton, Rosalind S. Guest, Belinda M. Needham-Shroshire, Nathan Lebwohl, Mark S. Nash, Barth A. Green.** Evaluation of a Training Program for Persons With SCI Paraplegia Using the Parastep 1 Ambulation System: Part 1. Ambulation Performance and Anthropometric Measures. *Archives of Physical Medicine and Rehabilitation.* August 1997, 78.

[30]. SIGMEDICS, INC. [Online] [Zitat vom: 26. 09 2014.] http://www.sigmedics.com/.

[31]. **Mayr W., Hofer C., Kern H., Bijak M., Lanmüller H., Rafolt D., Stöhr H., Unger E.** The European R&D Project RISE - Use of Electrical Stimulation to Restore Standing in Paraplegic With Long-Term Denervated Degenerated Muscles (DDM). *Proceedings of the 9th Vienna International Workshop on Functional Electrical Stimulation.* 2007.

[32]. Reha-Funtrike. [Online] OVG Marketing und Vertriebs GmbH, 2003.

[33]. **Biegelmeier, Kieback, Kiefer, Krefter.** *Schutz in elektrischen Anlagen - Band 1: Gefahren durch den elektrischen Strom.* Berlin : VDE Verlag, 2003.

[34]. **GmbH, DR. SCHUHFRIED MEDIZINTEHNIK.** Operating Instructions - Stimulette den2x. Wien : DR. SCHUHFRIED MEDIZINTEHNIK GmbH.

[35]. **T.Mohr, et al.** Increased Bone Mineral Density after Prolonged Electrically Induced Cycle Training of Paralyzed Limbs in Spinal Cord Injured Man. *Calcified Tissue International.* 1996, 61, S. 22-25.

[36]. **Hofer, Christian.** *Functional Electrical Stimulation of Human Denervated Muscle: Technical Equipment and Patient Study.* Wien : s.n., 2008.

[37]. TENSWELT. [Online] [Zitat vom: 13. 11 2014.] http://www.tenswelt.de/elektroden/stimex-ske/stimex-50x130mm.html.

[38]. **Panasonic.** ASQ1 Turquise Stroke Switches - Datasheet.

[39]. **Hengstler.** Incremental Encoders - Datasheet. *Hengstler.* 2001.

[40]. **Jürgen Dankert, Helga Dankert.** *Technische Mechanik - Statik, Festigkeitslehre, Kinematik/Kinetik.* 4.Auflage. s.l. : Teubner, 2006.

[41]. **Gressmann, Michael.** *Fahrradphysik und Biomechanik.* s.l. : Delius Klasing Verlag, 2005.

[42]. Deutscher Wetterdienst. [Online] [Zitat vom: 19. 08 2014.] http://www.deutscher-wetterdienst.de/lexikon/download.php?file=Standardatmosphaere.pdf.

[43]. **E. Rummich, E. Schmidt.** *Unterlagen zur Vorlesung Grundlagen der Elektrotechnik für MB und VT.* Wien : Institut für Elektrische Antriebe und Maschinen, 2007.

[44]. **E.Rummich, Th. Wolbank.** *Skriptum zur Vorlesung 327.040 Grundlagen der Elektronik für MB, WI-MB.* s.l. : Institut für Elektrische Antriebe und Maschinen, 2008.

[45]. **AUTODESK.** AUTODESK INVENTOR 2014 HELP. [Online] [Cited: 16 05 2014.] http://help.autodesk.com/view/INVNTOR/2014/ENU/?guid=GUID-B73B2C75-4AA4-4F9E-9BC4-4AB8D26C1765.

[46]. **L. Griffin, M.J. Decker, J.Y. Hwang, B. Wang, K. Kitchen, Z. Ding, J.L. Ivy.** Functional Electrical Stimulation Cycling Improves Body Composition, Metabolic and Neural Factors in Persons with Spinal Cord Injury. *Journal of Electromyography and Kinesiology.* 2009, 19, pp. 614-622.

[47]. **Frotzler A., Coupaud S., Perret C., Kakebeeke T.H., Hunt K.J., Nick de Donaldson, Eser P.** High-Volume FES-Cycling Partially Reverses Bone Loss in People with Chronic Spinal Cord Injury. *Bone.* 2008, 43, S. 169-176.

[48]. **Jerrold S Petrofsky, Chandler A. Phillips, Harfy H. Heaton, Roger M. Glaser.** Bicycle Ergometer for Paralyzed Muscle. *Journal of Clinical Engineering.* January-March 1984.

Appendix

A1 Technical Drawings

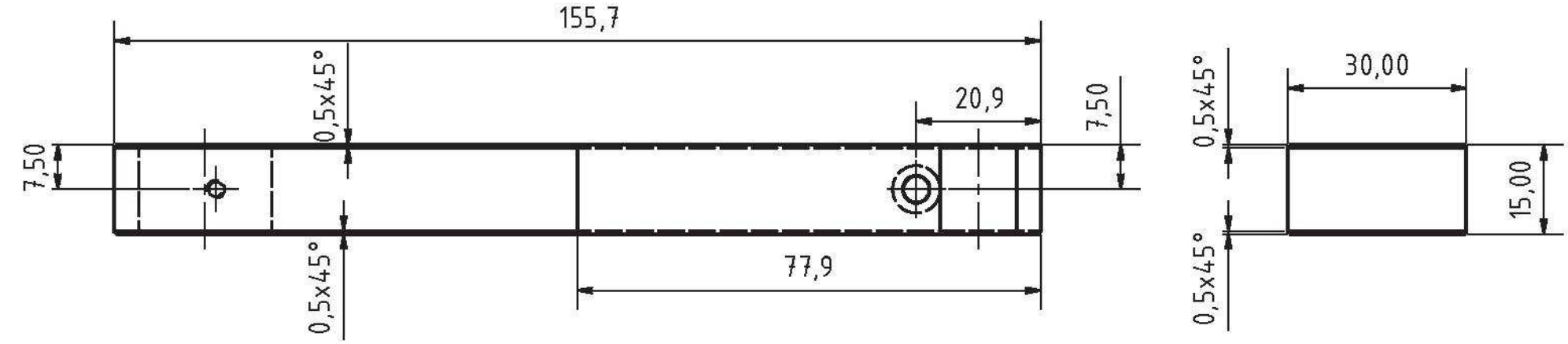

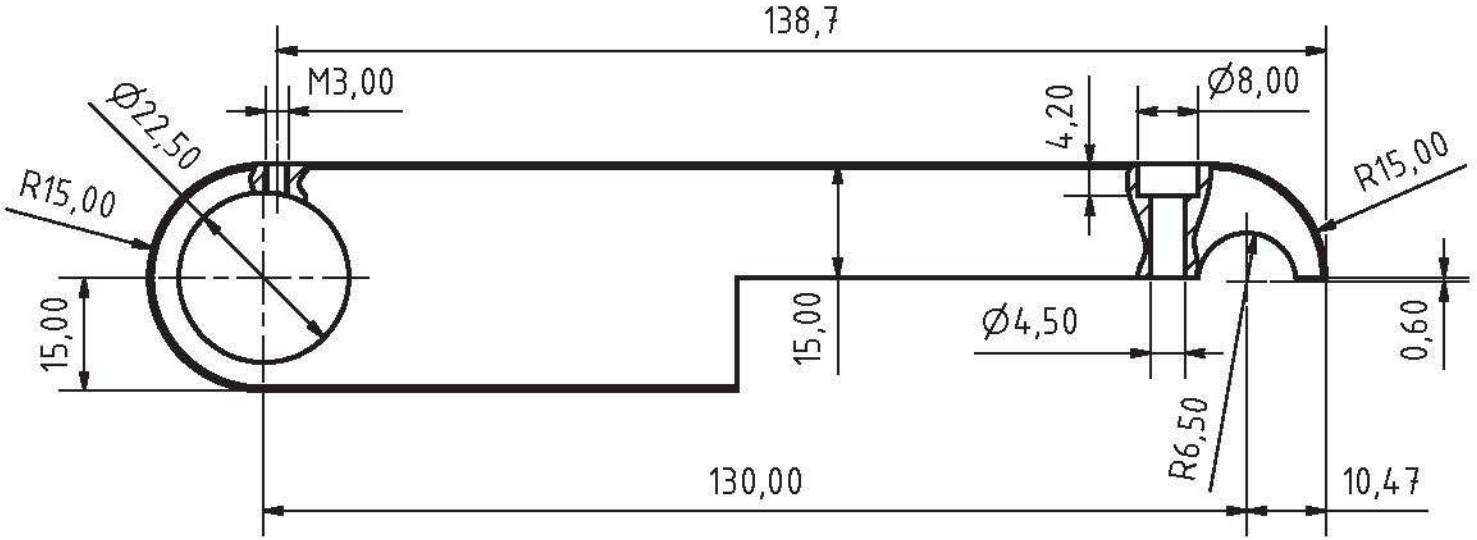

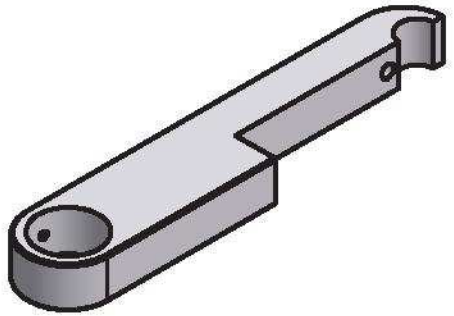

2 Stück
Material: Aluminium

					Datum	Name
				Gezeichnet	15.04.2013	Thomas Egger
				Kontrolliert		
				Norm		
Status	Änderungen	Datum	Name			

CPM-Oberteil

M 1:1

XXX

1

A4

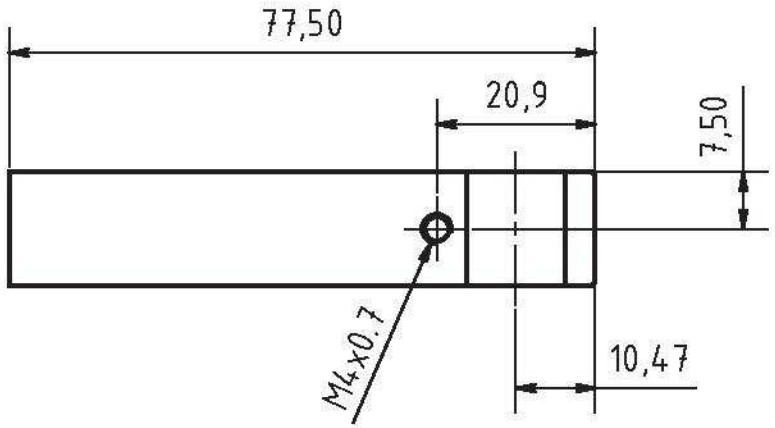

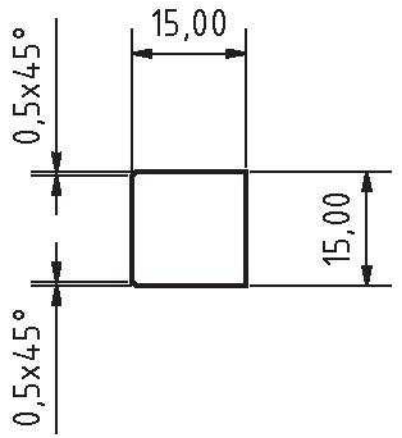

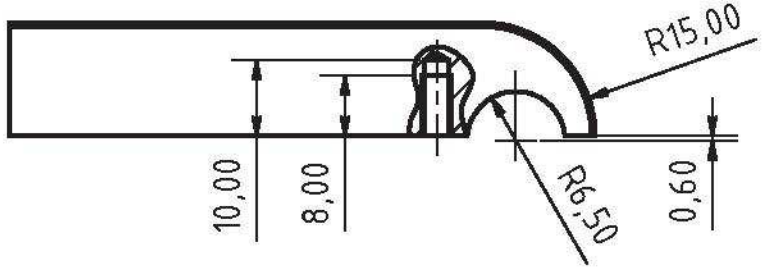

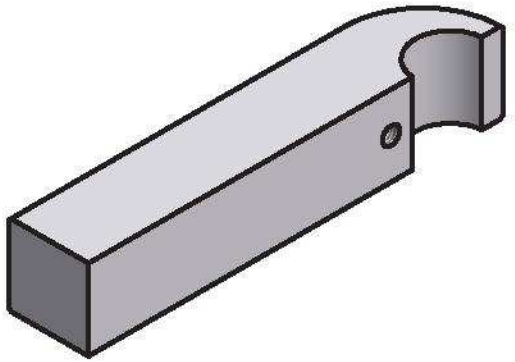

2 Stück
Material: Aluminium

					Datum	Name	CPM-Unterteil
				Gezeichnet	15.04.2013	Thomas Egger	
				Kontrolliert			
				Norm			
				M 1:1		XXX	1
Status	Änderungen	Datum	Name				A4

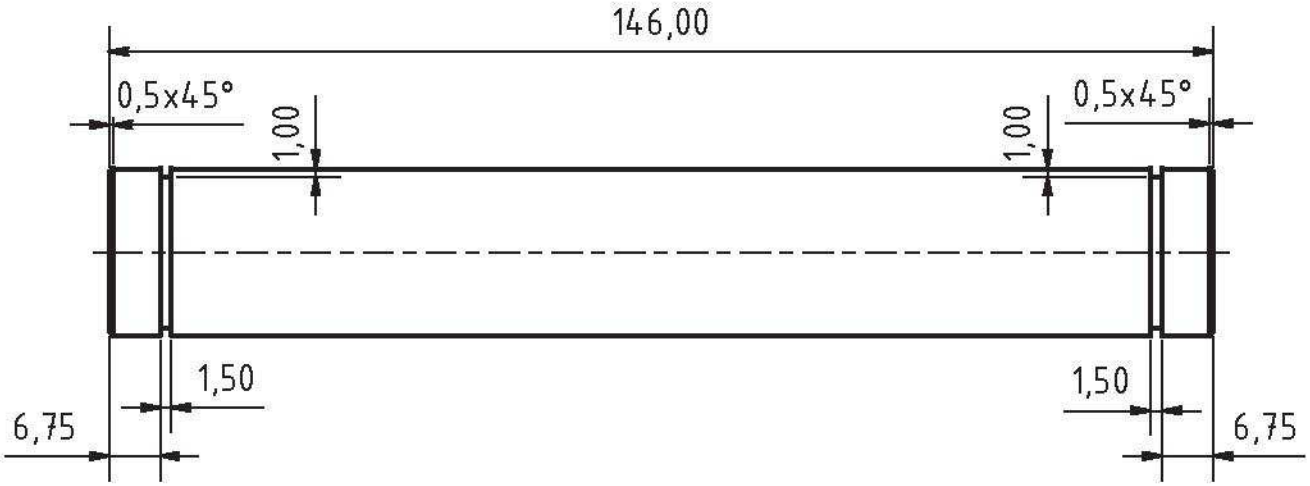

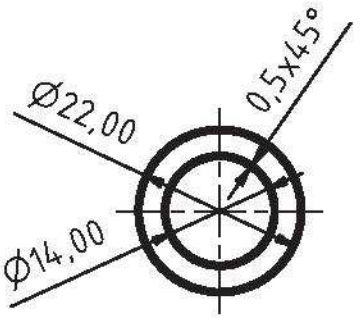

1 Stück
Material: Aluminium

					Datum	Name
				Gezeichnet	15.04.2013	Thomas Egger
				Kontrolliert		
				Norm		
				M 1:1	XXX	1 / A4
Status	Änderungen	Datum	Name			

CPM-Rohr

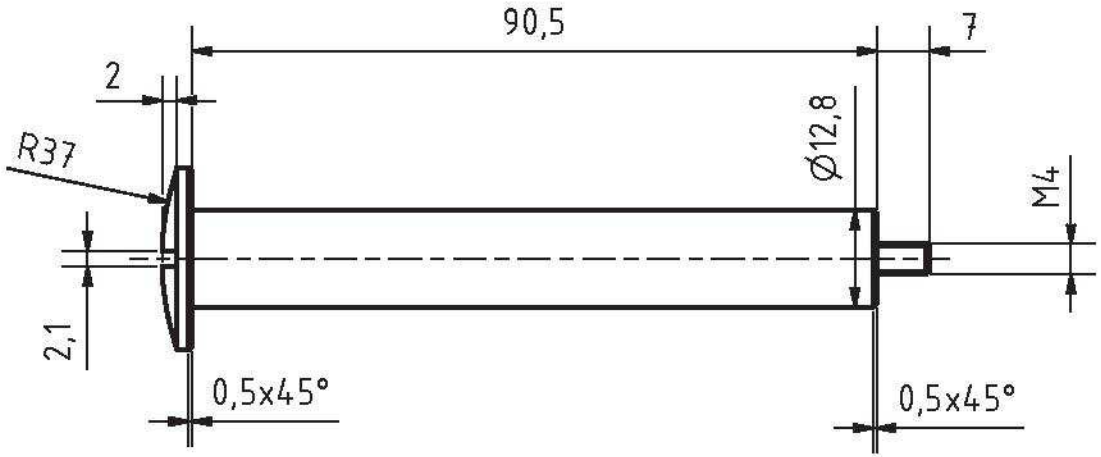

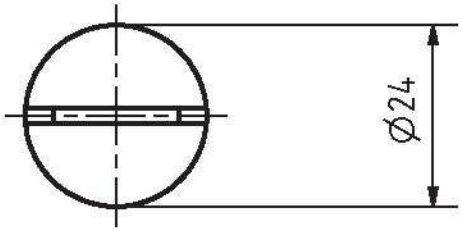

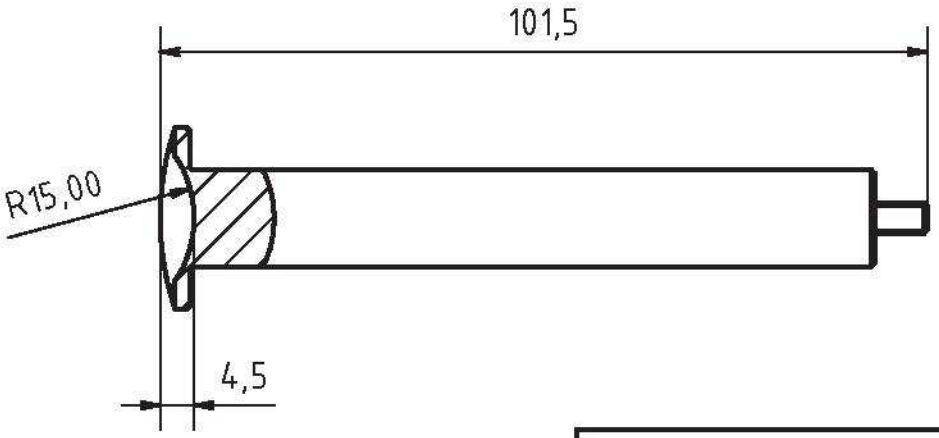

					Datum	Name
				Gezeichnet	11.04.2013	Thomas Egger
				Kontrolliert		
				Norm		
Status	Änderungen	Datum	Name			

Fixationsbolzen-V2

M 1:1

XXX

1

A4

1 Stück
Material: Stahl

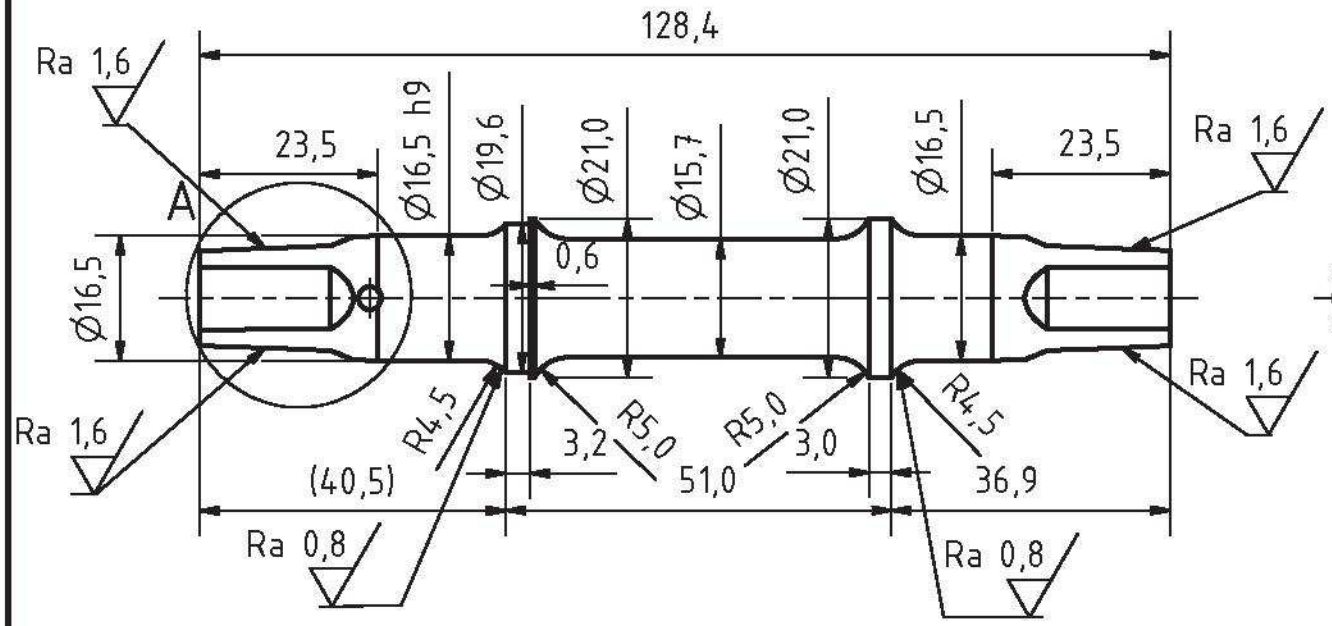

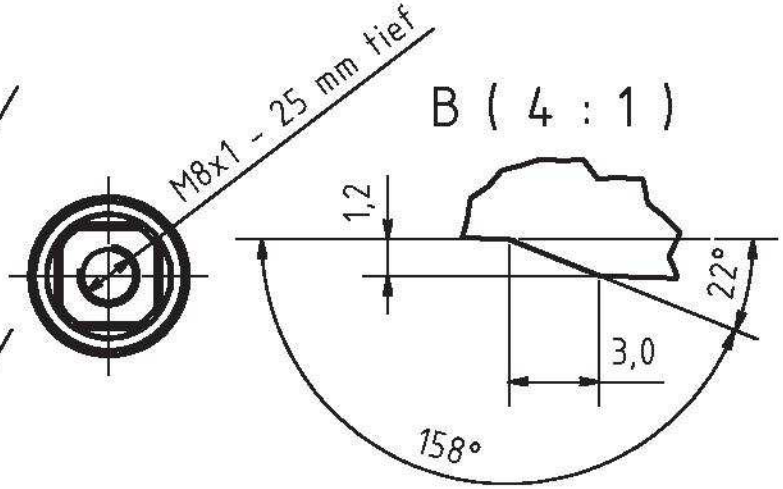

A (2 : 1)- Detail Vierkant

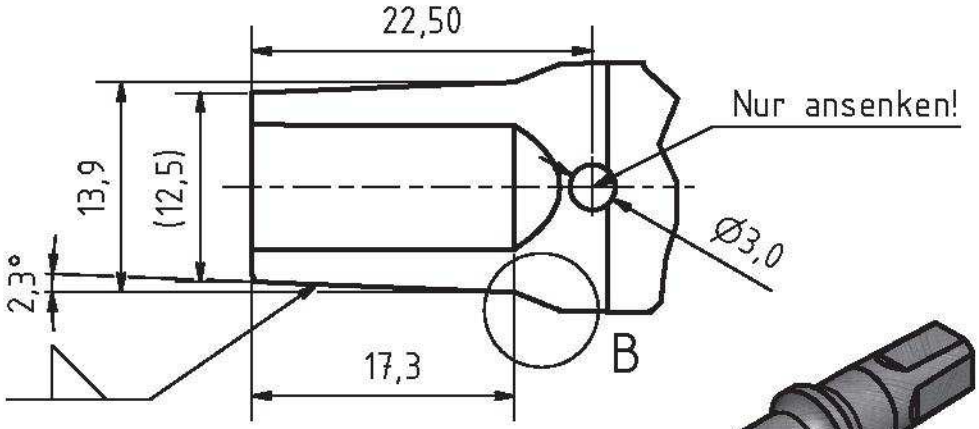

(2 : 1) - Detail Kegel

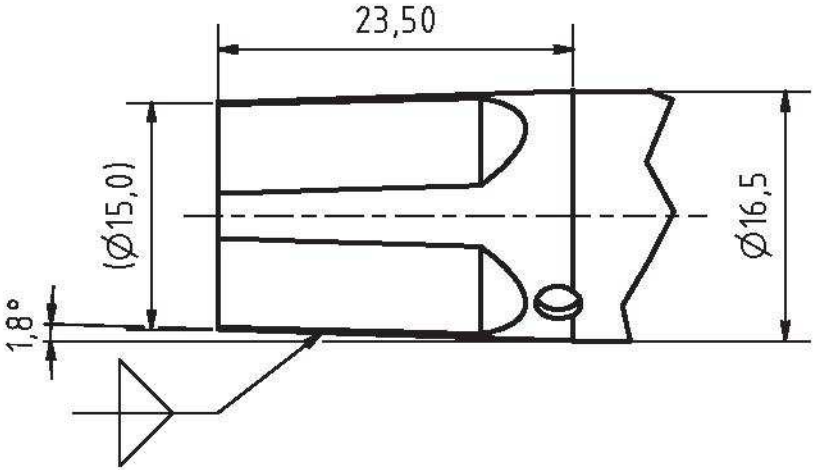

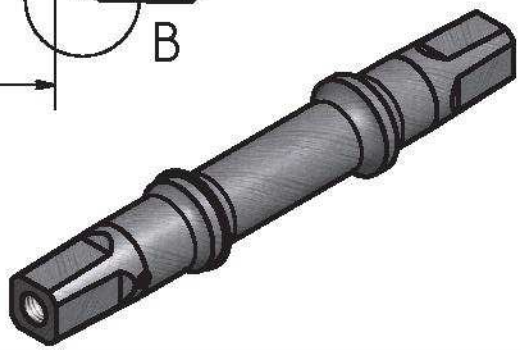

Material: Stahl

	Datum	Name	
Gezeichnet	22.05.2013	Thomas	BBS-Welle
Kontro..iert			
Norm			
M 1:1	XXX		1 A4

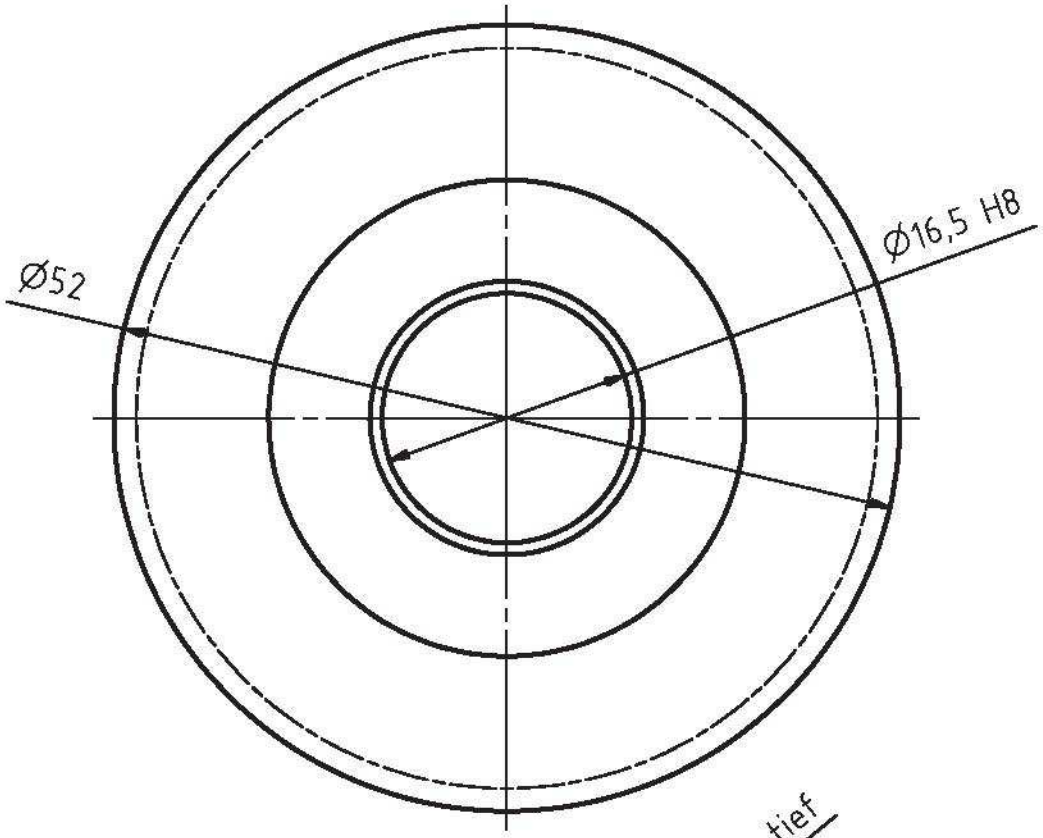

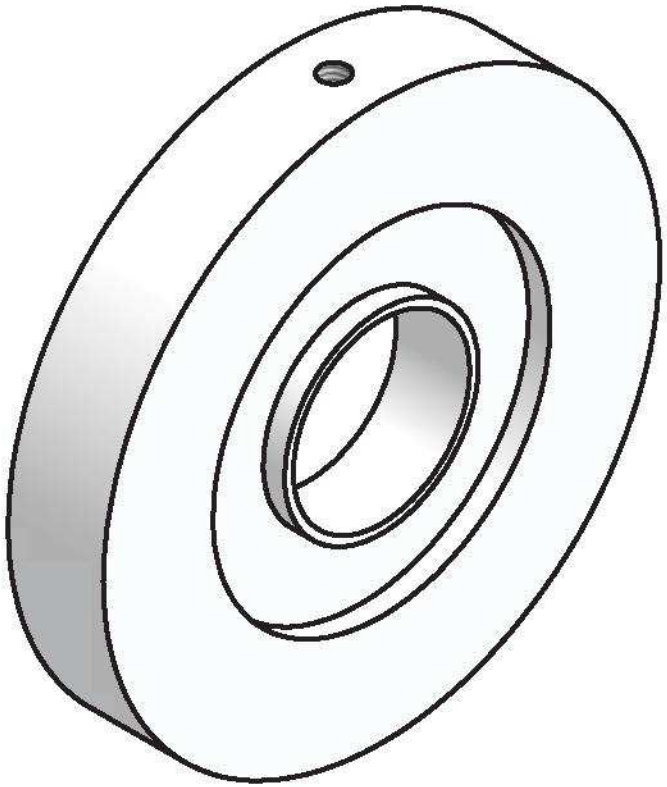

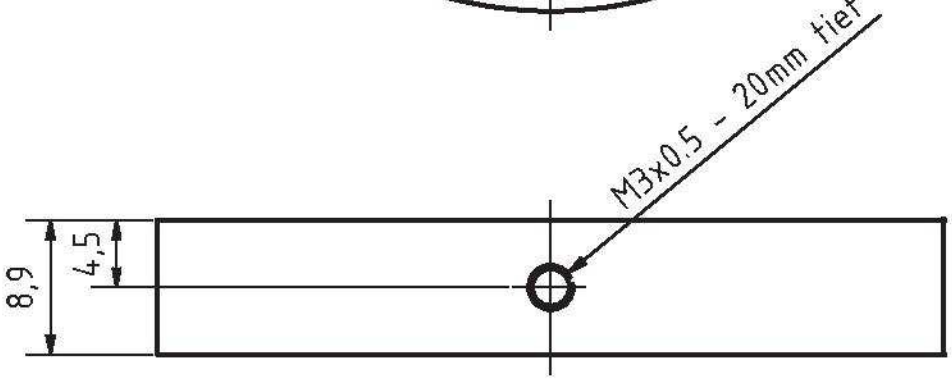

Material: Kunststoff

	Datum	Name	
Gezeichnet	29.05.2013	Thomas	BBS-Zahnrad_Nachbearb.
Kontrolliert			
Norm			
M 2:1	XXX		1 / A4

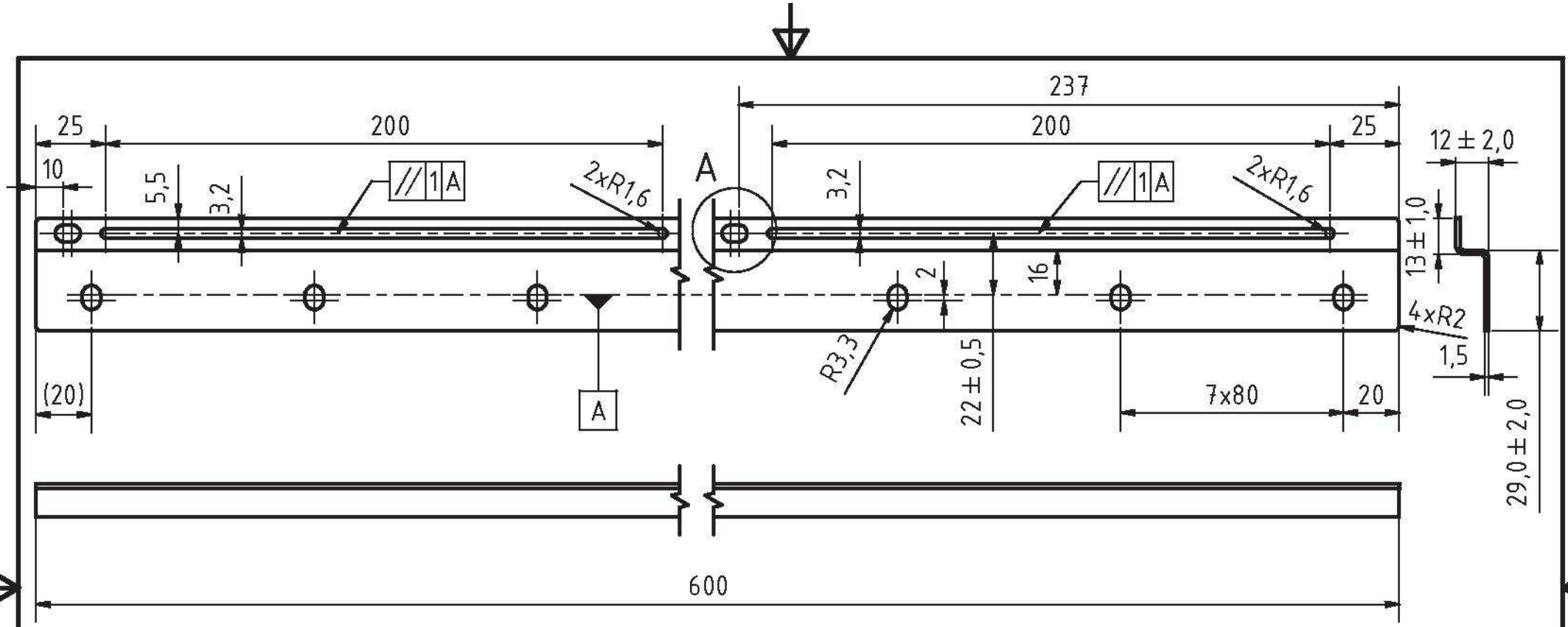

A (1 : 1)-Detail Langloch (2x)

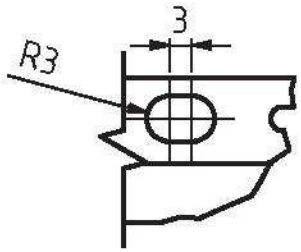

Material: Aluminium

	Datum	Name	
Gezeichnet	06.06.2013	Thomas	LS-Schiene
Kontrolliert			
Norm			
M 1:2	XXX		1 / A4

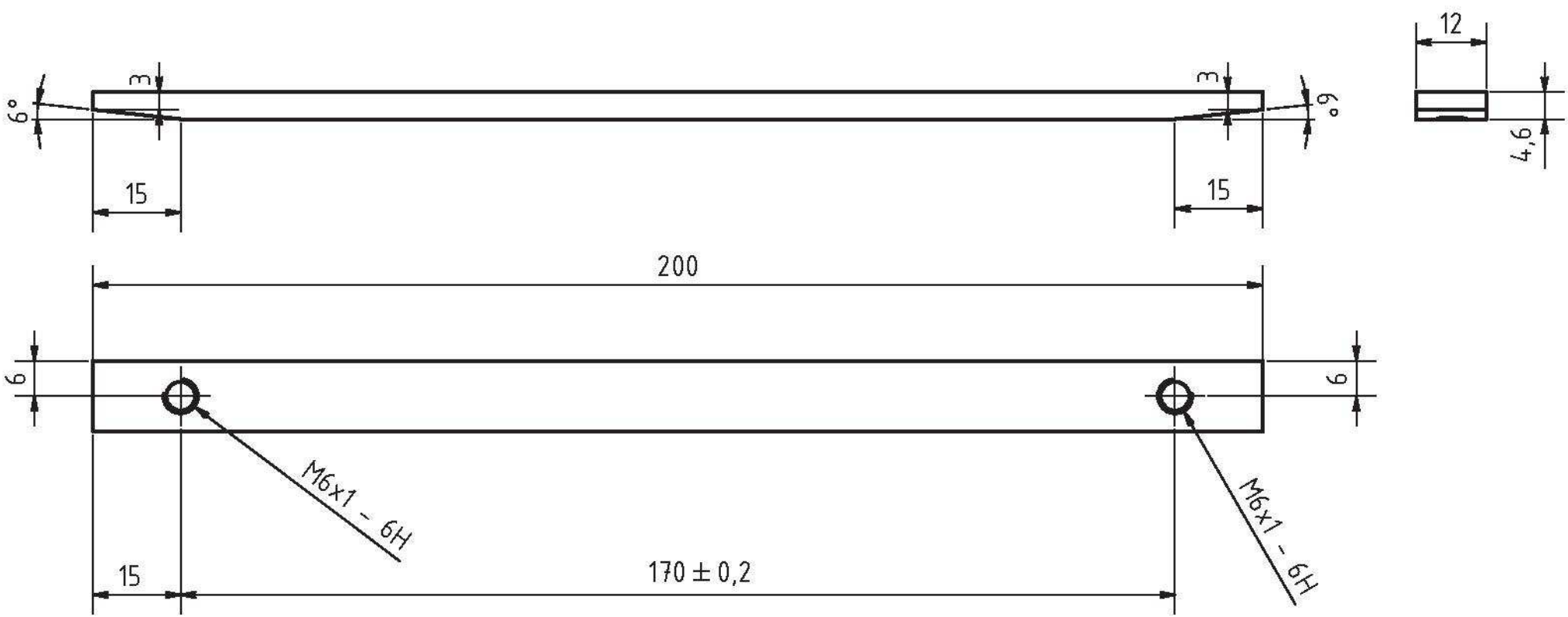

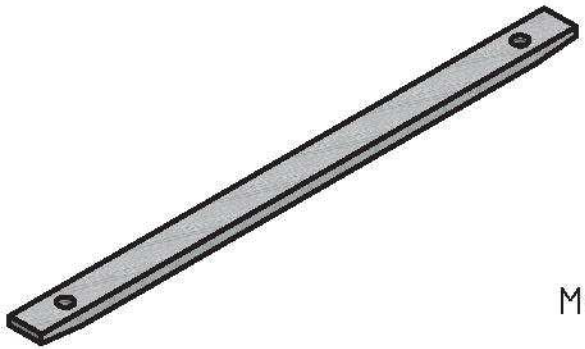

Material: Stahl

	Datum	Name	
Gezeichnet	07.06.2013	Thomas	LS-Anschlag
Kontrolliert			
Norm			
M 1:1	XXX		1 A4

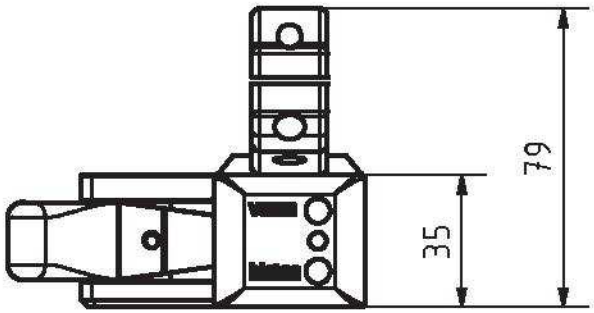

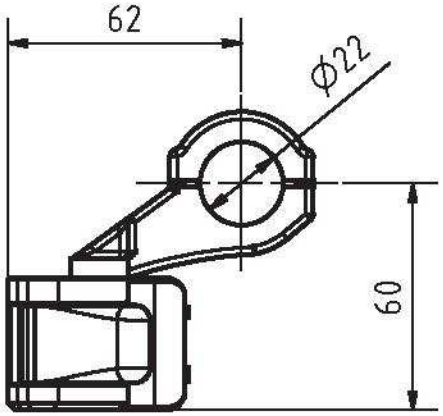

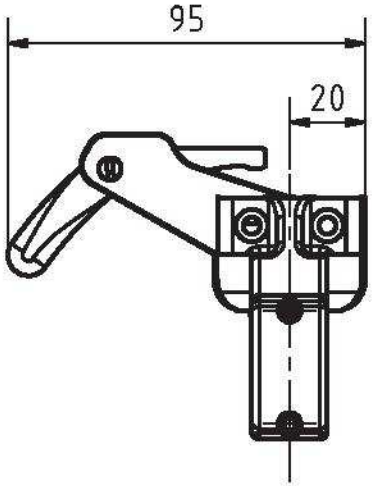

					Datum	Name	SBC-Gehäuse
				Gezeichnet	28.10.2014	Thomas	
				Kontrolliert			
				Norm			
				M 1:2		XXX	1 / A4
Status	Änderungen	Datum	Name				

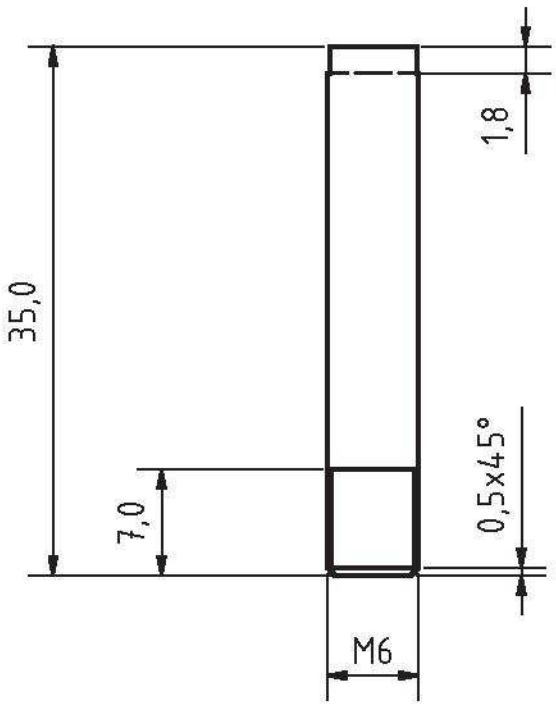

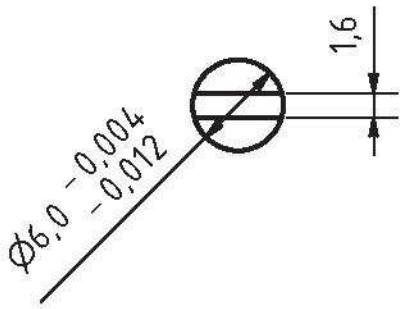

	Datum	Name	
Gezeichnet	10.07.2013	Thomas	SBC-Achse
Kontrolliert			
Norm			
M 2:1	XXX		1 A4

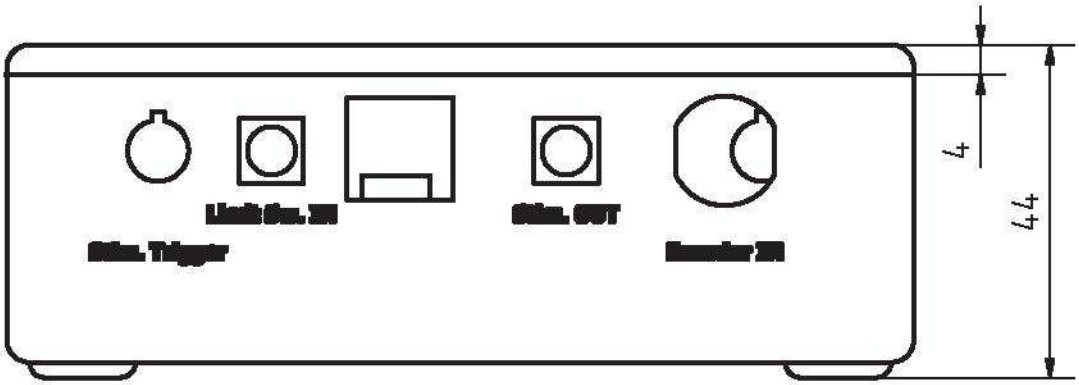

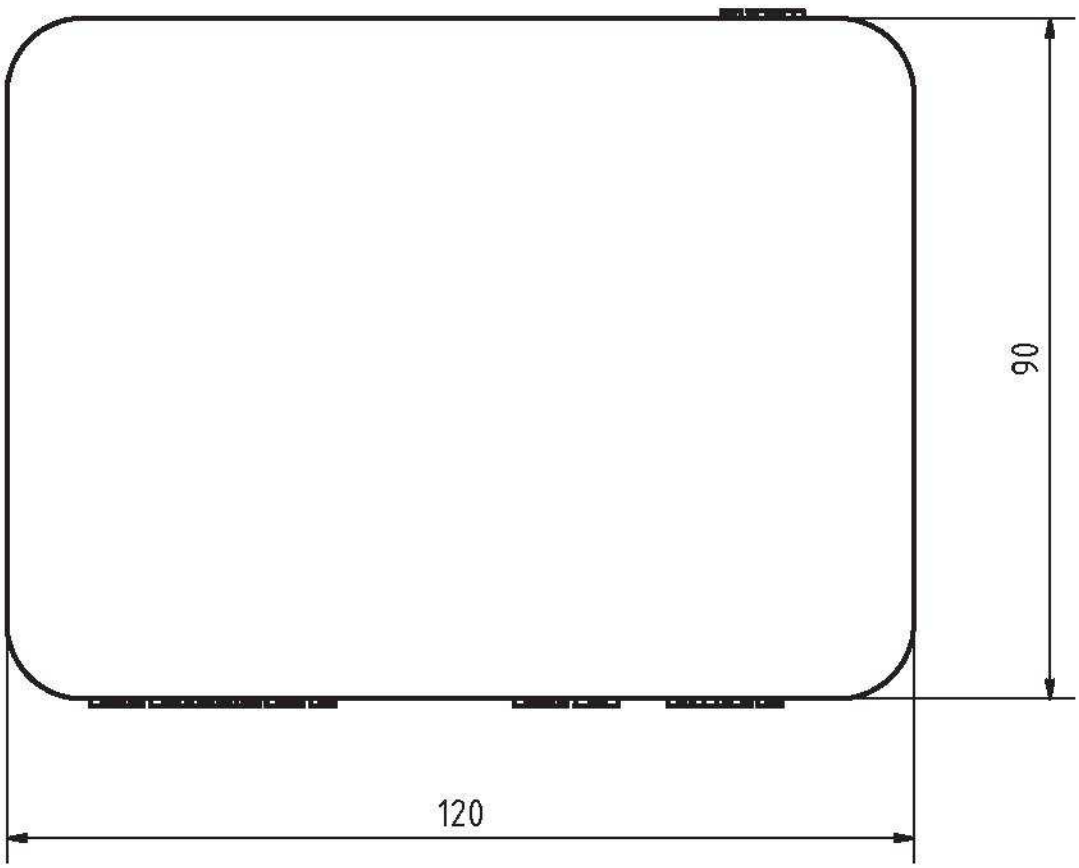

					Datum	Name	
				Gezeichnet	03.12.2013	Thomas	Controller Housing
				Kontrolliert			
				Norm			
				M 1:1		XXX	2
							A4
Status	Änderungen	Datum	Name				

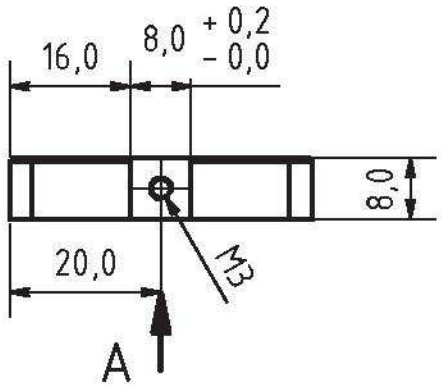

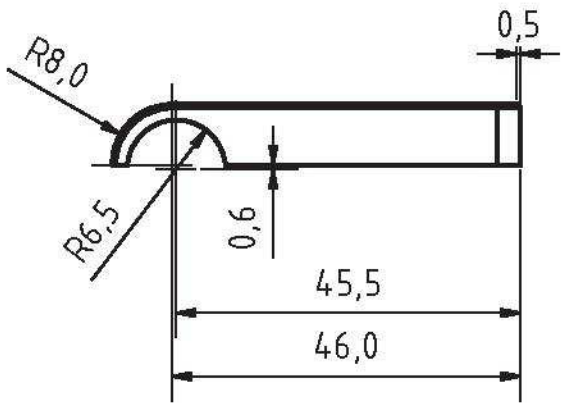

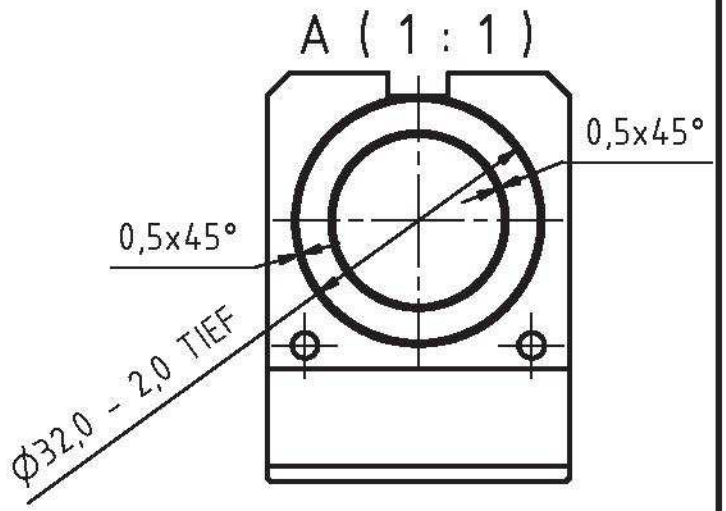

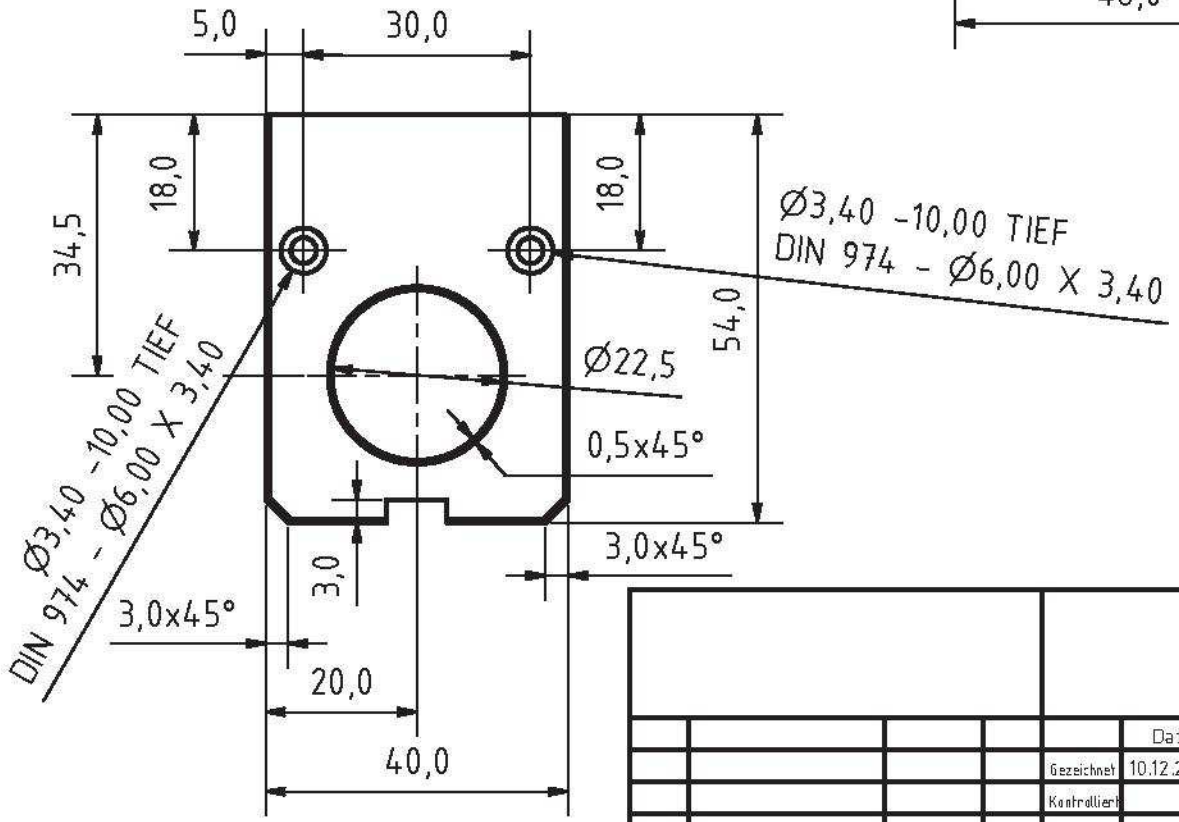

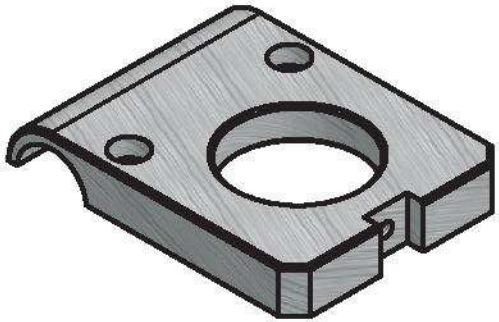

1 Stück
Material: Aluminium

					Datum	Name	
				Gezeichnet	10.12.2013	Thomas	EBC-Oberteil
				Kontrolliert			
				Norm			
					M 1:1	XXX	1 / A4
Status	Änderungen	Datum	Name				

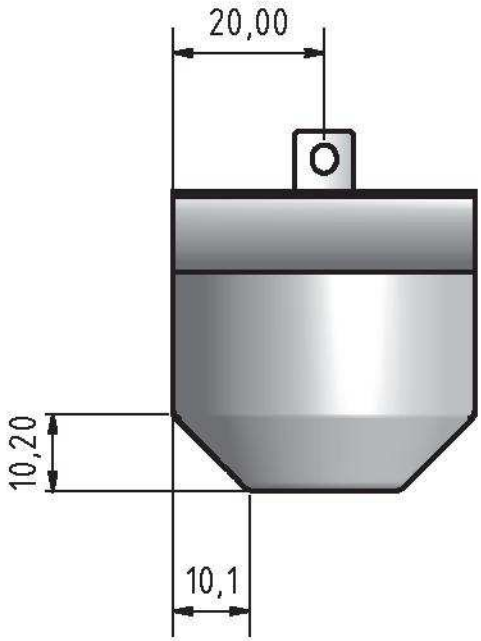

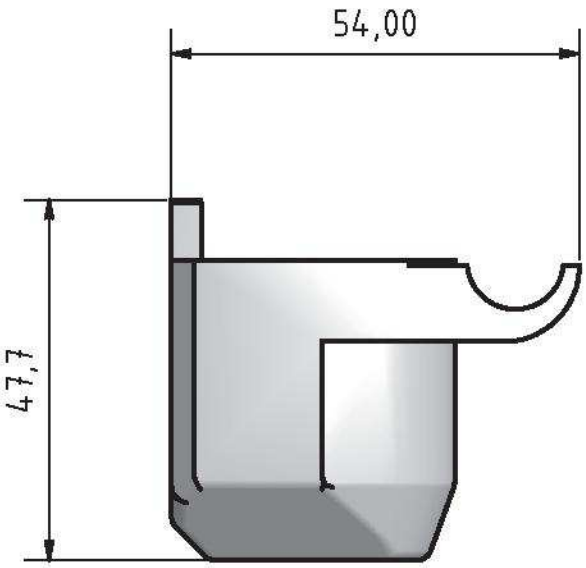

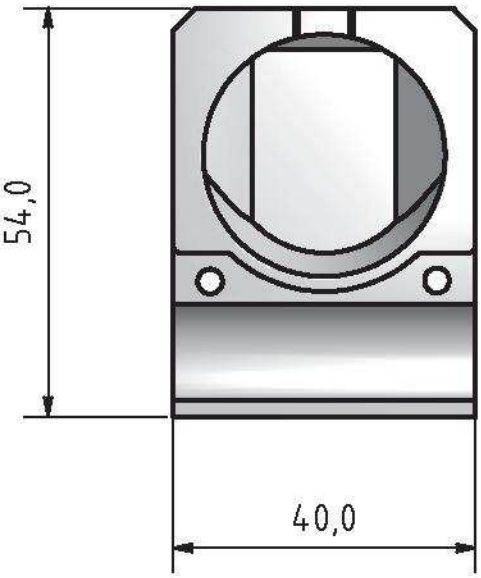

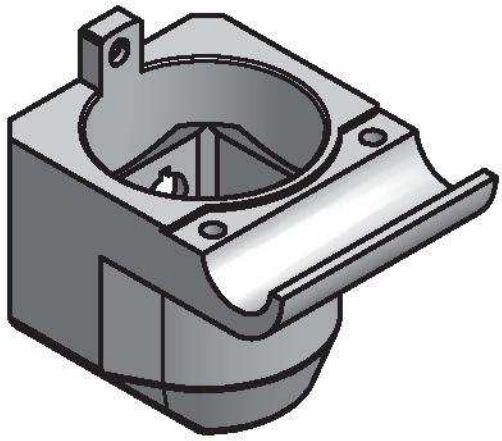

					Datum	Name		
				Gezeichnet	10.12.2013	Thomas	EBC-Unterteil	
				Kontrolliert				
				Norm				
							M 1:1	XXX 1 A4
Status	Änderungen	Datum	Name					

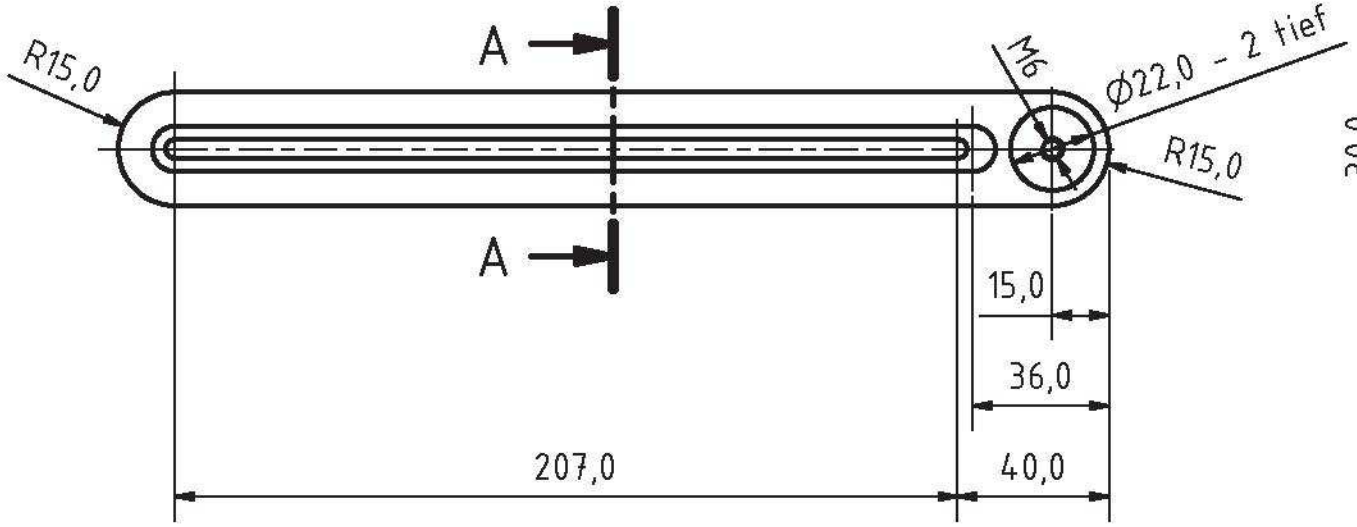

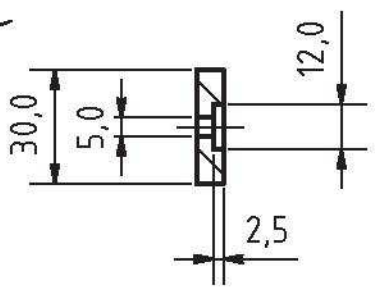

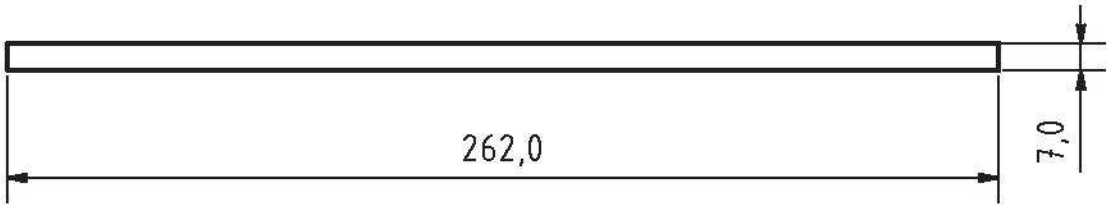

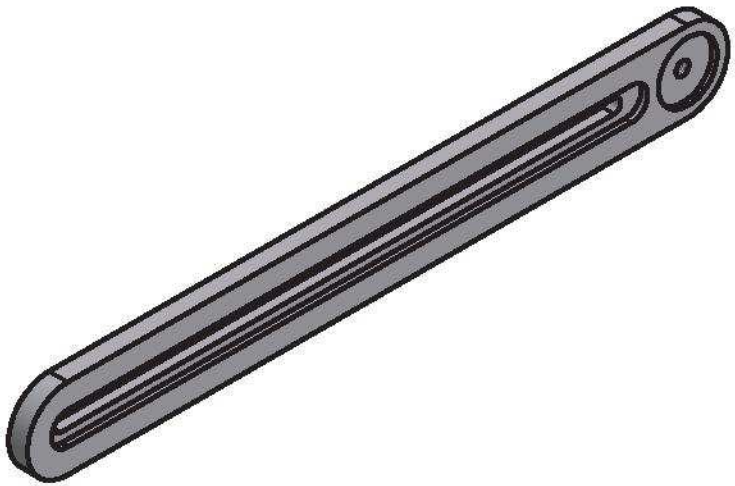

2 Stück
Material: Stahl

					Datum	Name
				Gezeichnet	10.01.2014	Thomas
				Kontrolliert		
				Norm		
Status	Änderungen	Datum	Name	M 1:2	XXX	1 / A4

PES-Anschlagschiene

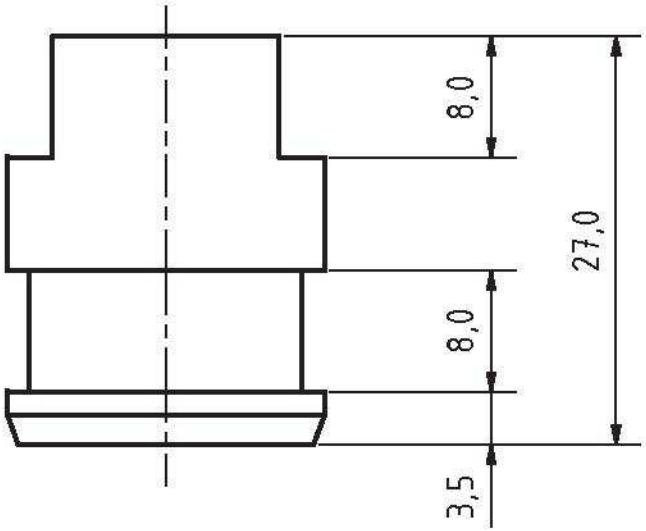

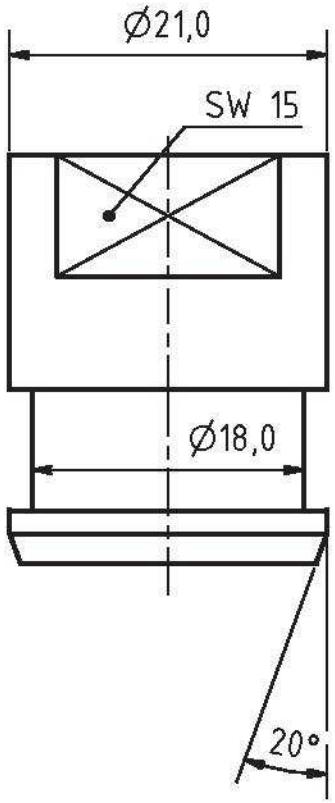

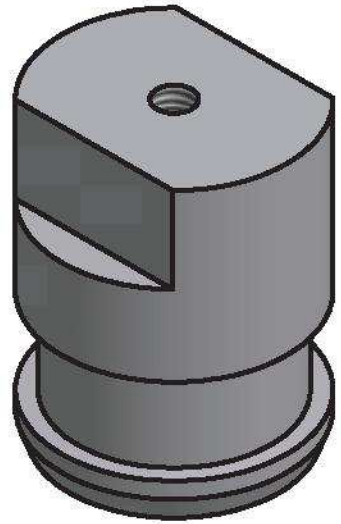

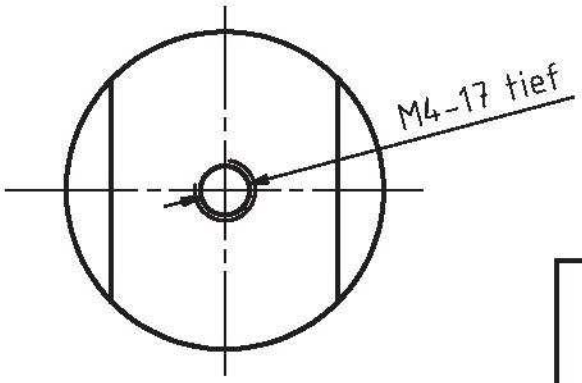

2 Stück
Material: Stahl

					Datum	Name	PES-Anschlagzylinder
				Gezeichnet	10.01.2014	Thomas	
				Kontrolliert			
				Norm			
				M 2:1	XXX		1
Status	Änderungen	Datum	Name				A4

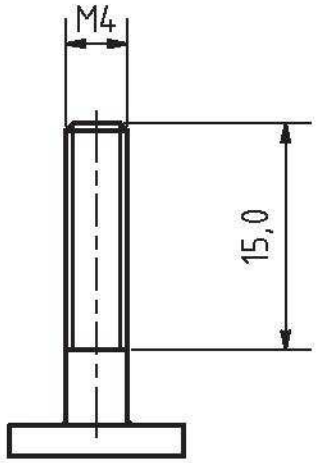

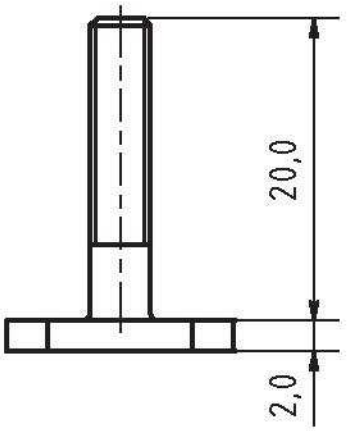

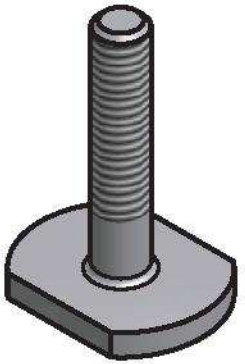

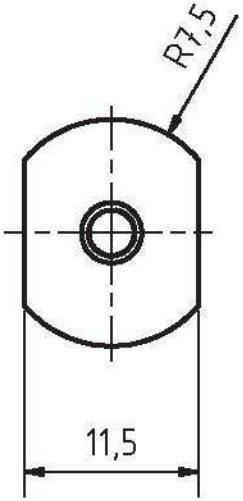

2 Stück
Material: Stahl

					Datum	Name
				Gezeichnet	10.01.2014	Thomas
				Kontrolliert		
				Norm		
				M 2:1	XXX	1 / A4
Status	Änderungen	Datum	Name			

PES-Anschlagbolzen

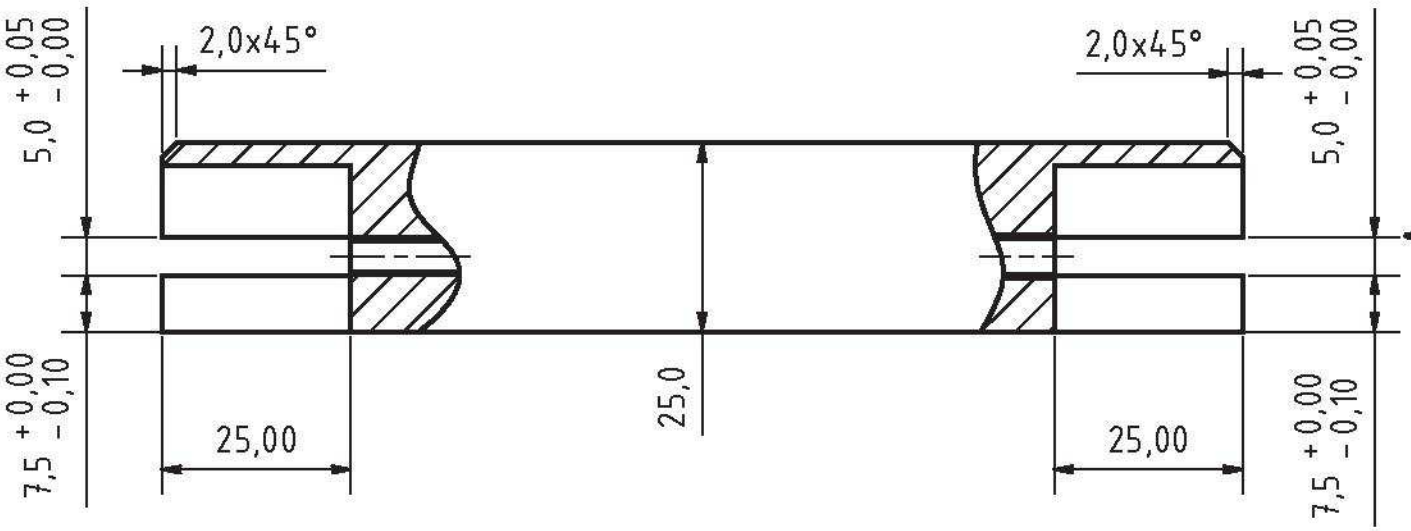

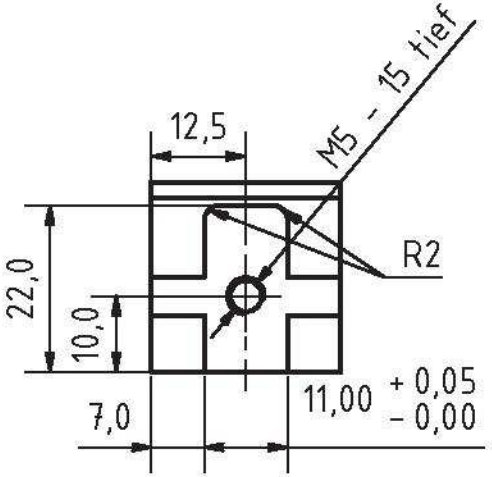

A (1 : 1)

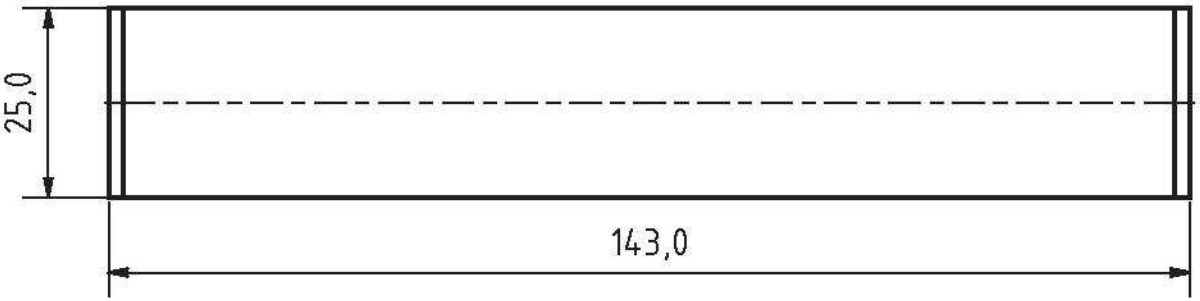

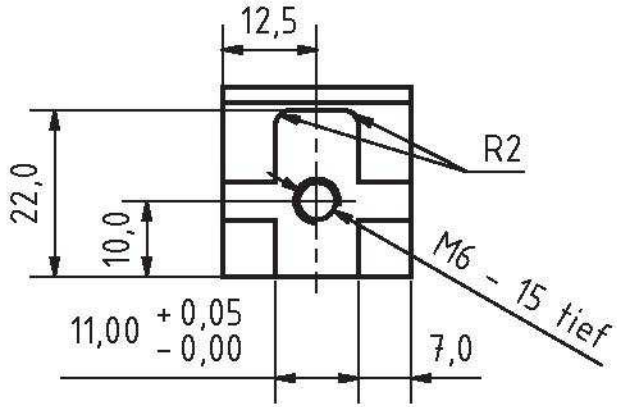

Material: Stahl
1 Stück

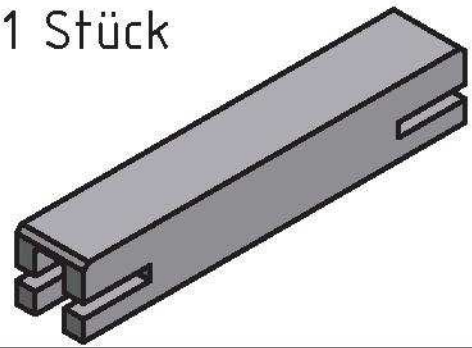

					Datum	Name
				Gezeichnet	15.01.2014	Thomas
				Kontrolliert		
				Norm		
				M 1:1	XXX	1
						A4
Status	Änderungen	Datum	Name			

ESC-Balken_horizontal

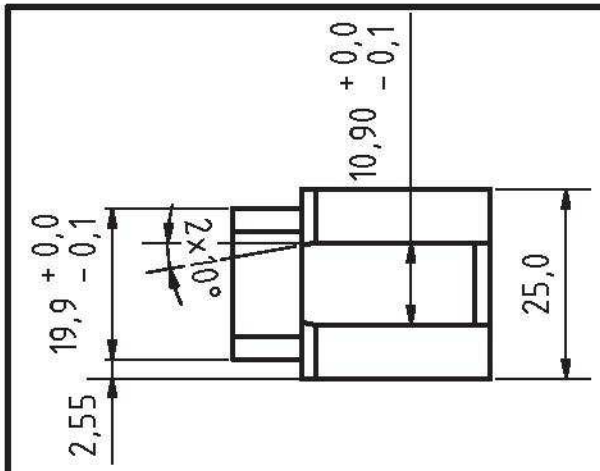

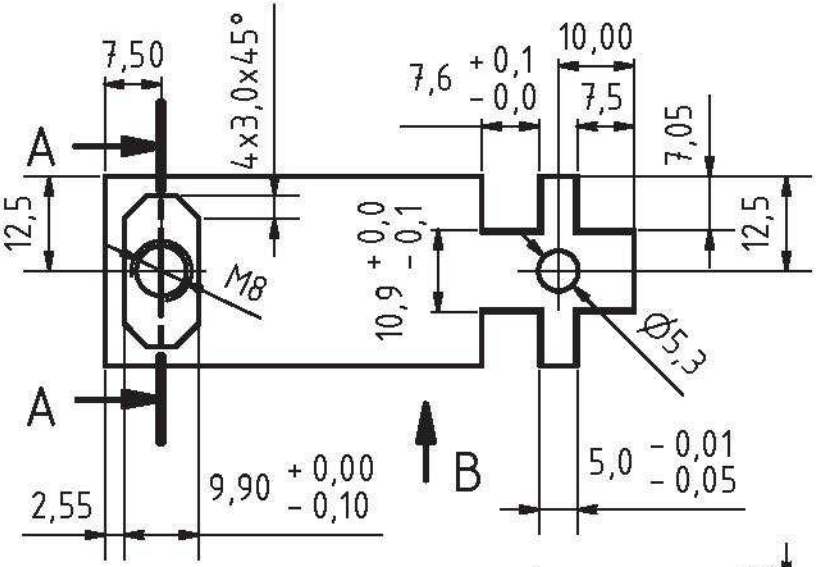

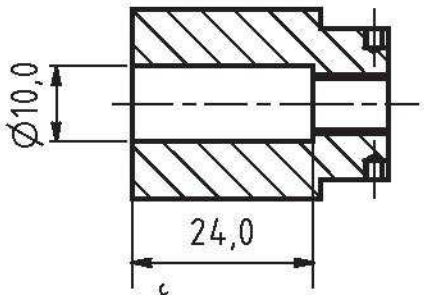

Material: Aluminium
1 Stück

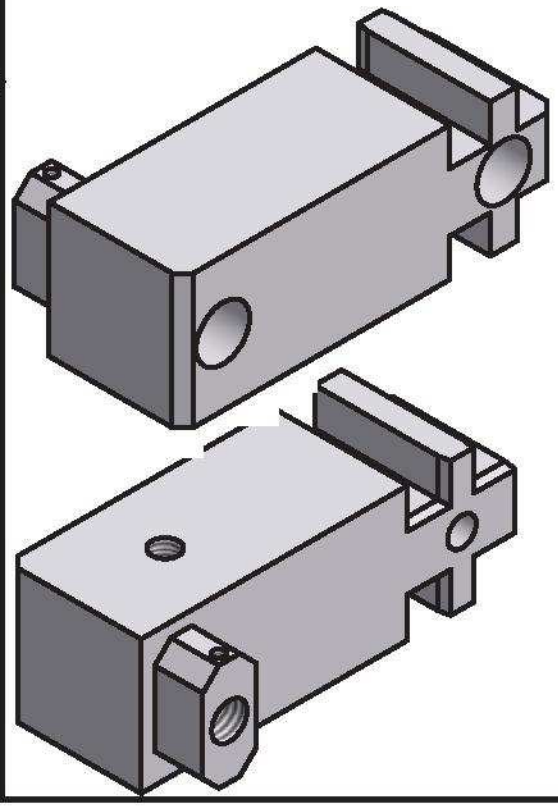

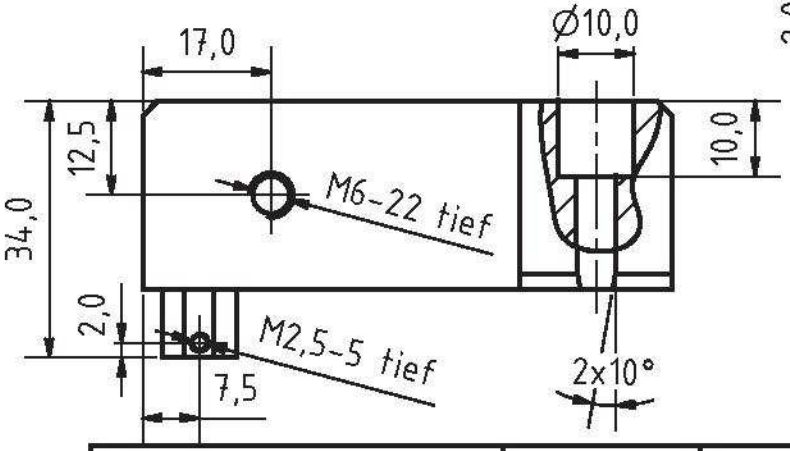

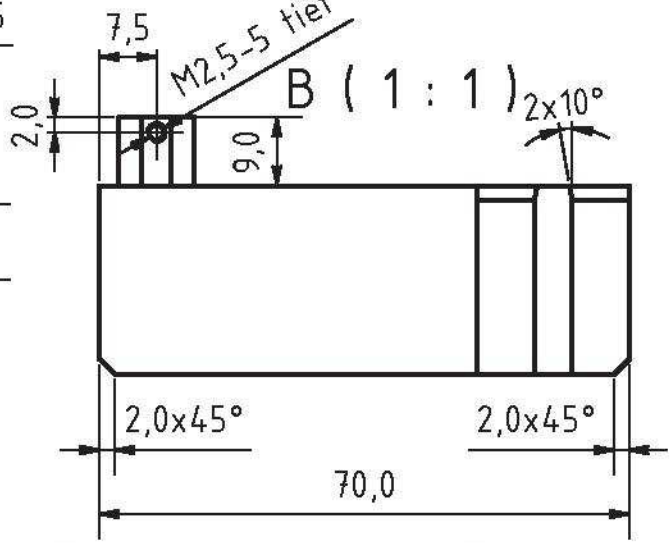

					Datum	Name
				Gezeichnet	15.01.2014	Thomas
				Kontrolliert		
				Norm		
Status	Änderungen	Datum	Name	M 2:1	XXX	1 A4

ESC-Balken_vertikal_fix

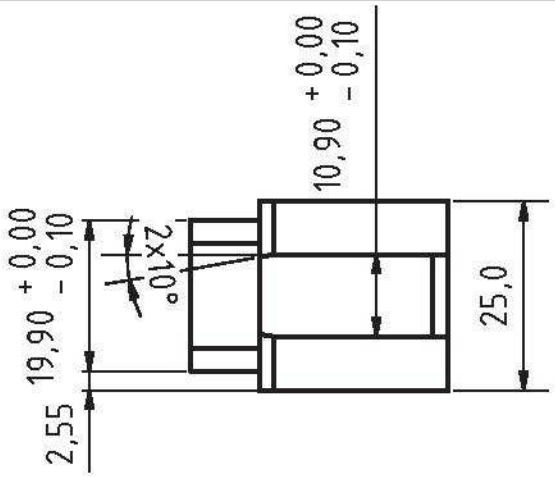

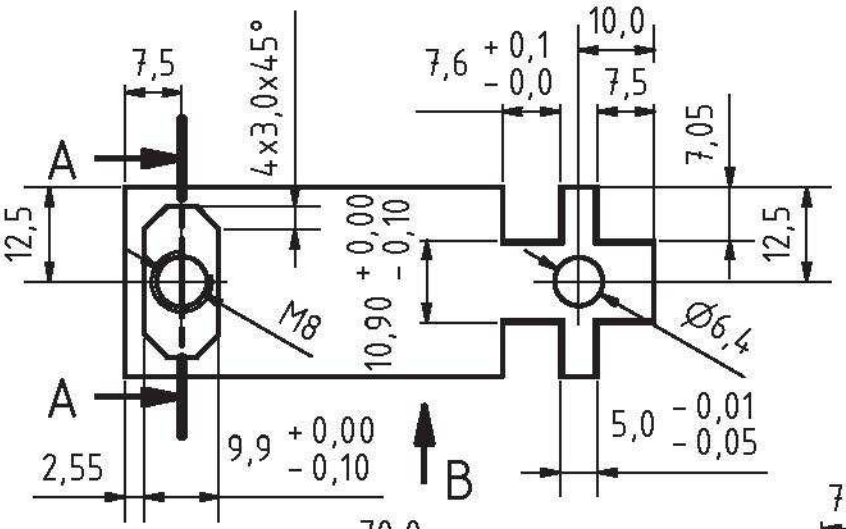

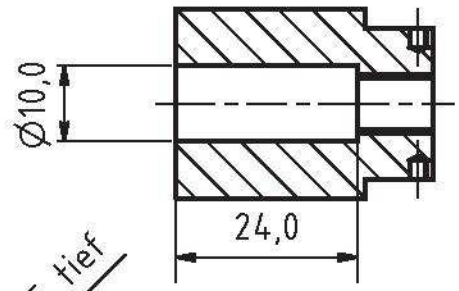

Material: Aluminium
1 Stück

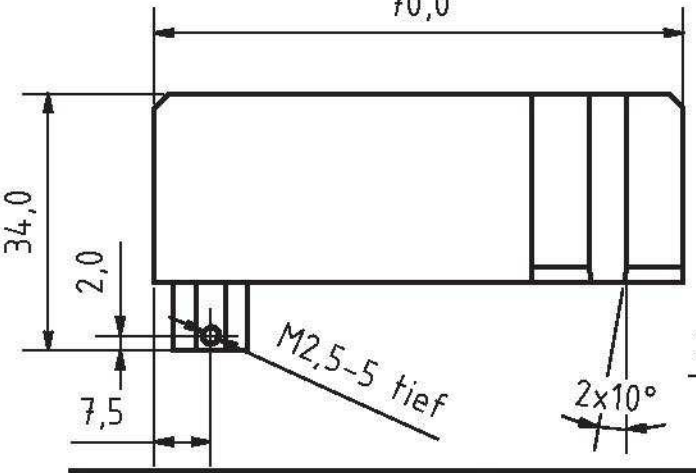

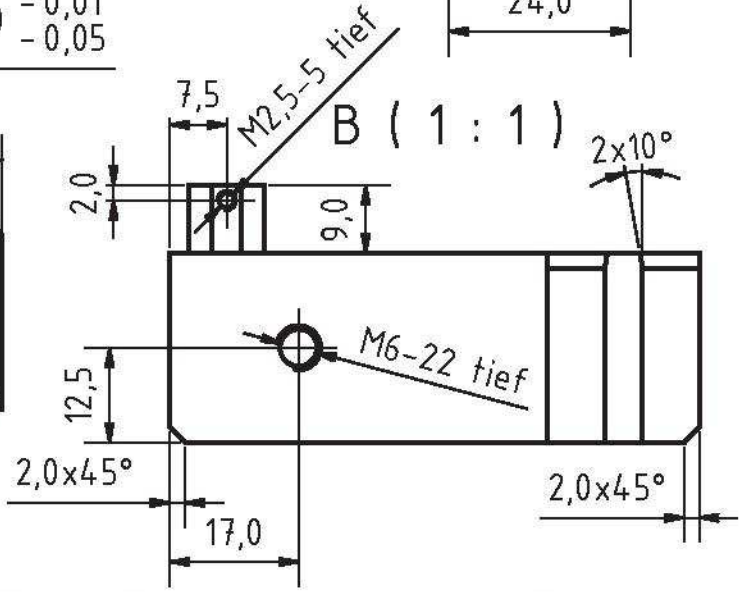

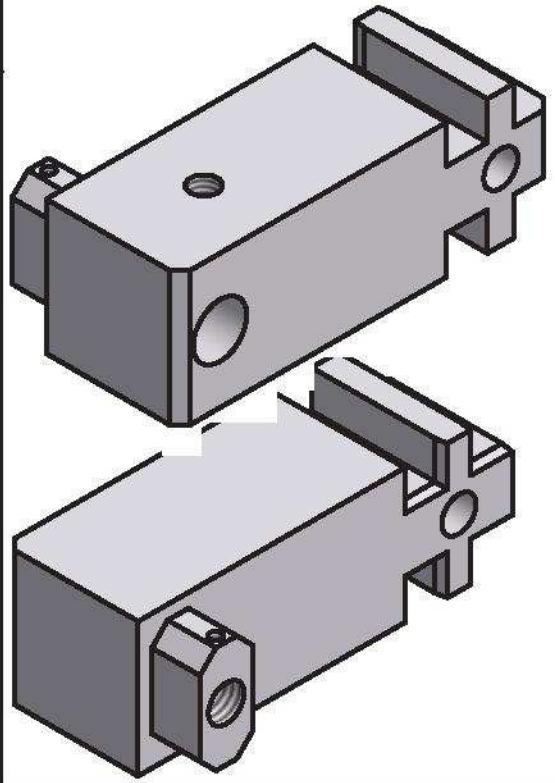

					Datum	Name
				Gezeichnet	16.01.2014	Thomas
				Kontrolliert		
				Norm		
				M 2:1	XXX	1
Status	Änderungen	Datum	Name			A4

ESC-Balken_vertikal_variabel

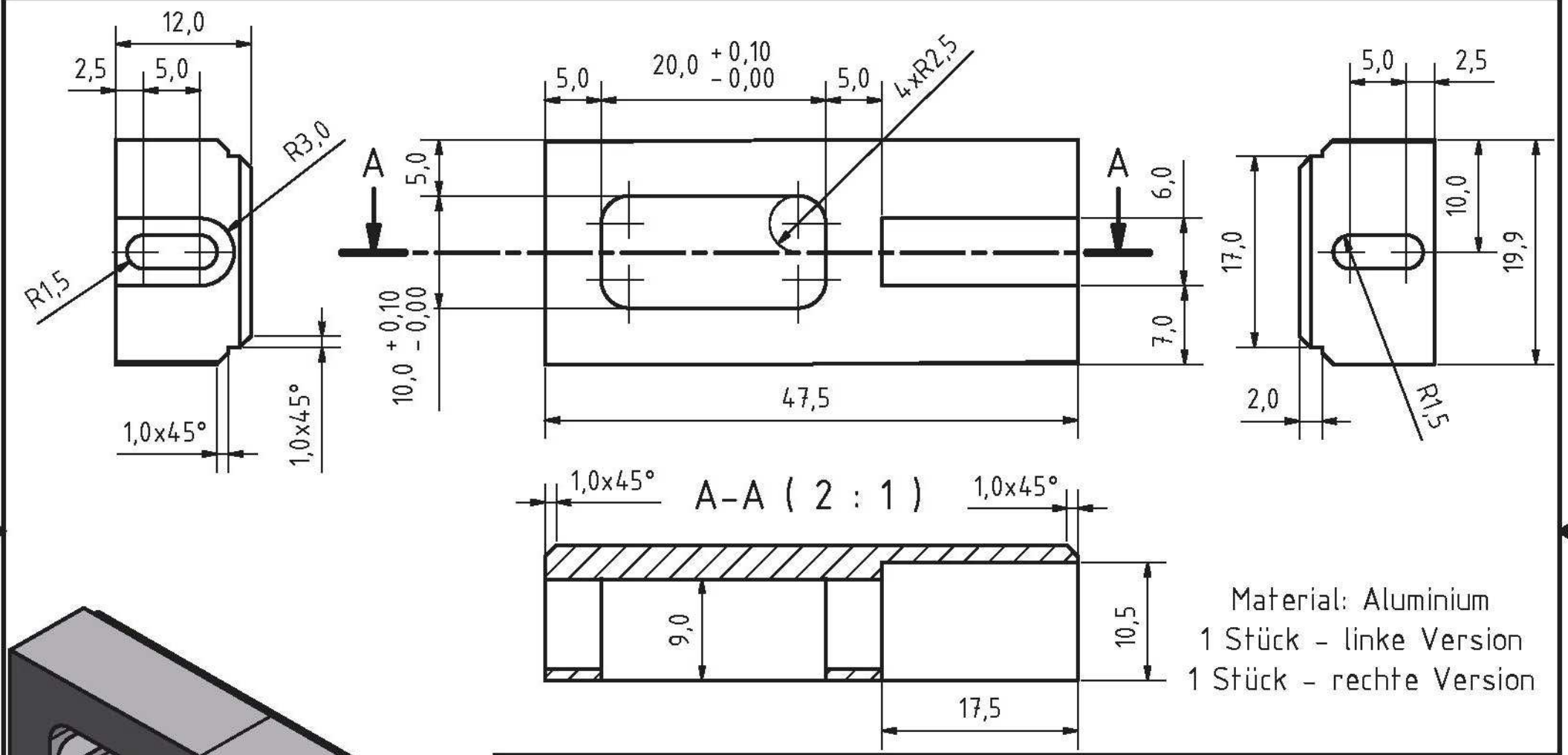

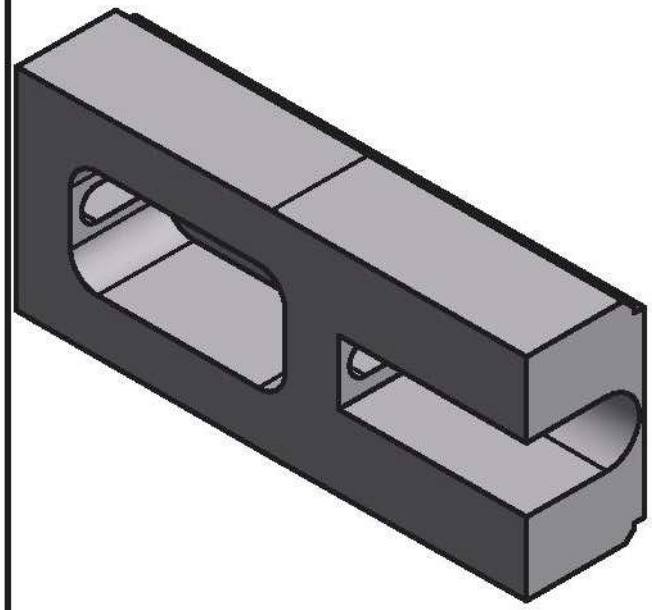

					Datum	Name
				Gezeichnet	16.01.2014	Thomas
				Kontrolliert		
				Norm		
Status	Änderungen	Datum	Name			

ESC-Klemmbacke_Rev1

M 2:1

XXX

1

A4

Version - links

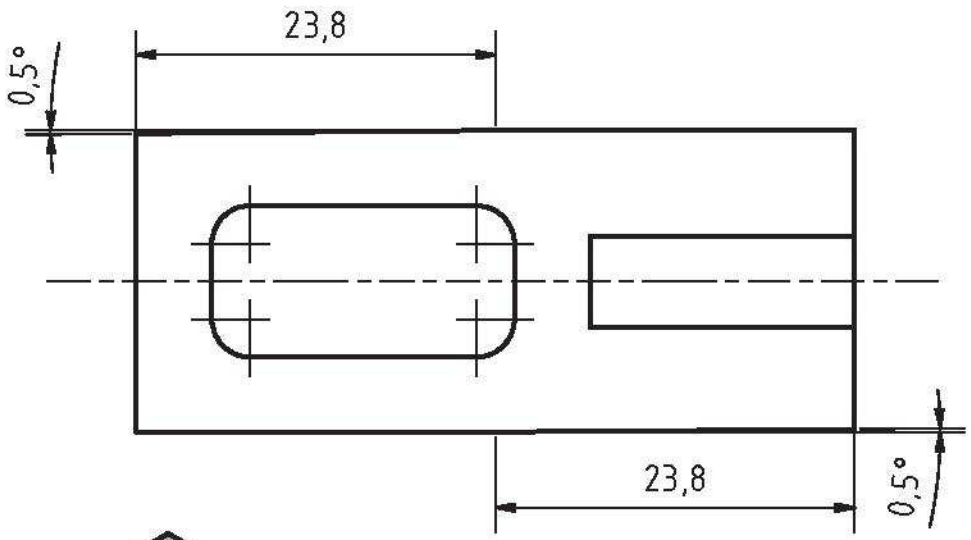

Version - rechts

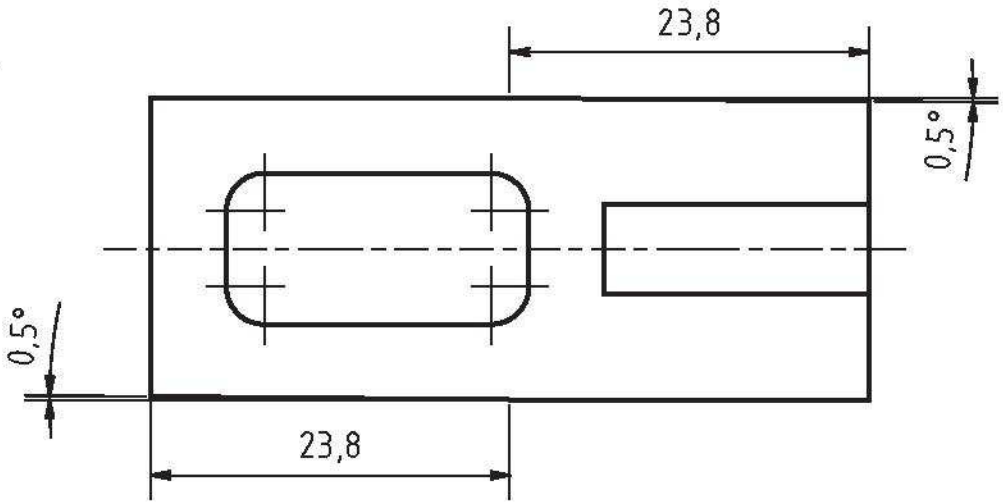

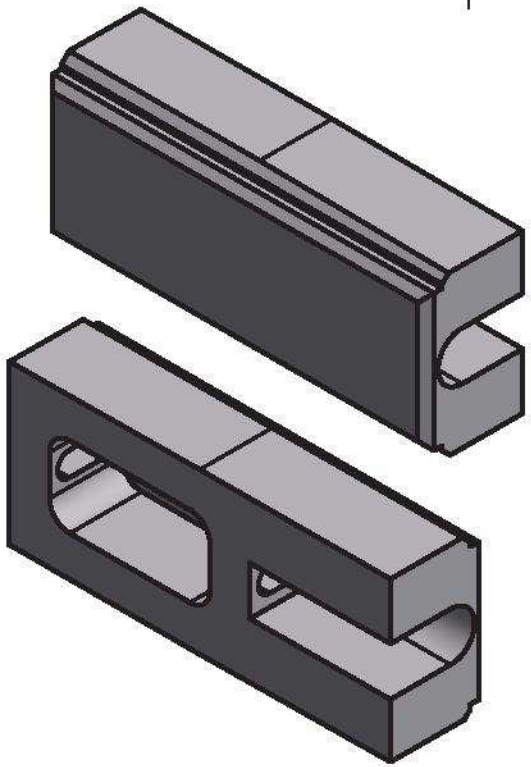

					Datum	Name	ESC-Klemmbacke_Rev1
				Gezeichnet	16.01.2014	Thomas	
				Kontrolliert			
				Norm			
				M 2:1	XXX		2 A4
Status	Änderungen	Datum	Name				

A-A (2 : 1)

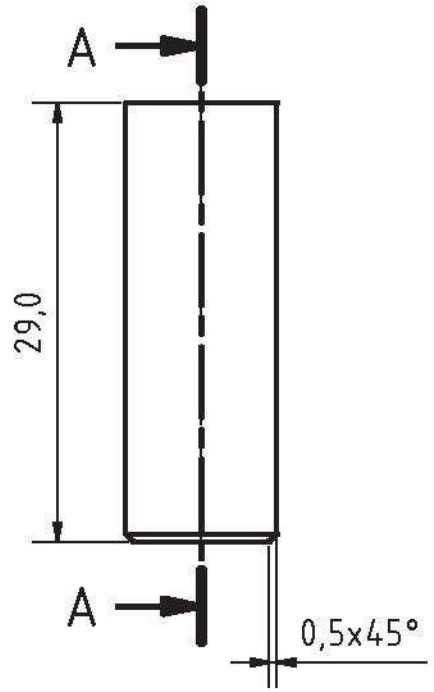

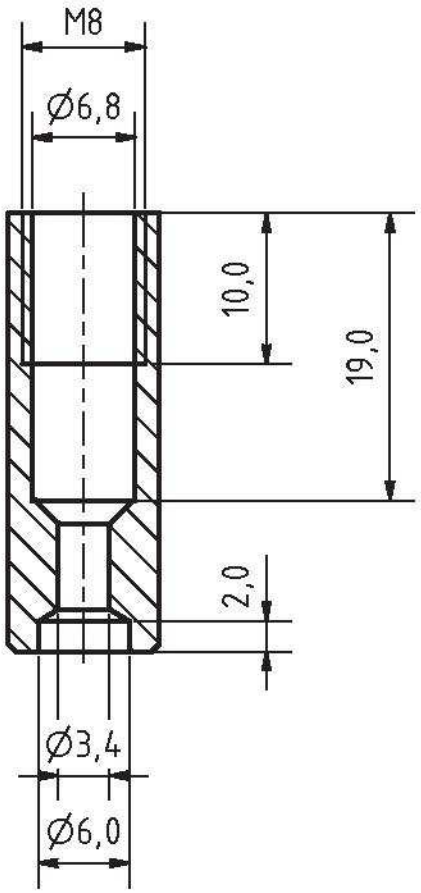

Material: Aluminium
2 Stück

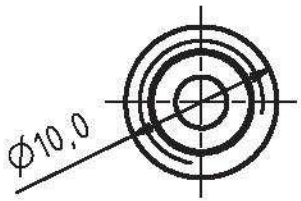

					Datum	Name	BC-Befestigung
				Gezeichnet	21.01.2014	Thomas	
				Kontrolliert			
				Norm			
				M 2:1		XXX	1
Status	Änderungen	Datum	Name				A4

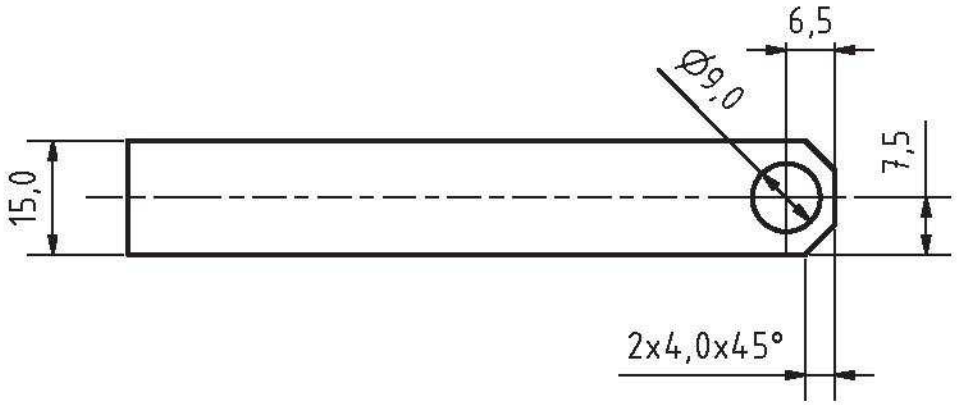

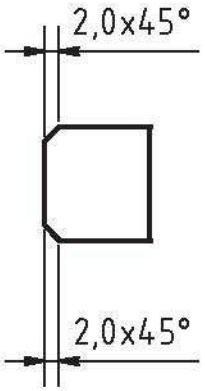

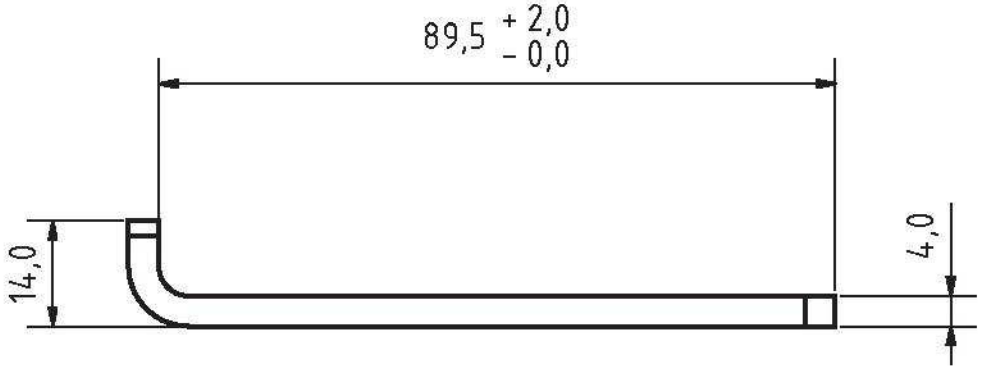

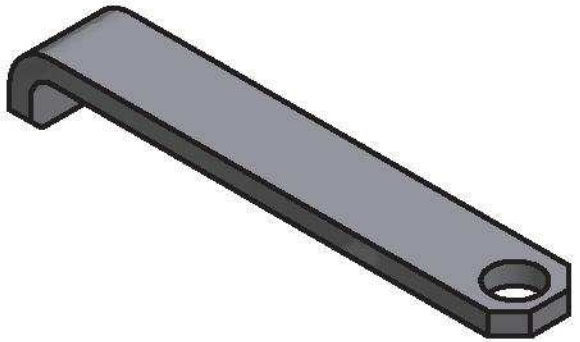

Material: Stahl
2 Stück

					Datum	Name	
				Gezeichnet	21.01.2014	Thomas	BC-Klemmlasche
				Kontrolliert			
				Norm			
					M 1:1	XXX	1
							A4
Status	Änderungen	Datum	Name				

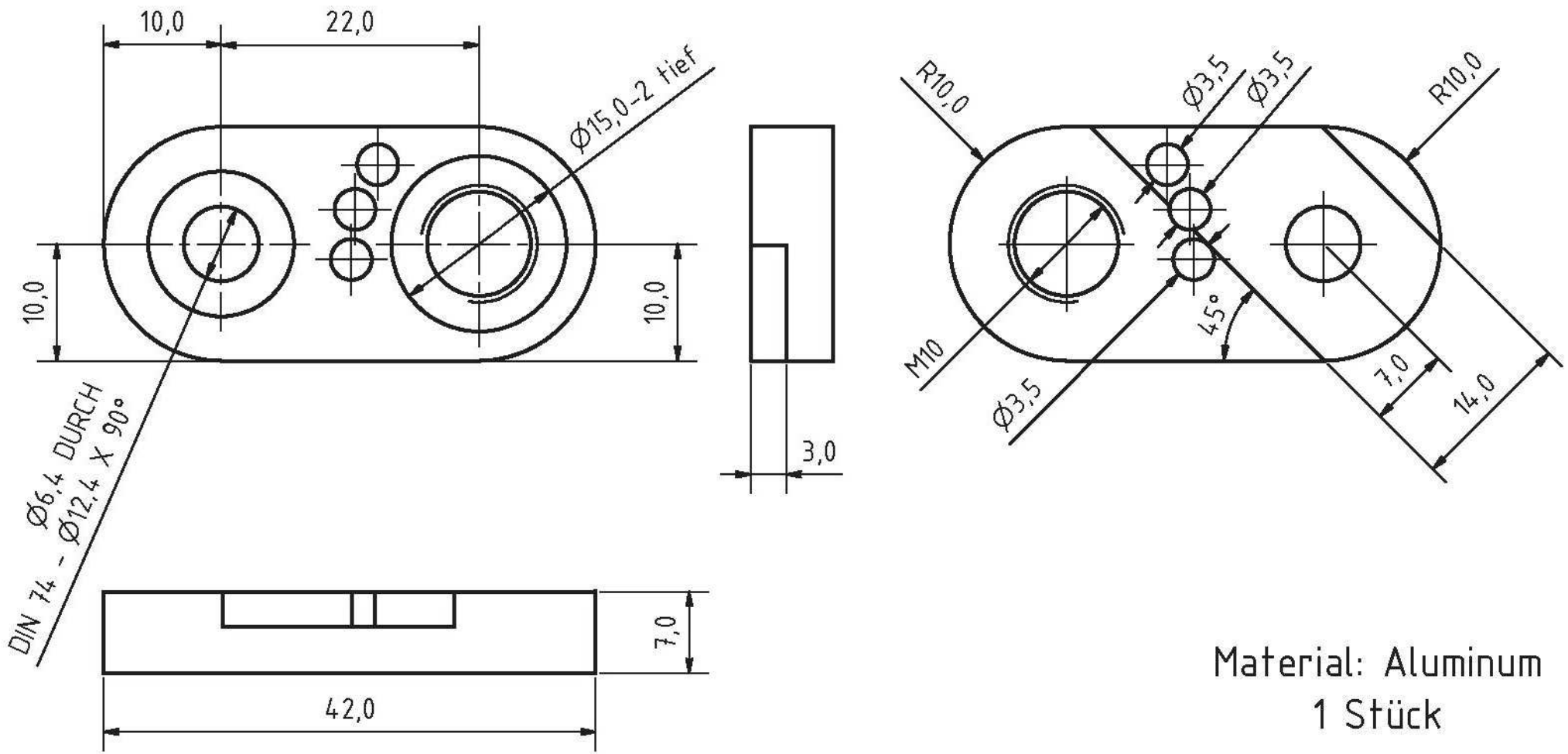

Material: Aluminum
1 Stück

					Datum	Name
				Gezeichnet	07.02.2014	Thomas
				Kontrolliert		
				Norm		
Status	Änderungen	Datum	Name			

CTA-Motageplatte

M 2:1

XXX

1

A4

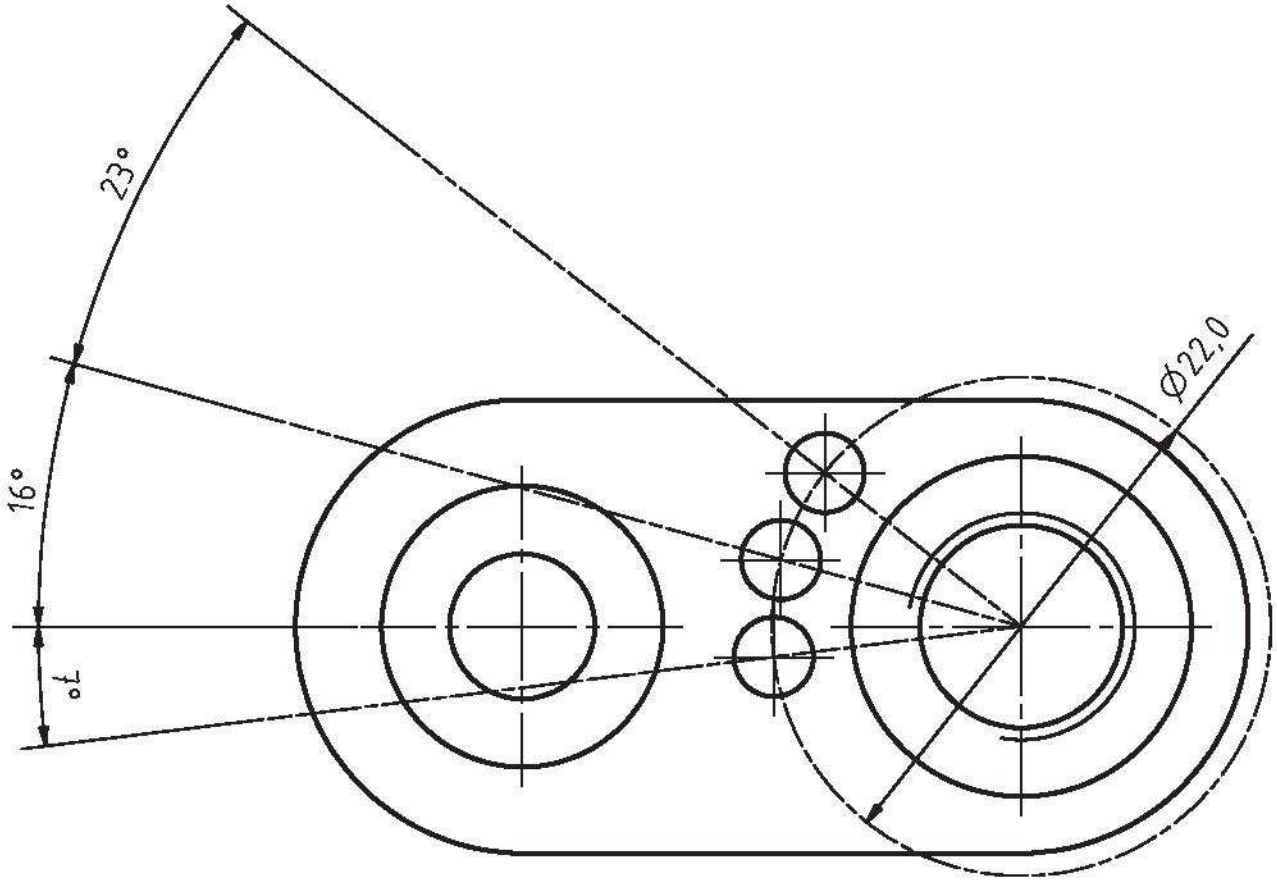

					Datum	Name	CTA-Motageplatte
				Gezeichnet	07.02.2014	Thomas	
				Kontrolliert			
				Norm			
				M 3:1		XXX	2
							A4
Status	Änderungen	Datum	Name				

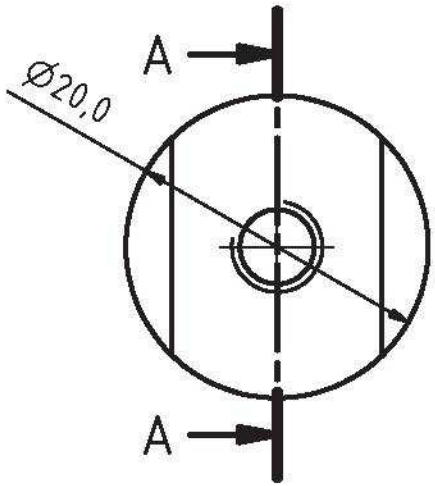

A–A (2 : 1)

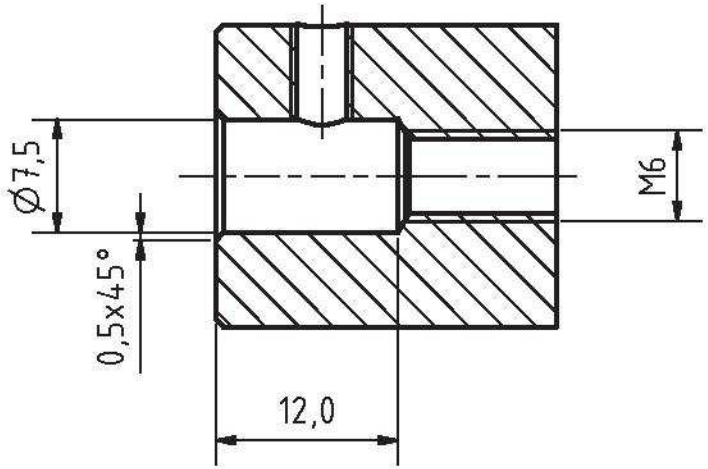

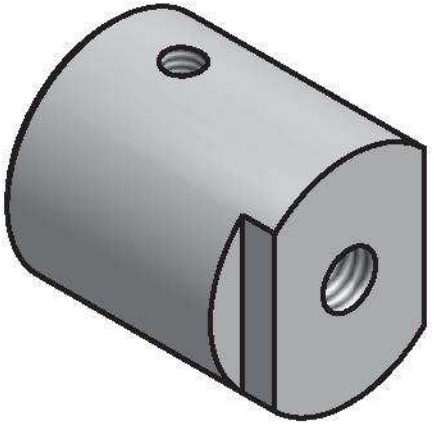

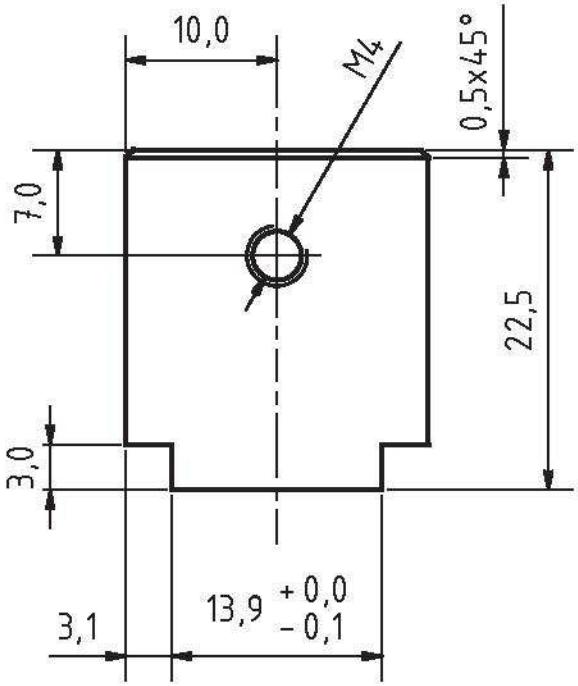

Material: Aluminium
1 Stück

					Datum	Name	CTA-Zylinder
				Gezeichnet	07.02.2014	Thomas	
				Kontrolliert			
				Norm			
				M 2:1		XXX	1 / A4
Status	Änderungen	Datum	Name				

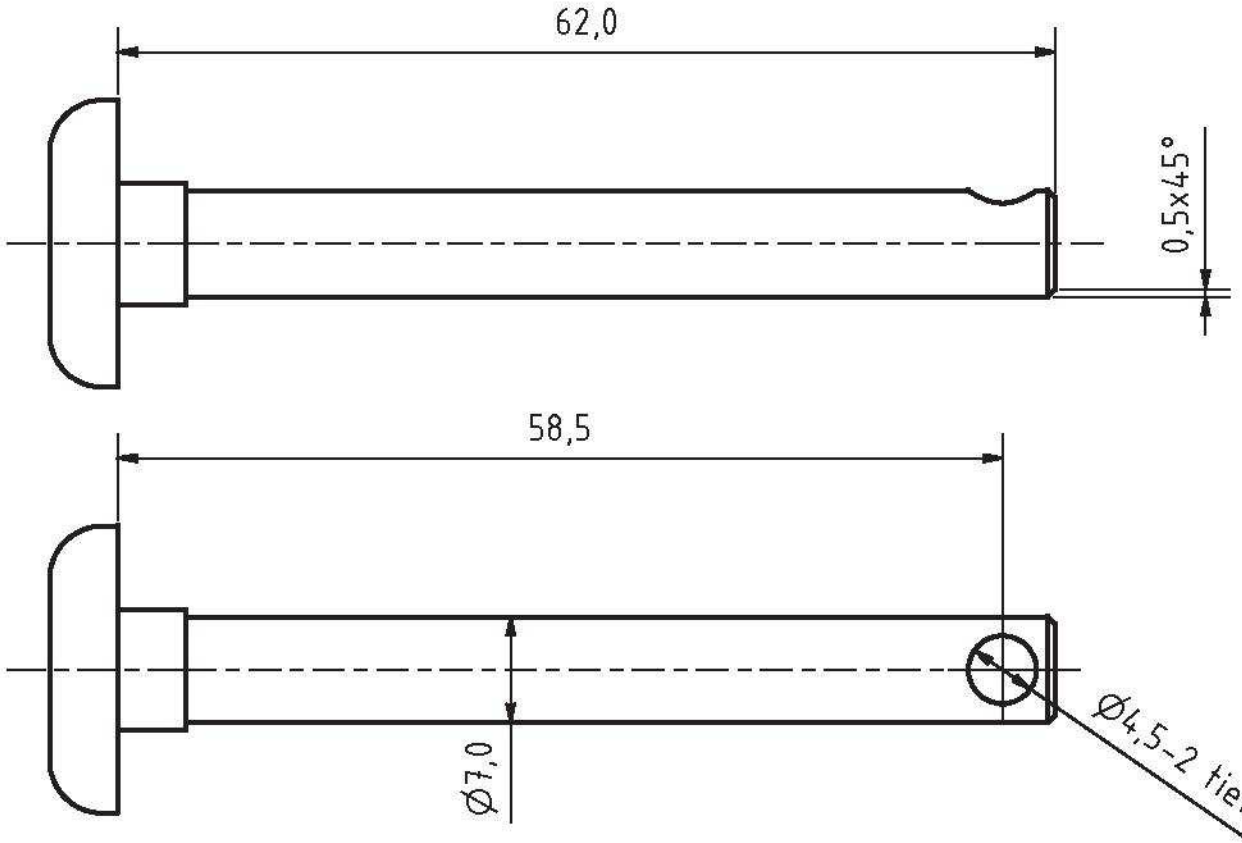

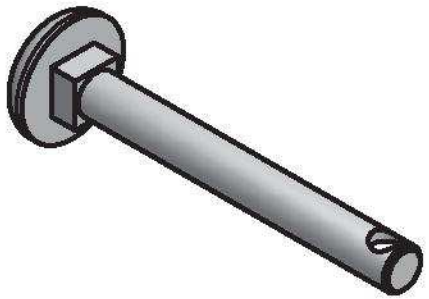

					Datum	Name	
				Gezeichnet	07.02.2014	Thomas	CTA-Befestigungsschraube
				Kontrolliert			
				Norm			
				M 2:1		XXX	1
							A4
Status	Änderungen	Datum	Name				

1 Stück
Nachbearbeitung

A2 Circuit Diagrams

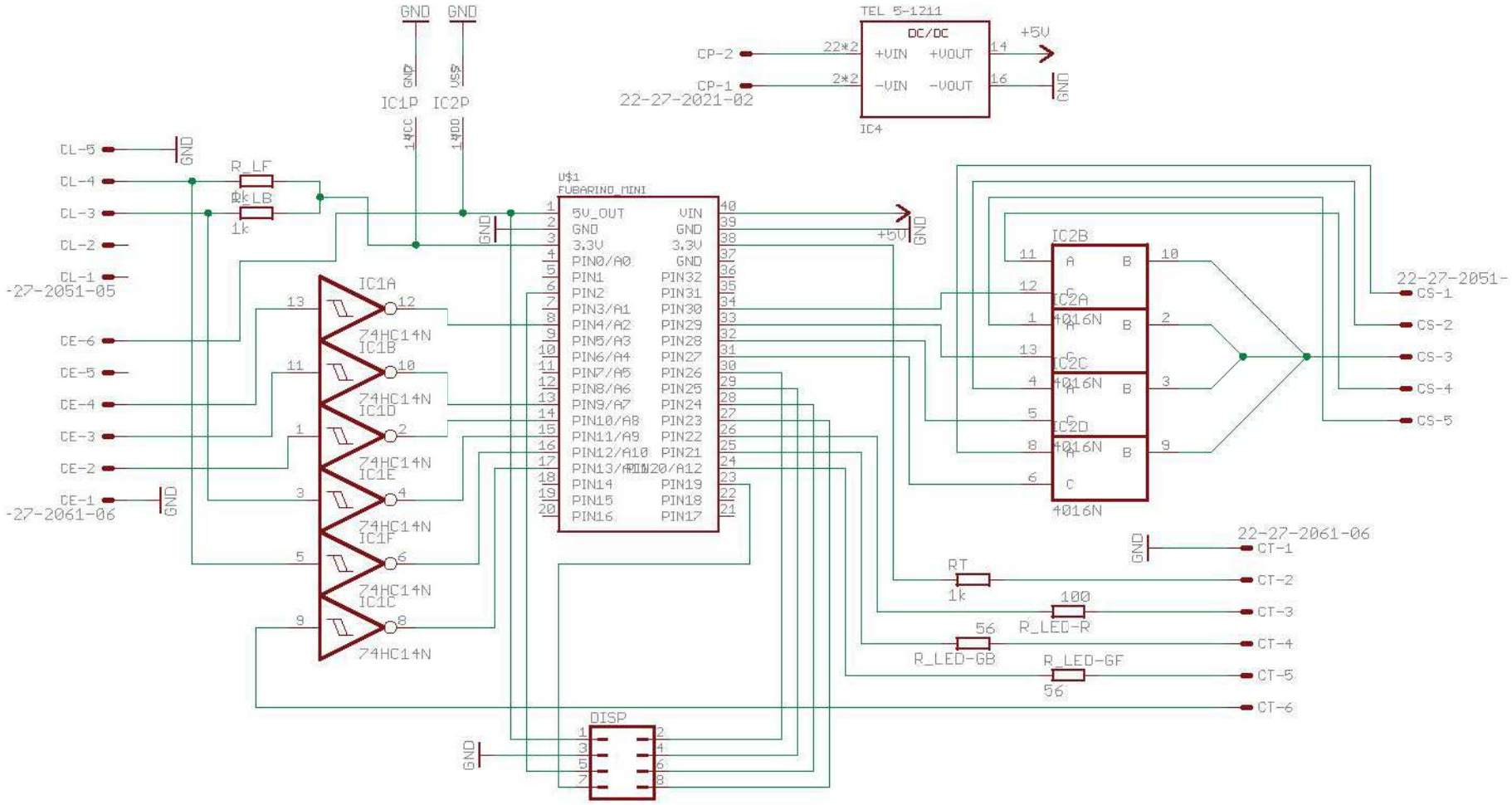

Controller - Circuit Board

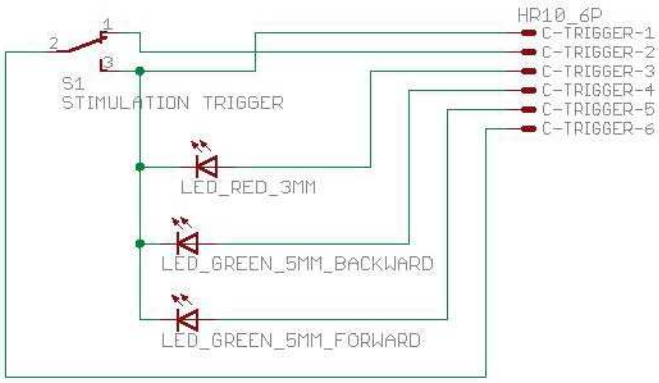

Stimulation Trigger - Circuit Diagram

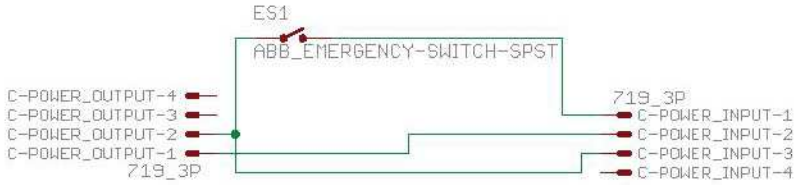

Emergency Switch - Circuit Diagram

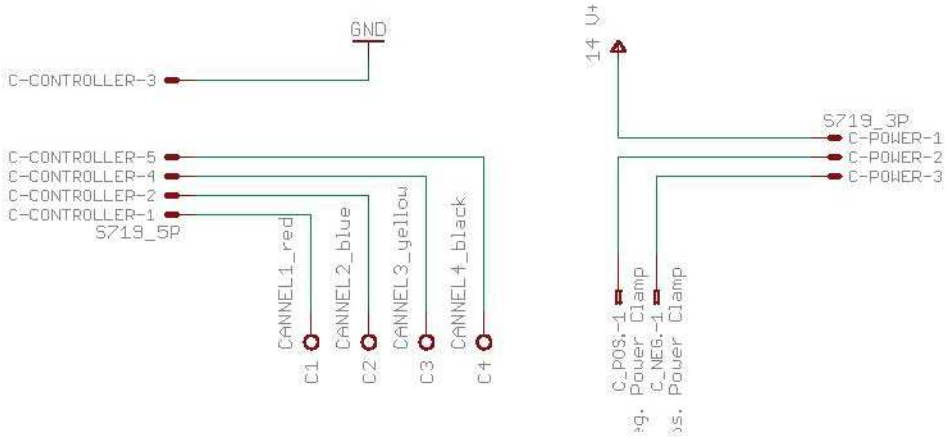

Stimulator Adaption - Circuit Diagram

A3 Calculation

A3.1 Function Test Calculation

Chapter A3.1 includes the calculations necessary to achieve the mean bicycle resistance force over three test trials as well as the power and mean power for one function test trial. Other function test trials were computed on the same way but are not added to the appendix because only the input files vary from this example calculation.

Technical Specifications

Variable Data:

$h := 200m$ % Sea level of the test track [m]

$T := 298.15K$ % T=Temperature at the test track [K]

$A := 0.48m^2$ % A=Air contact surface m²

$m_p := 76kg$ % Body weight of the driver [kg]

$m_f := 48.2kg$ % Bicycle weight [kg]

$m_{ges} := m_p + m_f$ % Overall weight [kg]

Constant Data:

$cw := 0.77$ % CW-Value for recumband bicycles [11]

$r := 85mm$ % r=Radius from the middle of the wheel till outer edge of the electric motor [mm]

$r_a := 235mm$ % r.a=Radius from the middle of the wheel till tread [mm]

$r_i := 212.5mm$ % r.i=Radius from the middle of the wheel till inner edge of wheel rim [mm]

$m_v := 1kg$ % Mass of frontal wheel [kg]

$m_{hr} := 5.4kg$ % Mass of backward wheel on the right side (when looking in driving direction), including electric motor [kg]

$p_0 := 1013.25 \cdot 10^2 Pa$ % Reference air pressure at sea level [Pa]

$T_0 := 293.15K$ % Reference temperature at sea level [K]

$R := 287.058 \frac{J}{kg \cdot K}$ % Universal gas constant [J/kg*K]

Test Data Import

Test Trial Data

$v := \text{READEXCEL}(\text{"C:\Daten\Fahrtest-Ampl1.xlsx"}, \text{"Tabelle1!C2:C21"}) \cdot \frac{m}{s}$

$t := \text{READEXCEL}(\text{"C:\Daten\Fahrtest-Ampl1.xlsx"}, \text{"Tabelle1!A2:A21"})$

$\Delta t := \text{READEXCEL}(\text{"C:\Daten\Fahrtest-Ampl1.xlsx"}, \text{"Tabelle1!D2:D21"}) \cdot s$

Bicycle Resistance Data

$v_w := \text{READEXCEL}(\text{"C:\Daten\Fahrradwiderstand.xlsx"}, \text{"Tabelle1!C2:C38"}) \cdot \frac{m}{s}$

$t_w := \text{READEXCEL}(\text{"C:\Daten\Fahrradwiderstand.xlsx"}, \text{"Tabelle1!A2:A38"})$

$\Delta t_w := \text{READEXCEL}(\text{"C:\Daten\Fahrradwiderstand.xlsx"}, \text{"Tabelle1!D2:D38"}) \cdot s$

$v_{w2} := \text{READEXCEL}(\text{"C:\Daten\Fahrradwiderstand.xlsx"}, \text{"Tabelle2!C2:C35"}) \cdot \frac{m}{s}$

$t_{w2} := \text{READEXCEL}(\text{"C:\Daten\Fahrradwiderstand.xlsx"}, \text{"Tabelle2!A2:A35"})$

$\Delta t_{w2} := \text{READEXCEL}(\text{"C:\Daten\Fahrradwiderstand.xlsx"}, \text{"Tabelle2!D2:D35"}) \cdot s$

$v_{w3} := \text{READEXCEL}(\text{"C:\Daten\Fahrradwiderstand.xlsx"}, \text{"Tabelle3!C2:C35"}) \cdot \frac{m}{s}$

$t_{w3} := \text{READEXCEL}(\text{"C:\Daten\Fahrradwiderstand.xlsx"}, \text{"Tabelle3!A2:A35"})$

$\Delta t_{w3} := \text{READEXCEL}(\text{"C:\Daten\Fahrradwiderstand.xlsx"}, \text{"Tabelle3!D2:D35"}) \cdot s$

Calculation of the Drag Force

$$p(h) := p_0 \cdot \left(1 - \frac{0.0065 \frac{K}{m} \cdot h}{T_0}\right)^{5.255}$$

$$\rho := \frac{p(h)}{R \cdot T} = 1.157 \frac{kg}{m^3}$$ % Air density at +23°C

$$F_L := \frac{1}{2} \cdot cw \cdot \rho \cdot A \cdot v^2$$ % Drag Force [N]

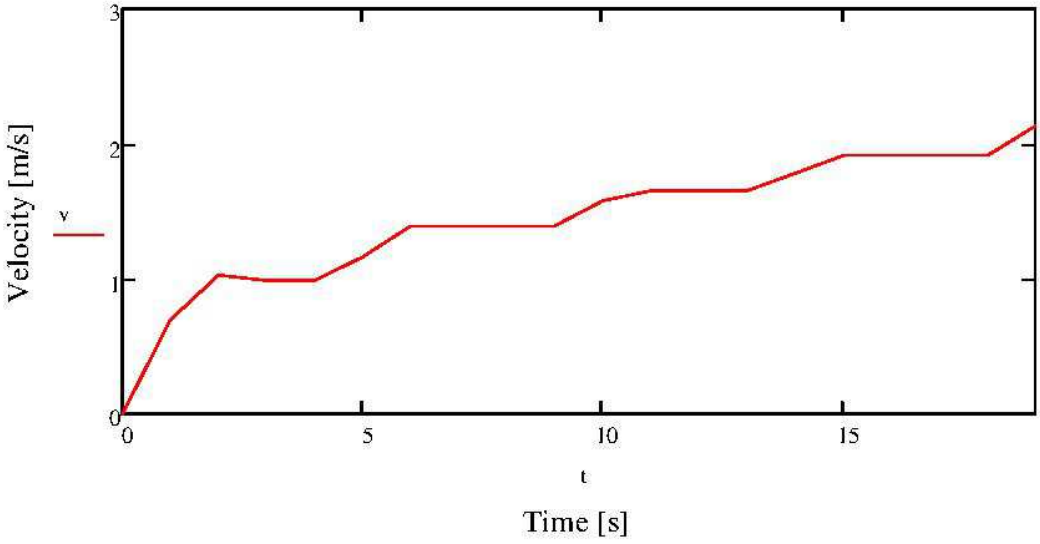

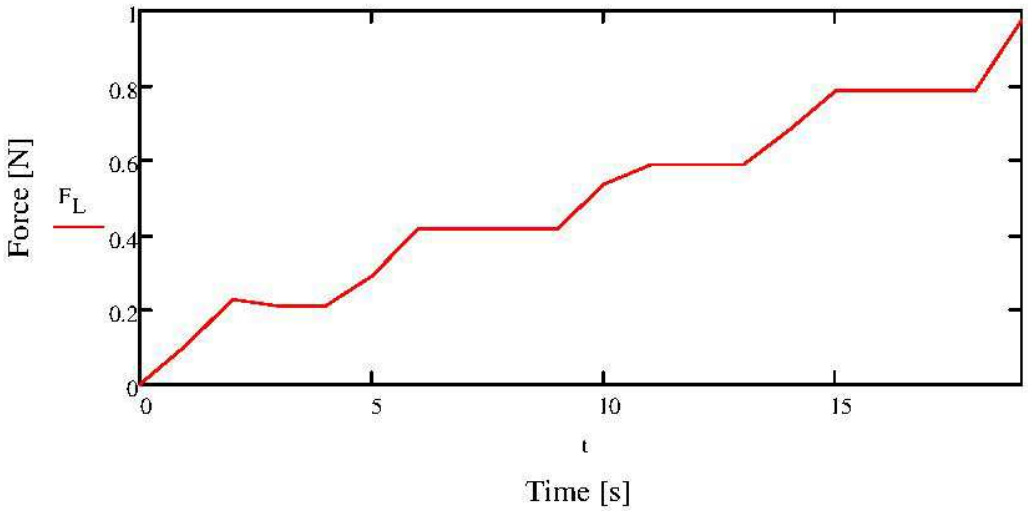

Calculation of the Translational Inertia Force

$a(v) :=$ | $D \leftarrow 0$ | $D_0 \leftarrow 0$ | for $i \in$ ORIGIN.. letzte(v) − 1 | $D_{i+1} \leftarrow \frac{v_{i+1} - v_i}{\Delta t_{i+1}}$ | return D

% Calculation of the acceleration vector

$F_a := m_{ges} \cdot a(v)$

% Translational force of inertia [N]

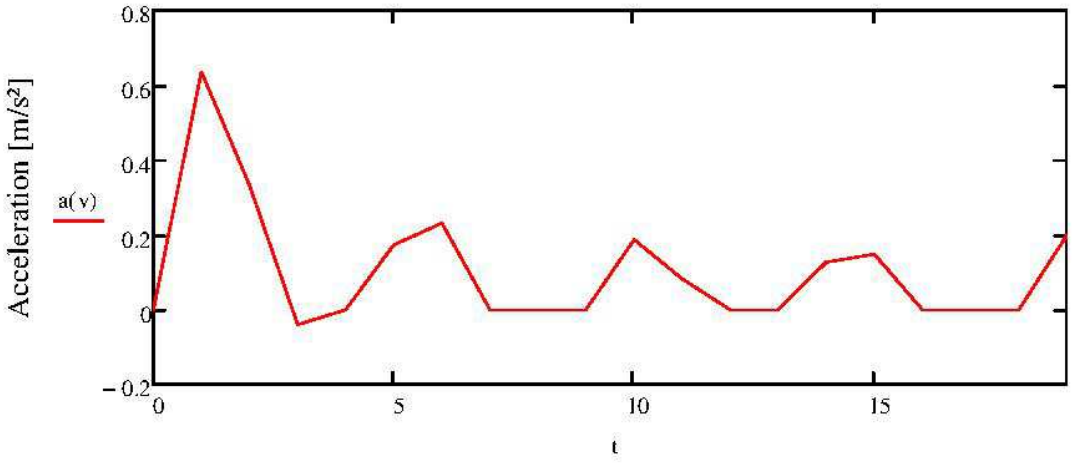

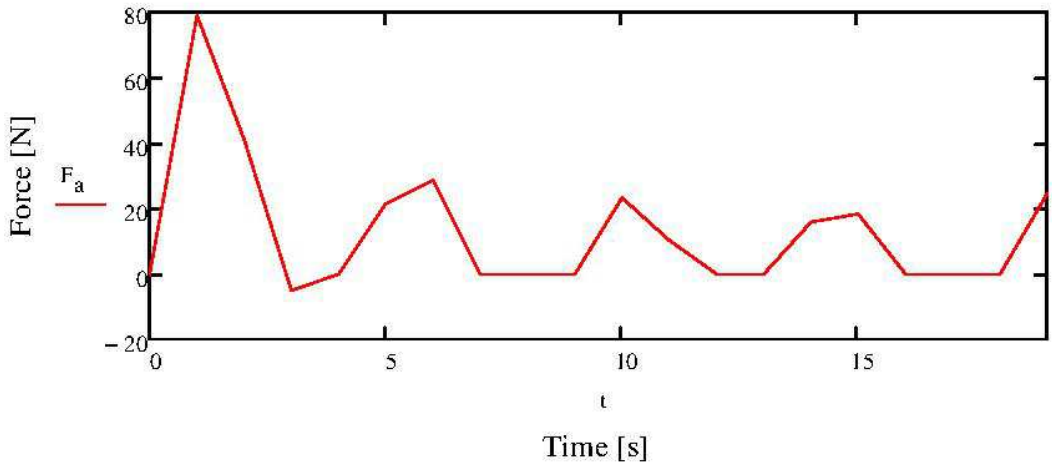

Calculation of the Rotational Inertia Force

$\omega := \frac{v}{r_a}$ % Angular velocity

$\omega_{Punkt} := \frac{a(v)}{r_a}$ % Angular acceleration

Moments of Inertia

$I_v := m_v \cdot \frac{\left(r_a^2 + r_i^2\right)}{2}$ % Of the frontal wheel

$I_{hl} := I_v$ % Of the left backward wheel (in driving direction)

$I_{hr} := m_v \cdot \frac{\left(r_a^2 + r_i^2\right)}{2} + \left(m_{hr} - m_v\right) \cdot r^2$ % Of the right backward wheel (in driving direction)

Torque Produced by Moments of Inertia

$M_{Iv} := I_v \cdot \omega_{Punkt}$ % Of the frontal wheel

$M_{Ihl} := M_{Iv}$ % Of the left backward wheel (in driving direction)

$M_{Ihr} := I_{hr} \cdot \omega_{Punkt}$ % Of the right backward wheel (in driving direction)

Forces Produced by Torque

$F_{Iv} := \frac{M_{Iv}}{r_a}$ % Of the frontal wheel

$F_{Ihl} := F_{Iv}$ % Of the left backward wheel (in driving direction)

$F_{Ihr} := \frac{M_{Ihr}}{r_a}$ % Of the right backward wheel (in driving direction)

$F_{Iges} := F_{Iv} + F_{Ihl} + F_{Ihr}$ % Rotational Inertia Force

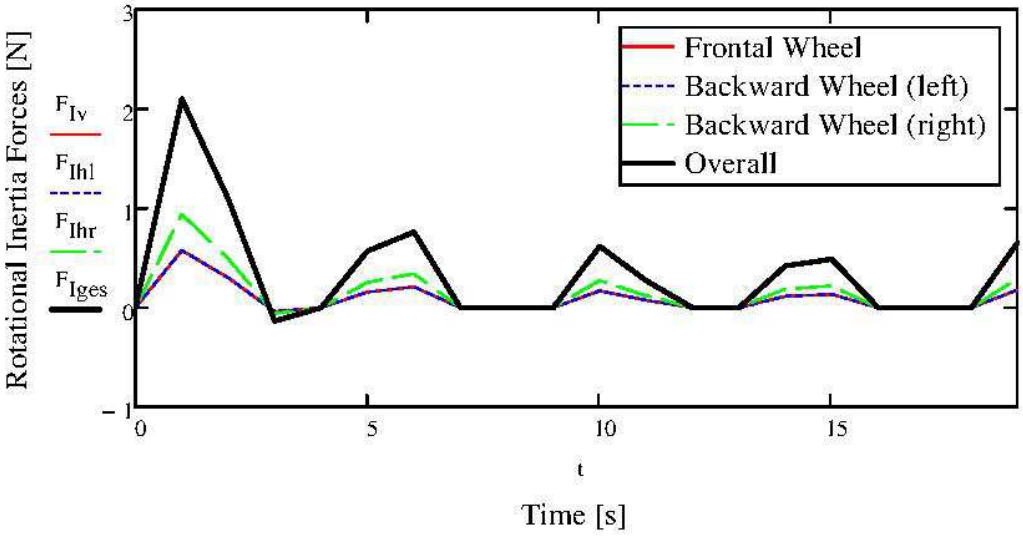

Calculation of the Bicycle Resistance Force (BRF) "Fr"

Assumptions for the calculation of the BRF

- Driving force Fa=0
- Even testtrial=> Potential energy can be neglected
- No breaking while test trial
- Inertia force acts as driving force=> Positive algebraic sign
- Air pressure of the bicycle wheels = 8 bar

Trial Number One

$v_{wg} := \mathrm{strgltt}(t_w, v_w)$

%Smoothening of the velocity vector with the least square methode

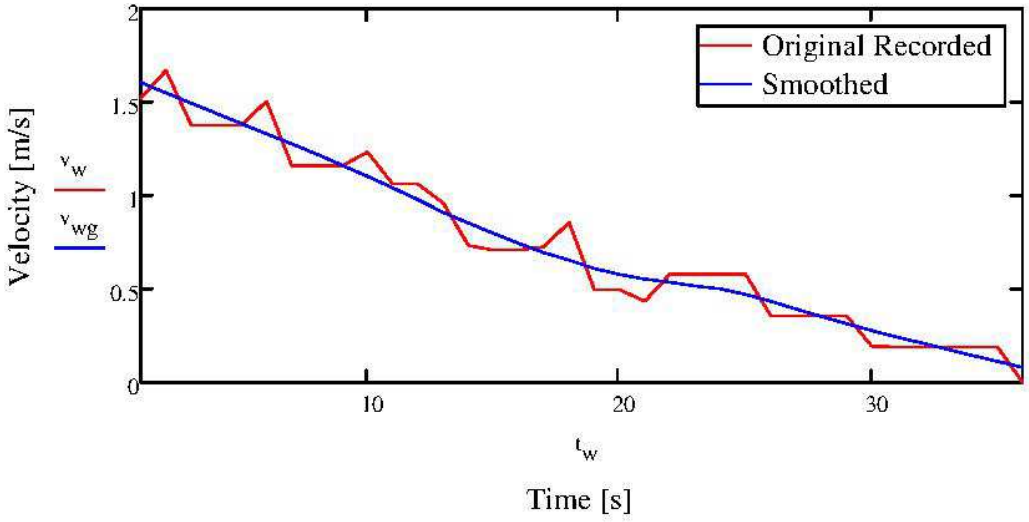

Calculation of the Acceleration Vector

$$a_w(v_w) := \left| \begin{array}{l} D \leftarrow 0 \\ D_0 \leftarrow 0 \\ \text{for } i \in \text{ORIGIN}..\text{letzte}(v_w) - 1 \\ \quad D_{i+1} \leftarrow \dfrac{v_{w_{i+1}} - v_{w_i}}{\Delta t_{w_{i+1}}} \\ \text{return } D \end{array} \right.$$

%Acceleration vector without smoothening

$$a_{wg}(v_{wg}) := \left| \begin{array}{l} D \leftarrow 0 \\ D_0 \leftarrow 0 \\ \text{for } i \in \text{ORIGIN}..\text{letzte}(v_{wg}) - 1 \\ \quad D_{i+1} \leftarrow \dfrac{v_{wg_{i+1}} - v_{wg_i}}{\Delta t_{w_{i+1}}} \\ \text{return } D \end{array} \right.$$

%Acceleration vector with smoothening

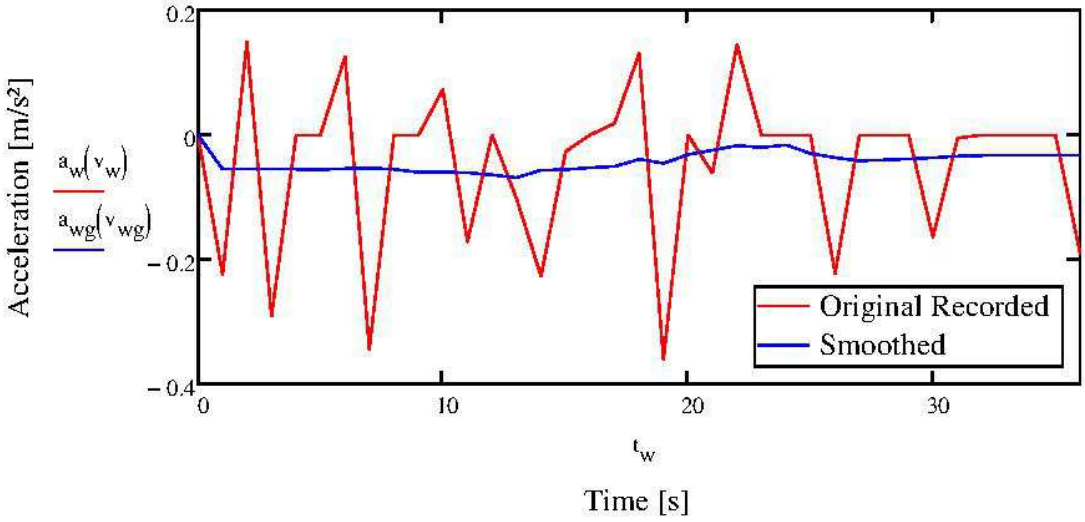

$F_{aw} := -\left(m_{ges} \cdot a_{wg}(v_{wg})\right)$ % Translational force of inertia

$\omega_w := \frac{v_{wg}}{r}$

$\omega_{Punktw} := \frac{a_{wg}(v_{wg})}{r}$

$M_{Ivw} := I_v \cdot \omega_{Punktw}$

$M_{Ihlw} := M_{Ivw}$

$M_{Ihrw} := I_{hr} \cdot \omega_{Punktw}$

$F_{Ivw} := \frac{M_{Ivw}}{r_a}$

$F_{Ihlw} := F_{Ivw}$

$F_{Ihrw} := \frac{M_{Ihrw}}{r_a}$

$F_{Igesw} := -\left(F_{Ivw} + F_{Ihlw} + F_{Ihrw}\right)$ % Rotational force of inertia

$F_{Lw} := \frac{1}{2} \cdot cw \cdot \rho \cdot A \cdot v_{wg}^{2}$ % Drag force

$F_r := F_{aw} + F_{Igesw} - F_{Lw}$ % Bicycle resistance force

$F_{rg} := strgltt(t_w, F_r)$ % Smoothing of BRF

$F_{rm} := mittelwert(F_r) = 5.524\,N$ % BRF mean value

$F_{rmg} := mittelwert(F_{rg}) = 5.544\,N$ % Smoothed BRF mean value

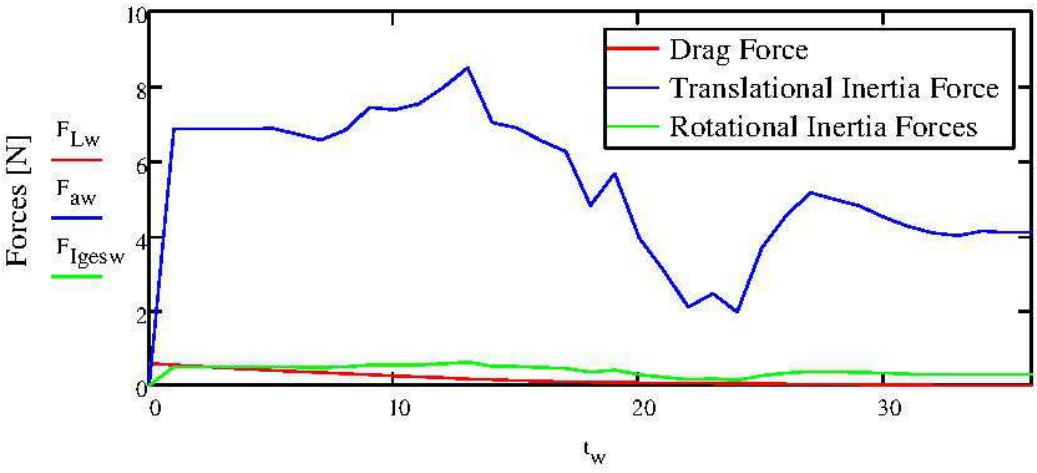

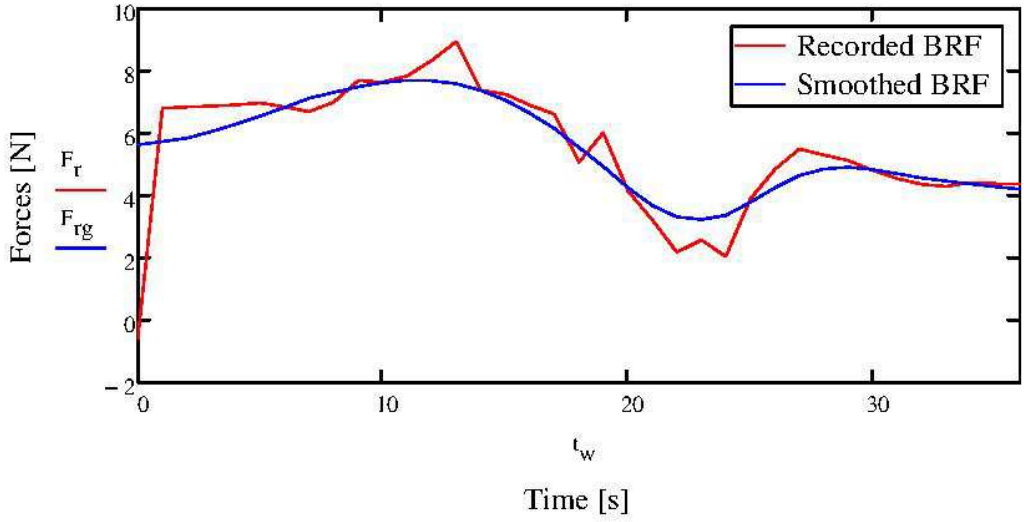

Trial Two

$v_{wg2} := \text{strgltt}(t_{w2}, v_{w2})$ %Smoothening of the velocity vector with the least square methode

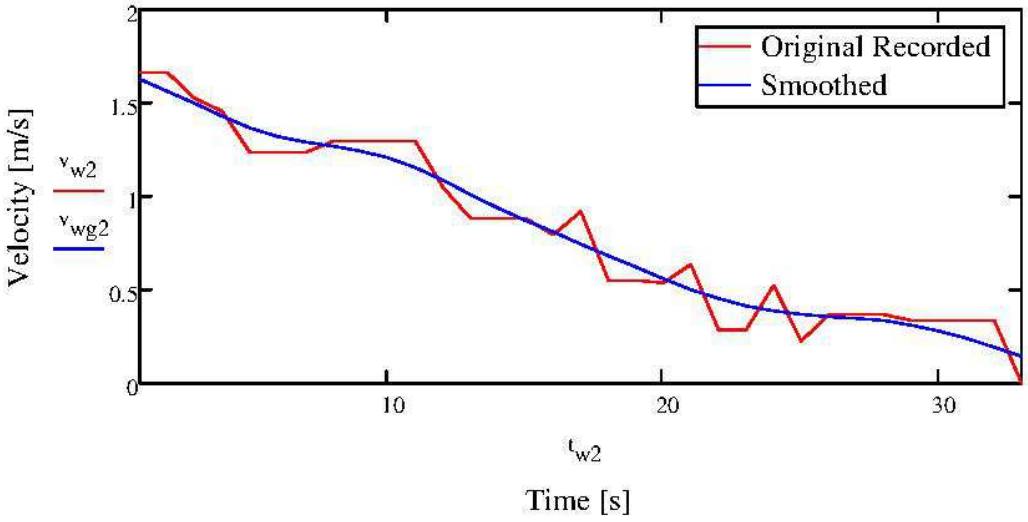

Calculation of the Acceleration Vector:

$a_{w2}(v_{w2}) :=$ %Acceleration vector without smoothening

$D \leftarrow 0$

$D_0 \leftarrow 0$

for $i \in \text{ORIGIN} .. \text{letzte}(v_{w2}) - 1$

$$D_{i+1} \leftarrow \frac{v_{w2_{i+1}} - v_{w2_i}}{\Delta t_{w2_{i+1}}}$$

return D

$a_{wg2}(v_{wg2}) :=$ %Acceleration vector with smoothening

$D \leftarrow 0$

$D_0 \leftarrow 0$

for $i \in \text{ORIGIN} .. \text{letzte}(v_{wg2}) - 1$

$$D_{i+1} \leftarrow \frac{v_{wg2_{i+1}} - v_{wg2_i}}{\Delta t_{w2_{i+1}}}$$

return D

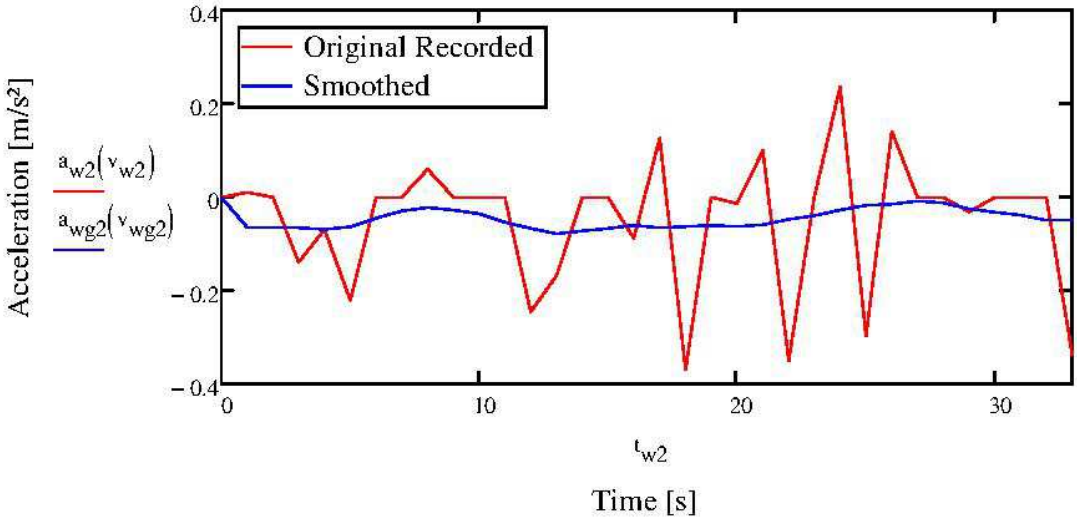

$F_{aw2} := -(m_{ges} \cdot a_{wg2}(v_{wg2}))$ % Translational force of inertia

$\omega_{w2} := \frac{v_{wg2}}{r}$

$\omega_{Punktw2} := \frac{a_{wg2}(v_{wg2})}{r}$

$M_{Ivw2} := I_v \cdot \omega_{Punktw2}$

$M_{Ihlw2} := M_{Ivw2}$

$M_{Ihrw2} := I_{hr} \cdot \omega_{Punktw2}$

$F_{Ivw2} := \frac{M_{Ivw2}}{r_a}$

$F_{Ihlw2} := F_{Ivw2}$

$F_{Ihrw2} := \frac{M_{Ihrw2}}{r_a}$

$F_{Igesw2} := -(F_{Ivw2} + F_{Ihlw2} + F_{Ihrw2})$ % Rotational force of inertia

$F_{Lw2} := \frac{1}{2} \cdot cw \cdot \rho \cdot A \cdot v_{wg2}^2$ % Drag force

$F_{r2} := F_{aw2} + F_{Igesw2} - F_{Lw2}$ % Bicycle resistance force

$F_{rg2} := strgltt(t_{w2}, F_{r2})$ % Smoothing of BRF

$F_{rm2} := mittelwert(F_{r2}) = 5.876\,N$ % BRF mean value

$F_{rmg2} := mittelwert(F_{rg2}) = 5.863\,N$ % Smoothed BRF mean value

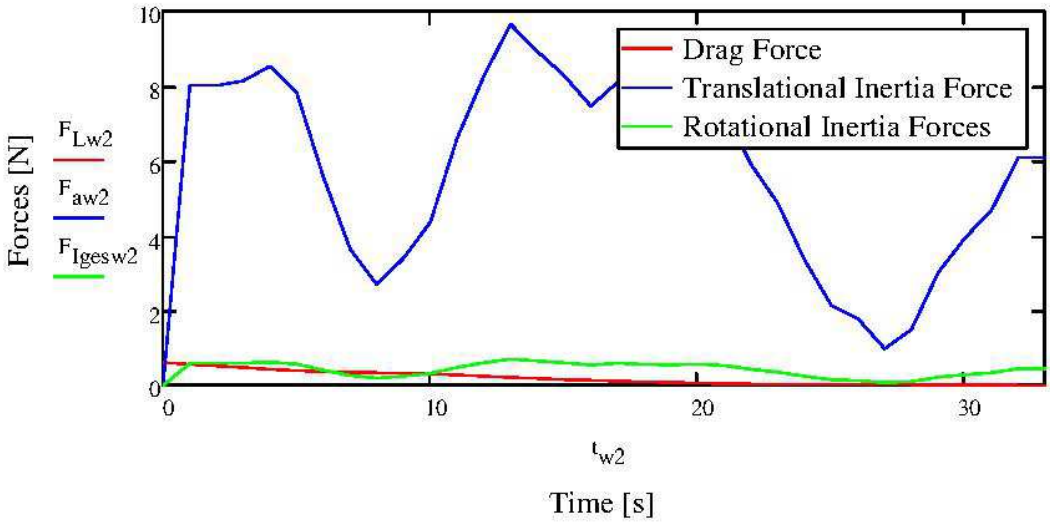

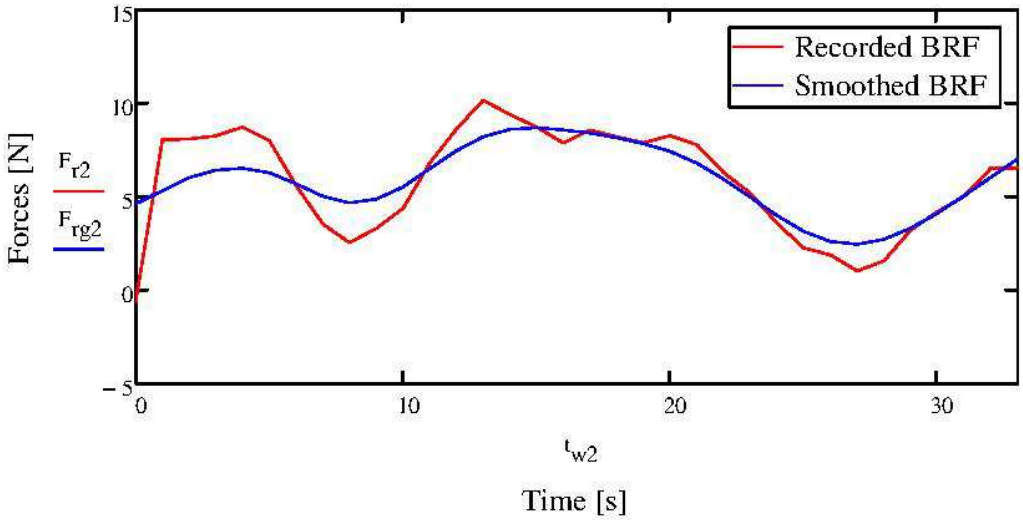

Trial Three

$v_{wg3} := strgltt(t_{w3}, v_{w3})$ %Smoothening of the velocity vector with the least square methode

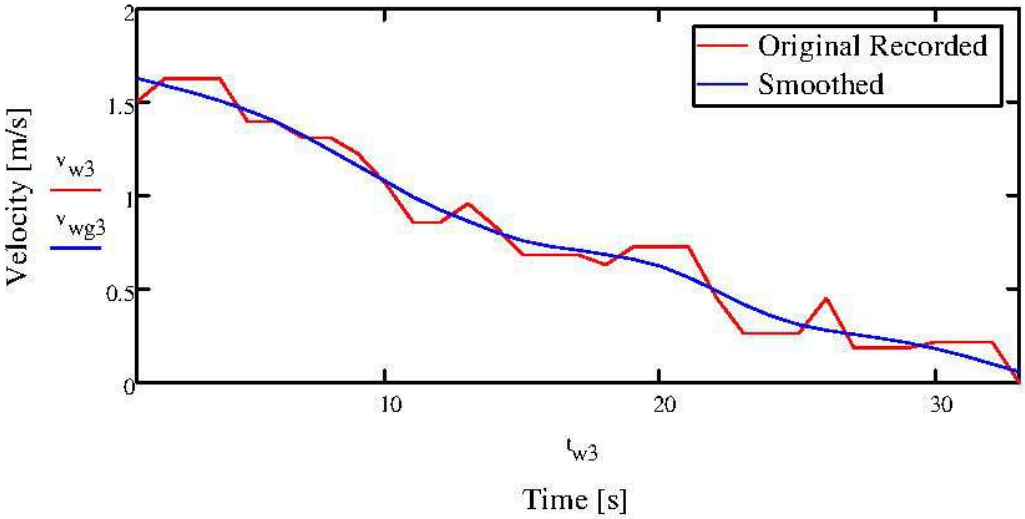

Calculation of the Acceleration Vector

$a_{w3}(v_{w3}) :=$ %Acceleration vector without smoothening

$D \leftarrow 0$

$D_0 \leftarrow 0$

for $i \in ORIGIN .. letzte(v_{w3}) - 1$

$$D_{i+1} \leftarrow \frac{v_{w3_{i+1}} - v_{w3_i}}{\Delta t_{w3_{i+1}}}$$

return D

$a_{wg3}(v_{wg3}) :=$ %Acceleration vector with smoothening

$D \leftarrow 0$

$D_0 \leftarrow 0$

for $i \in ORIGIN .. letzte(v_{wg3}) - 1$

$$D_{i+1} \leftarrow \frac{v_{wg3_{i+1}} - v_{wg3_i}}{\Delta t_{w3_{i+1}}}$$

return D

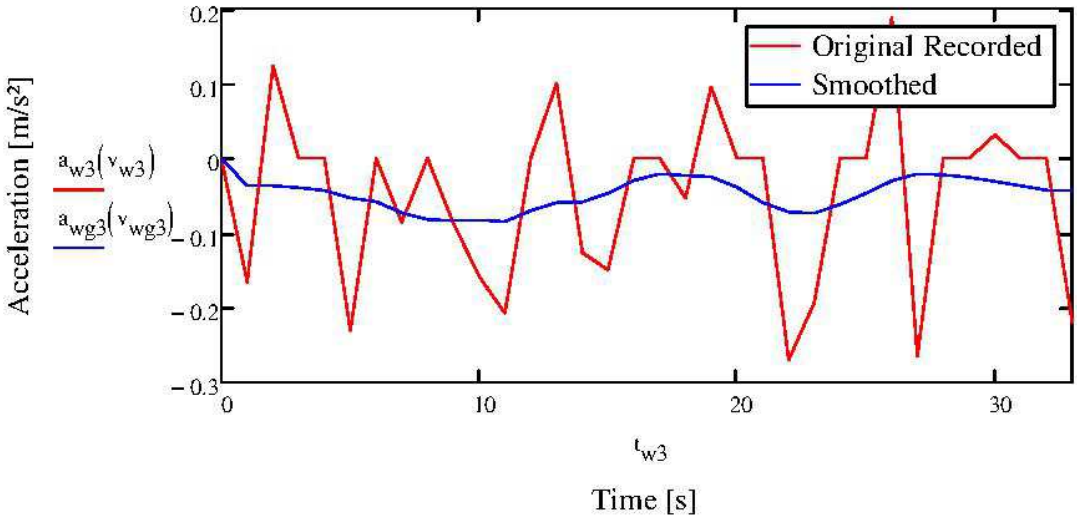

$F_{aw3} := -(m_{ges} \cdot a_{wg3}(v_{wg3}))$ % Translational force of inertia

$\omega_{w3} := \frac{v_{wg3}}{r}$

$\omega_{Punktw3} := \frac{a_{wg3}(v_{wg3})}{r}$

$M_{Ivw3} := I_v \cdot \omega_{Punktw3}$

$M_{Ihlw3} := M_{Ivw3}$

$M_{Ihrw3} := I_{hr} \cdot \omega_{Punktw3}$

$F_{Ivw3} := \frac{M_{Ivw3}}{r_a}$

$F_{Ihlw3} := F_{Ivw3}$

$F_{Ihrw3} := \frac{M_{Ihrw3}}{r_a}$

$F_{Igesw3} := -(F_{Ivw3} + F_{Ihlw3} + F_{Ihrw3})$ % Rotational force of inertia

$F_{Lw3} := \frac{1}{2} \cdot cw \cdot \rho \cdot A \cdot v_{wg3}^2$ % Drag force

$F_{r3} := F_{aw3} + F_{Igesw3} - F_{Lw3}$ % Bicycle resistance force

$F_{rg3} := \text{strgltt}(t_{w3}, F_{r3})$ % Smoothing of BRF

$F_{rm3} := \text{mittelwert}(F_{r3}) = 6.11\,\text{N}$ % BRF mean value

$F_{rmg3} := \text{mittelwert}(F_{rg3}) = 6.098\,\text{N}$ % Smoothed BRF mean value

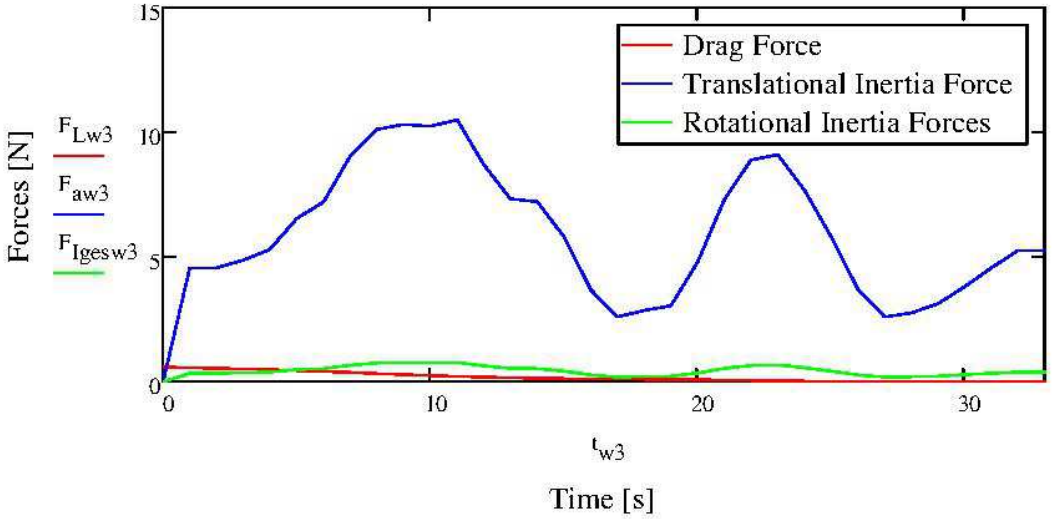

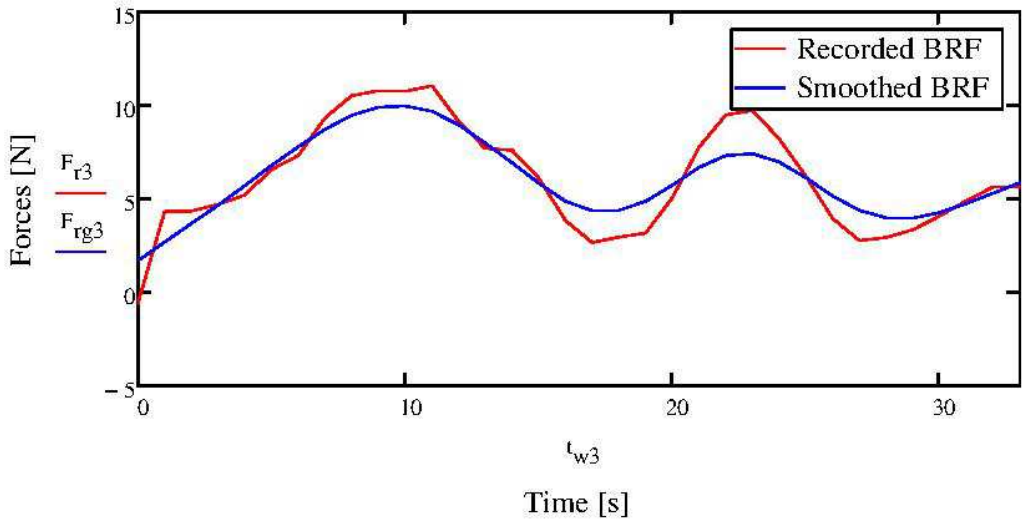

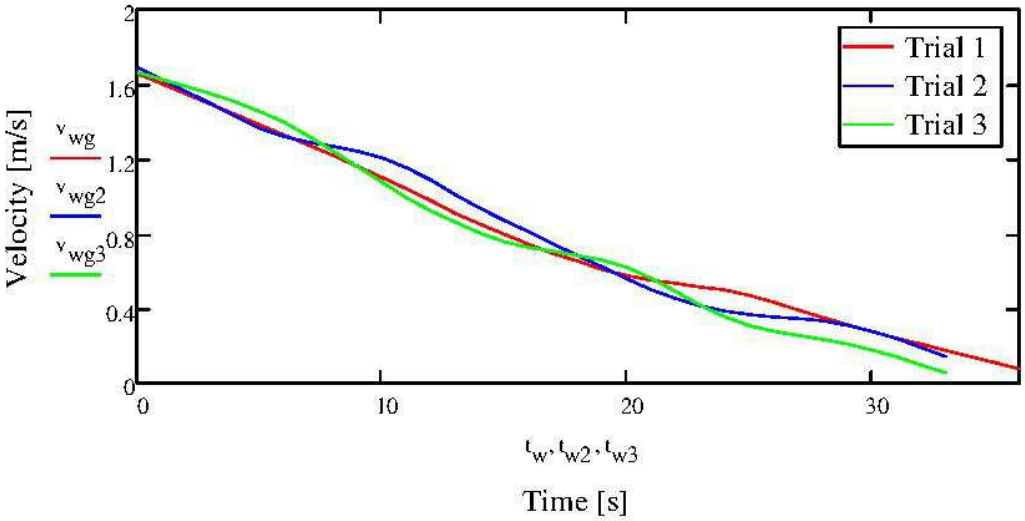

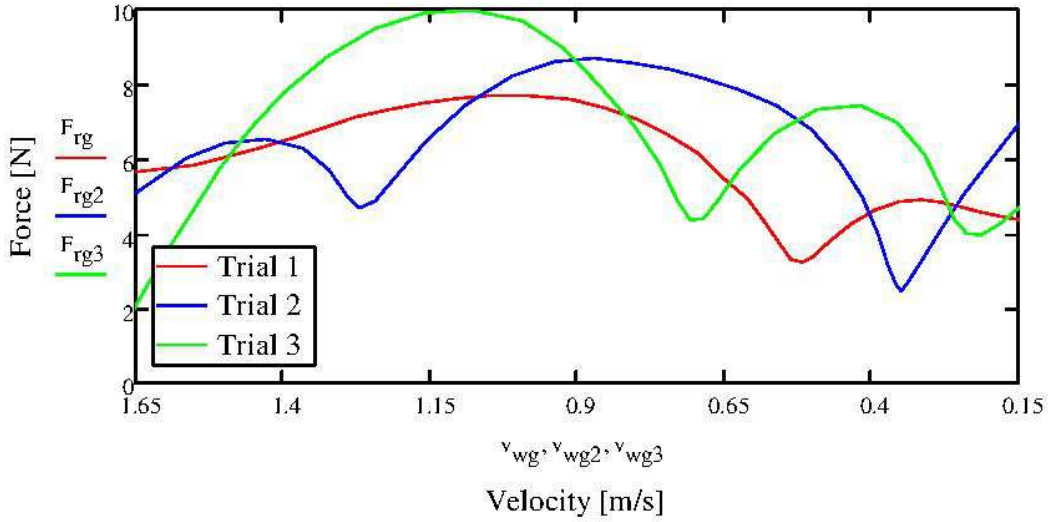

BRF mean value out of 3 trials

$$F_{rmges} := \frac{\text{mittelwert}(F_{rm}) + \text{mittelwert}(F_{rm2}) + \text{mittelwert}(F_{rm3})}{3} = 5.837\,\text{N}$$

Power Calculation

$P_L := \overrightarrow{(F_L \cdot v)}$ % Power of the drag force

$P_a := \overrightarrow{\left|(F_a + F_{Iges}) \cdot v\right|}$ % Power of the inertia forces

$P_r := F_{rmges} \cdot v$ % Power of the bicycle resistance

$P_{ges} := P_L + P_a + P_r$ % Overall Power

$P_{gesg} := kgltt(t, P_{ges}, 3)$ %Smoothed over all power (for depiction)

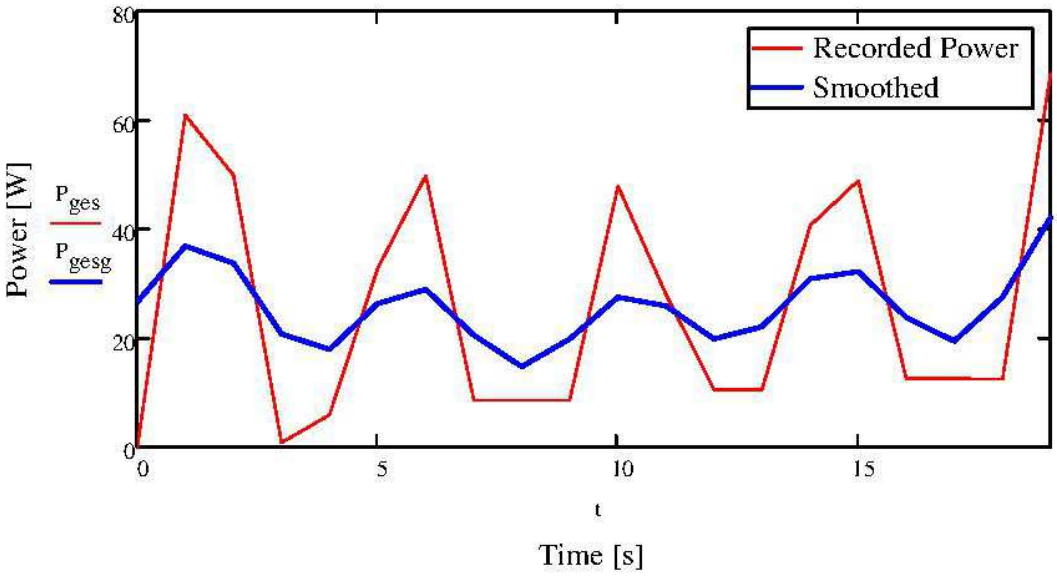

Mean Power

$P_m := \text{mittelwert}(P_{ges})$ % Mean power

$P_m = 26.009\ \text{W}$

$P_{mw} :=$
$D \leftarrow 0$
for $i \in \text{ORIGIN}..\text{letzte}(P_{ges}) - 1$
$D_i \leftarrow \text{mittelwert}(P_{ges})$
$D_{\text{letzte}(P_{ges})} \leftarrow D_{\text{letzte}(D)}$
return D

% Generation of a mean power vector (for depiction)

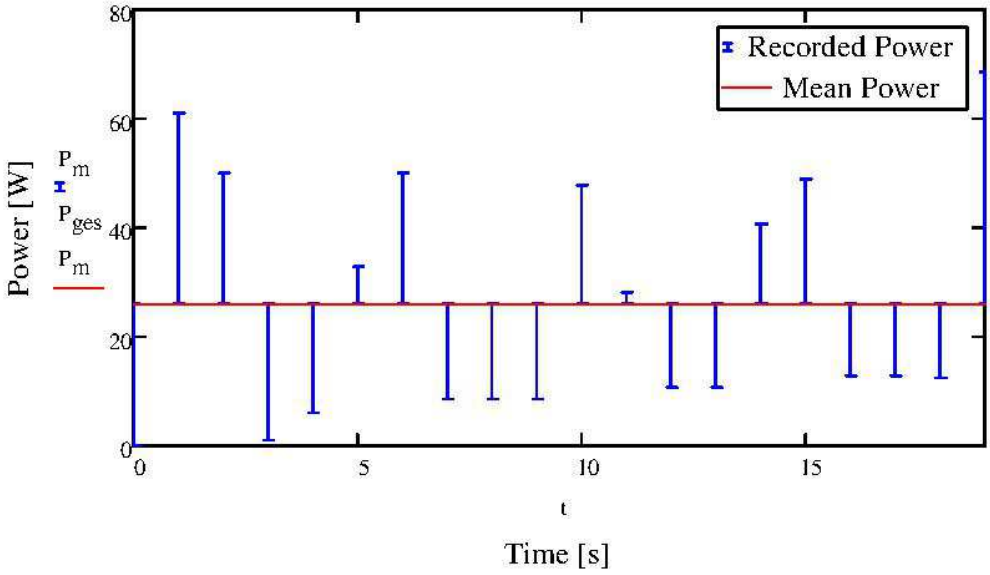

A3.2 ESC Calculation

Dimensions

$a1 := 11mm$

$a2 := 25mm$

$a3 := 7mm$

$b1 := 7.5mm$

$b2 := 12.5mm$

$b3 := 3mm$

$h_v := 54.5mm$ Lenght of the vertical beam

$l_h := 119.5mm$ Lenght of the horizontal beam

$A_7 := a3 \cdot b1 = 52.5 \cdot mm^2$

$A_{12} := a3 \cdot b2 = 87.5 \cdot mm^2$

$A_3 := a1 \cdot b3 = 33 \cdot mm^2$

$A_{25} := a2 \cdot a2 = 625 \cdot mm^2$

Calculation of the upper overall center of gravity

$$y_s := \frac{2 \cdot a3 \cdot b1 \cdot \frac{b1}{2} + 2 \cdot a3 \cdot b2 \cdot \left(a2 - \frac{b2}{2}\right) + a1 \cdot b3 \cdot \left(a2 - \frac{b3}{2}\right)}{2 \cdot A_7 + 2 \cdot A_{12} + A_3} = 14.219\,mm$$

$$y_7 := \frac{b1}{2} - y_s = -10.469\,mm$$

$$y_{12} := a2 - y_s - \frac{b2}{2} = 4.531\,mm$$

$$y_3 := a2 - y_s - \frac{b3}{2} = 9.281\,mm$$

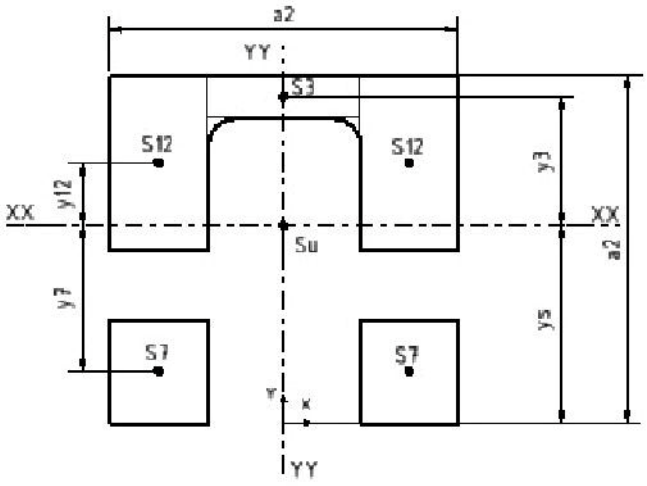

Force and bending moment

$F_k := 8000N$ Clamping force

$M := F_k \cdot h_v$ Resulting torque at the guide rails

Youngs modulus (E)

$$E_{Steel} := 210000 \frac{N}{mm^2}$$

Section modulus (I)

$$I_3 := \frac{a1 \cdot b3^3}{12} = 24.75 \cdot mm^4$$

$$I_7 := \frac{a3 \cdot b1^3}{12} = 246.094 \cdot mm^4$$

$$I_{12} := \frac{a3 \cdot b2^3}{12} = 1.139 \times 10^3 \cdot mm^4$$

$$I_{25} := \frac{a2 \cdot a2^3}{12} = 3.255 \times 10^4 \cdot mm^4$$

The overall section modulus Ixx was calculated under the assumption that no relative movement is possible between the areas I7 and I12.

$$I_{XX} := 2 \cdot \left(I_{12} + y_{12}^2 \cdot A_{12} \right) + I_3 + y_3^2 \cdot A_3 + 2 \left(I_7 + y_7^2 \cdot A_7 \right) = 2.074 \times 10^4 \cdot mm^4$$

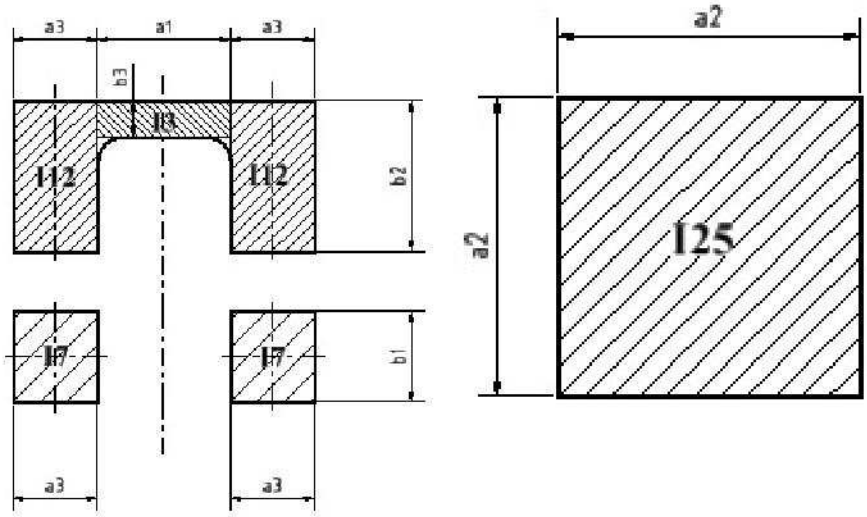

Horizontal beam - deflection at the middle (x=lh/2)

To estimate the resulting maximal deflection of the horizontal beam it was assumed as beam stressed by two bending moments at the ends.

$$x := \frac{l_h}{2}$$

$$w_x := \frac{\left(F_k \cdot h_v \cdot x - M \cdot l_h\right) \cdot x^2}{2 \cdot E_{Steel} \cdot I_{25} \cdot l_h} = -0.057\,mm$$

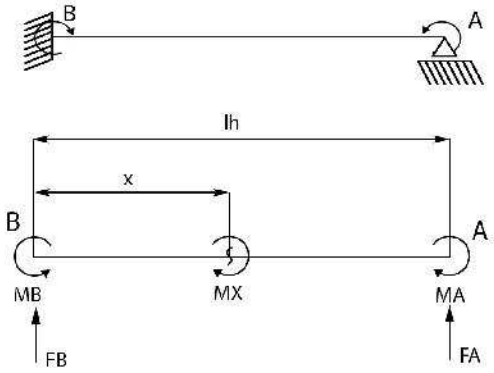

Deflection of the upper reinforced guiding beams

To estimate the resulting maximal deflection at the end of the guide rails they were assumed as cantilever beam and stressed by a force at the end.

$$F_1 := 17440N$$

$$l_B := 25mm$$

$$w_{XX} := \frac{F_1 \cdot l_B^{\,3}}{3 \cdot E_{Steel} \cdot I_{XX}} = 0.021 \cdot mm$$

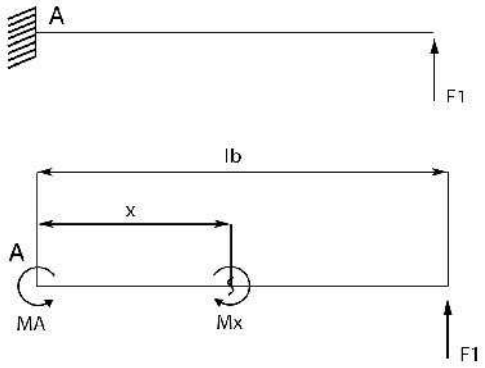

A4 Test Trial Checklist

- Subject data: weight, age, sex, kind of injury, injury since, FES training since injury

- Test trail conditions (slope, trail surface)

- Wind conditions

- Electrode type

- Electrode conductive material

- Take picture to assess wind contact surface, with yard stick
- Measurement of knee angle in backward position

Result:

- Take a picture of knee angle in backward position
- Measurement of knee angle in forward position

Result:

- ☐ Take a picture of knee angle in forward position

- ☐ Measurement of fence position

Result:

- ☐ Take a picture of fence position

- ☐ Measurement of electrode position

Result:

- ☐ Take a picture of electrode position

- ☐ Adjusted stimulator amplitude

Result:

- ☐ Adjusted stimulator frequency

Result:

- ☐ Adjusted pulse width

  Result:

- ☐ Measurement of the ambient temperature

Result: